

IMPROVED LABORATORY TRANSITION PROBABILITIES FOR Sm II
AND APPLICATION TO THE SAMARIUM ABUNDANCES OF THE SUN
AND THREE *r*-PROCESS RICH, METAL-POOR STARS

(short title: Sm Transition Probabilities and Abundances)

J. E. Lawler, E. A. Den Hartog

Department of Physics, University of Wisconsin, Madison, WI 53706;

eadenhar@wisc.edu, jelawler@wisc.edu

C. Sneden

Department of Astronomy and McDonald Observatory, University of Texas,
Austin, TX 78712; chris@verdi.as.utexas.edu

and J. J. Cowan

Homer L. Dodge Department of Physics and Astronomy, University of
Oklahoma, Norman, OK 73019; cowan@nhn.ou.edu

ABSTRACT

Radiative lifetimes, accurate to $\pm 5\%$, have been measured for 212 odd-parity levels of Sm II using laser-induced fluorescence. The lifetimes are combined with branching fractions measured using Fourier-transform spectrometry to determine transition probabilities for more than 900 lines of Sm II. This work is the largest-scale laboratory study to date of Sm II transition probabilities using modern methods. This improved data set has been used to determine a new solar photospheric Sm abundance, $\log \varepsilon = 1.00 \pm 0.03$, from 26 lines. The spectra of three very metal-poor, neutron-capture-rich stars also have been analyzed, employing between 55 and 72 Sm II lines per star. The abundance ratios of Sm relative to other rare earth elements in these stars are in agreement, and are consistent with ratios expected from rapid neutron-capture nucleosynthesis (the *r*-process).

Subject headings: atomic data — stars: abundances stars: Population II — Sun: abundances

1. INTRODUCTION

Improved transition probability data for numerous Rare Earth (RE) spectra have been determined over the last decade. A complete review by Biémont & Quinet (2003) has over 500 citations. Work on the second spectra (singly ionized) during the last decade includes: La II (Li & Zhankui 1999, Zhiguo et al. 1999, Lawler et al. 2001a, Derkatch et al. 2002), Ce II (Palmeri et al. 2000, Zhang et al. 2001b), Pr II (Ivarsson et al. 2001), Nd II (Den Hartog et al. 2003), Sm II (Scholl et al. 2002, Xu et al. 2003b), Eu II (Zhang et al. 2000, Lawler et al. 2001c; Rostohar et al. 2001, Den Hartog et al. 2002), Gd II (Zhang et al. 2001a, Xu et al. 2003a), Tb II (Den Hartog et al. 2001; Lawler et al. 2001b), Dy II (Curry et al. 1997; Wickliffe et al. 2000), Ho II (Den Hartog et al. 1999; Lawler et al. 2004), Tm II (Anderson et al. 1996; Wickliffe & Lawler 1997, Rieger et al. 1999, Quinet et al. 1999a), Yb II (Zhao et al. 1996, Pinnington et al. 1997, Taylor et al. 1997, Biémont et al. 1998, Li et al. 1999, Yu & Maleki 2000), Lu II (Den Hartog, et al. 1998; Quinet et al. 1999b; Fedchak et al. 2000). Many of the recent experimental studies have combined radiative lifetimes from laser induced fluorescence (LIF) measurements with emission branching fractions measured using a Fourier transform spectrometer (FTS). This approach to determining atomic transition probabilities in complex spectra has proved to be quite reliable.

A major motivation for the intense, multi-year effort on RE and other heavy element spectroscopy arises from stellar elemental abundance studies. High-resolution, high signal-to-noise spectra on a variety of targets from very large ground-based telescopes and the Hubble Space Telescope are providing data that are reshaping our views on the chemical evolution of our Galaxy. Old metal-poor Galactic halo stars provide a fossil record of the chemical make-up of our Galaxy when it, and the Universe, were very young (e.g., Gratton & Sneden 1994; McWilliam et al. 1995; Cowan et al. 1995; Sneden et al. 1996, Ryan et al. 1996, Cayrel et al. 2004). Recent abundance determinations of heavy neutron capture (*n*-capture) elements in very metal-poor stars have yielded new insights on the roles of the *r*(apid)- and *s*(low)-processes in the initial burst of Galactic nucleosynthesis. Substantial progress is occurring due to improvements in both observational data and laboratory data needed for analysis of the spectra (e.g. Cowan et al. 2002; Sneden et al. 2003; Simmerer et al. 2004).

The RE's are among the most spectroscopically accessible of the *n*-capture elements. Large numbers of transitions of singly ionized RE species appear in the spectrum of the Sun and in stars over a significant temperature range. In addition to work on metal-poor stars, the solar abundances of several of these elements have been brought into agreement with meteoric abundances through improvements in the transition probability database (e.g. Bord et al. 1998; Den Hartog et al. 1998; Lawler et al. 2001b).

In this paper we apply LIF/FTS experimental techniques to determine accurate data for a very large number of ionized samarium transitions. In the recent study of Xu et al.(2003b), theoretical branching fractions of Sm II have been combined with experimental lifetimes. The spectrum of Sm II is very complex;

there is a substantial breakdown of Russell- Saunders or LS coupling for most odd-parity levels in combination with extensive configuration mixing and relativistic effects. Therefore another one of the motivations for the work described herein is to test the relativistic Hartree Fock calculations by Xu et al. (2003b).

The above-mentioned studies on La II, Eu II, Tb II, and Ho II (whose nuclei have odd atomic numbers Z and only odd mass numbers N in their naturally occurring isotopes) included measurements of both transition probabilities along with isotope shift and/or hyperfine structure data. Although Sm ($Z = 62$) has seven abundant isotopes, all but two of them have even N 's. Therefore most of the blue and near UV lines of Sm II are rather narrow with no resolved structure in our spectra with resolving powers up to 10^6 . Several of the strong blue and near UV lines of Sm II do have detectable structure and this opens the possibility of isotopic abundance determinations. Masterman et al. (2003) reported an extensive study of the isotopic and hyperfine structure of strong Sm II lines in the blue region. In the present study, we have concentrated on determining transition probabilities. We measured radiative lifetimes using time-resolved laser-induced fluorescence for 212 odd-parity levels of Sm II. These were combined with branching fractions measured using FTS data to yield gf -values for over 900 transitions of Sm II. This new data set was used to re-assess Sm abundances in the solar photosphere and in three r -process rich, metal-poor stars. The possibility of determining Sm isotopic abundances is discussed. We conclude with a brief review of the n -capture elemental abundances in metal-poor halo stars.

2. OVERVIEW OF THE SECOND SPECTRUM OF SAMARIUM

Figure 1 is a partial Grotrian diagram for singly ionized Sm constructed from energy levels tabulated by Martin et al. (1978). The even-parity levels of the $4f^6(7F)6s$ sub-configuration are all known. The $4f^6(7F)5d$ sub-configuration also appears to be complete in Martin et al., but a detailed analysis by Wyart & Bauche-Arnoult (1981) led them to reject two “high J ” levels listed by Martin et al. (Our figure labels this sub-configuration as \sim known.) The first unknown even-parity levels are part of the $4f^6(5D)6s$ and $4f^6(5D)5d$ sub-configurations. These unknown even-parity levels have low J values and start about $15,500 \text{ cm}^{-1}$ according to Cowan Code (Cowan 1981) calculations (private communication: J.-F. Wyart 2005, D. Bord 2005). Fortunately, knowledge of even-parity levels below $20,000 \text{ cm}^{-1}$ is nearly complete. These low even-parity levels are sufficiently well isolated that they are relatively pure LS levels that can be assigned with confidence.

The situation for odd-parity levels is not as satisfactory. The lowest odd-parity level is the $4f^7\ ^8S_{7/2}$. This level is the only odd-parity level that is sufficiently isolated to be cleanly assigned. Martin et al. (1978) lists only tentative assignments for all higher odd-parity levels. Four extensively mixed configurations contribute to the band of odd-parity levels which starts at $21,250 \text{ cm}^{-1}$. These configurations are $4f^66p$, $4f^56s5d$, $4f^56s^2$, and $4f^55d^2$. Xu et al. (2003b) point out that these four overlapping configurations have 13,628 levels

and that the complete $4f^7$ configuration, which also overlaps the other four configurations, has an additional 327 levels. A complete analysis of the low odd-parity configurations is a formidable task. It is not necessary to diagonalize a $13,955 \times 13,955$ or larger matrix, because J (in addition to parity) is a good quantum number. Many of the levels in the five configurations are quite high in energy and do not strongly interact with the low odd-parity levels. However, even if the analysis is limited to the lowest sub-configurations built on the 7F and 6H parents (the $4f^6({}^7F)6p$, $4f^5({}^6H)6s5d$, $4f^5({}^6H)6s^2$, and $4f^5({}^6H)5d^2$ sub-configuration as denoted in Figure 1), this still includes more than 400 levels. The lack of assignment of the odd-parity levels is a problem which is discussed in more detail in § 4.

All of the transitions studied in this work are from odd-parity upper levels. These levels decay primarily in the blue and near UV to the $4f^6({}^7F)6s$ even-parity levels. A substantial number of weaker transitions in the yellow and red to the $4f^6({}^7F)5d$ even-parity levels were also measured in this work. The odd-parity levels in this study thus have significant $4f^6({}^7F)6p$ or $4f^56s5d$ components.

3. RADIATIVE LIFETIME MEASUREMENTS

Radiative lifetimes of 212 odd-parity levels of Sm II have been measured using time-resolved laser-induced fluorescence (LIF) on a slow ($\sim 5 \times 10^4$ cm/s) atom/ion beam. The apparatus and technique are the same as used for many other species and have been described in detail elsewhere. Only a brief discussion is given here. The reader is referred to recent work in Eu I, II, and III (Den Hartog et al. 2002) for a more detailed description.

The beam of Sm atoms and ions is produced using a hollow cathode discharge sputter source. A large-bore hollow cathode is lined with samarium foil. A pulsed argon discharge, operating at ~ 0.4 torr with $10 \mu\text{s}$ duration, 10 A pulses, is used to sputter the samarium. The hollow cathode is closed on one end except for a 1 mm hole, through which the samarium atoms and ions are extracted into a low pressure (10^{-4} torr) scattering chamber. This beam is intersected at right angles by a nitrogen laser-pumped dye laser beam 1 cm below the cathode bottom. The laser is tunable over the range 2050 - 7200 Å with the use of frequency doubling crystals, is pulsed at ~ 30 Hz repetition rate with a ~ 3 ns pulse duration, and has a 0.2 cm^{-1} bandwidth. The laser is used to selectively excite the level to be studied. Selective excitation eliminates the possibility of cascade radiation from higher-lying levels.

Fluorescence is collected in a direction orthogonal to both the laser and atomic/ionic beams through a pair of fused-silica windows which form an f/1 optical system. Optical filters, either broadband colored glass filters or narrow-band multi-layer dielectric filters, are typically inserted between the two lenses to cut down on scattered laser light and to block cascade radiation from lower levels. A RCA 1P28A photomultiplier tube (PMT) is used to detect the fluorescence. The signal from the PMT is recorded and averaged over 640 shots using a Tektronix SCD1000 digitizer. Data are recorded with the laser tuned on and off the excitation transition. A linear least-square fit to a single exponential

is performed on the background-subtracted fluorescence decay to yield the lifetime of the level. The lifetime is measured twice for each level, using a different excitation transition whenever feasible. This redundancy helps ensure that the transitions are identified correctly in the experiment, classified correctly and are free from blends.

With only two exceptions, the lifetimes reported here have an uncertainty of $\pm 5\%$. To achieve this level of fidelity and maintain it over the full dynamic range of the experiment (2 ns to $1.5 \mu s$), the possible systematic errors in these measurements must be well understood and controlled. They include electronic bandwidth limitations, cascade fluorescence, Zeeman quantum beats and atomic motion time-of-flight effects, among others. These systematic effects are discussed in detail elsewhere, (See, for example, Den Hartog et al. 1999; 2002) and will not be discussed further here. As a means of verifying that the measurements are within the stated uncertainties, we perform periodic end-to-end tests of the experiment by measuring a set of well known lifetimes. These cross-checks include lifetimes of Be I (Weiss 1995), Be II (Yan et al. 1998) and Fe II (Guo et al. 1992; Biémont et al. 1991), covering the range from 1.8–8.8 ns. An Ar I lifetime is measured at 27.85 ns (Volz & Schmoranzer 1998). He I lifetimes are measured in the range 95 – 220 ns (Kono & Hattori 1984).

The results of our lifetime measurements of 212 odd-parity levels of Sm II are presented in Table 1. Energy levels are from the tabulation by Martin et al. (1978). Air wavelengths are calculated from the energy levels using the standard index of air (Edlén 1953, 1966). The uncertainty of the lifetimes is $\pm 5\%$ with two exceptions which are noted in the table.

Also presented in Table 1 is a comparison of our results with those from other LIF lifetime measurements available in the literature. We find that our lifetimes agree very well with the 35 lifetimes reported by Biémont et al. (1989) with the exception of 4 levels: 21508, 25940, 26821 and 28930 cm^{-1} . In all four of these cases we measured our lifetime with 2 different excitation transitions. In the case of the 21508 cm^{-1} level, our lifetime is nearly an order of magnitude longer than what they measured. We speculate that they may have used the 4648.2 Å transition to excite this level. We observe a very strong blend 0.08 Å to the blue of this transition, which may have been inadvertently measured instead. No obvious explanation can be found for the factor of 2 - 2.5 disagreement on the 25940 and 26821 cm^{-1} levels. In addition to measuring each lifetime using two transitions, careful optical filtering was also used, so our confidence in our lifetimes is high. In the case of the 28930 cm^{-1} level, they report a lifetime $\sim 25\%$ lower than ours. Here again, there is no obvious reason for the disagreement. With the three most serious discrepancies removed from the averages, we see a mean difference between our measurements and theirs of 1.0% and an rms difference of 6.7%.

We find excellent agreement with the laser-fast beam measurements of 82 lifetimes by Scholl et al. (2002). All our measurements are within 10% of theirs, and the vast majority are well within 5%. The mean difference between our measurements and theirs is 1.0% and an rms difference of 3.0%. We do not see quite as good agreement with the LIF measurements of Xu et al. (2003b).

Yet they are still all within 15% of our measurements with a mean difference between our measurements and theirs of 5.2% and an rms difference of 7.0%. The agreement with the 18 laser-fast beam lifetimes of Vogel et al (1988) is excellent except for the 30% discrepancy at 27285 cm^{-1} . When this discrepancy is omitted we see a mean difference between our measurements and theirs of 1.0% and an rms difference of 1.8%. They single out the 27285 cm^{-1} level in their discussion as having comparatively large uncertainties. Our lifetime of this level was measured on two different transitions with narrowband, off-line filtering in both cases. Our confidence in this lifetime is high, especially as our value is in good agreement with those of both Biémont et al. (1989) and Scholl et al. (2002).

4. BRANCHING FRACTIONS AND ATOMIC TRANSITION PROBABILITIES

The 1.0 meter FTS at the National Solar Observatory (NSO) was used in this work on Sm II. This instrument is uniquely suited for spectroradiometry on complex RE atoms and ions. It provides: (1) a limit of resolution as small as 0.01 cm^{-1} , (2) wave number accuracy to 1 part in 10^8 , (3) broad spectral coverage from the UV to IR, and (4) the capability of recording a million point spectrum in 10 minutes (Brault 1976). An FTS is insensitive to any small drift in source intensity since an interferogram is a simultaneous measurement of all spectral lines. The combination of branching fractions from FTS spectra with radiative lifetimes from LIF measurements has resulted in greatly improved atomic transition probabilities for the first and second spectra of many elements.

The emission sources for Sm spectra were commercially manufactured, sealed hollow cathode discharge (HCD) lamps with fused silica windows containing either argon or neon fills. We operated these lamps at currents significantly above the manufacturers' recommendation, but used forced air cooling to prevent overheating. The NSO 1.0 m FTS fitted with the UV beam splitter was used to record spectra during our February 2000 observing run. Spectra of the Ar-filled lamp operating with a discharge current of 27 mA (61 co-adds), 27 mA (50 co-adds), 22 mA (4 co-adds), and 18 mA (68 co-adds), were taken with the "super blue" silicon diode detectors and no additional filtering. The term "co-add" refers to a coherently added interferogram. These spectra cover the $8,000\text{ cm}^{-1}$ to $35,000\text{ cm}^{-1}$ region with a limit of resolution of 0.053 cm^{-1} . Spectra of the Ne-filled lamp operating at 23 mA (10 co-adds) and at 17 mA (10 co-adds) were taken using an identical setup. An additional spectrum of the Ar-Sm lamp at 27 mA (50 co-adds) was taken with the same set-up during our February 2002 observing run. Branching fraction measurements were made almost entirely on the Ar-Sm spectra: the Ne-Sm spectra were used only to separate Ar + Sm line blends. The three Ar-Sm spectra with the 50 or more co-adds and a lamp current of 27 mA were most useful: the lower current Ar-Sm spectra were used primarily to check for optical depth errors on the very strongest lines.

The HCD lamps used in this study operate with relatively low buffer gas pressures and thus are not in local thermodynamic equilibrium (LTE). This is

not a problem because the absolute scale of a transition probability is provided by the radiative lifetime of the upper level in every case. Doppler broadening tends to dominate the emission line shapes in these low pressure lamps. Such narrow line shapes can produce radiation trapping or optical depth error. By comparing spectra from the Ar-Sm lamp operating at different currents, we verified that radiation trapping is not a problem. The sputtering rate of Sm in the hollow cathode discharge, and the total Sm density in the plasma, are strongly increasing function of discharge current.

The establishment of an accurate relative radiometric calibration or efficiency is critical to a branching fraction experiment. Detectors, spectrometer optics, lamp windows, and any other components in the light path or any reflections which contribute to the detected signal (such as due to light reflecting off the back of the hollow cathode), all have wavelength-dependent optical properties which must be taken into account when determining the ratio of line intensities at different wavelengths. Fortunately the radiometric efficiency of the FTS is a smoothly varying functions of wavelength. An excellent way to determine the relative radiometric efficiency of an FTS is to compare well-known branching ratios for sets of lines widely separated in wavelength, to the intensities measured for the same lines. Sets of Ar I and Ar II lines have been established for this purpose in the range of 4300 to 35000 cm⁻¹ by Adams & Whaling (1981), Danzmann & Kock (1982), Hashiguchi & Hasikuni (1985), and Whaling et al. (1993), . These provide an excellent means of calibrating our FTS spectra since the argon lines are measured in the exact experimental arrangement and at the exact same time as are the Sm II lines. A spectrum of a tungsten lamp, recorded before and after the 2002 Ar-Sm spectra, was used to interpolate between Ar reference lines to improve the relative radiometric calibration of the 2002 data. The use of a tungsten lamp is of some value near the dip in the FTS sensitivity at 12,500 cm⁻¹ from the aluminum mirror coatings, and between 10,000 and 9,000 cm⁻¹ where the Si detector response is rapidly decreasing.

All possible transition wave numbers between known energy levels of Sm II satisfying both the parity change and $\Delta J = -1, 0, \text{ or } 1$ selection rules were computed and used during analysis of FTS data. Energy levels from Martin et al. (1978) were used to determine possible transition wave numbers. Levels from Martin et al. (1978) are available in electronic form from Martin et al. (2000)¹.

Branching fraction measurements were attempted on all 212 levels from the lifetime experiment, and were completed on 185 levels. Some of the levels for which branching fractions could not be completed had a strong branch beyond the UV limit of our spectra, or had a strong branch which was severely blended. Typically an upper level, depending on its J value, has about 30 possible transitions to known lower levels. More than 40,000 possible spectral line observations were studied during the analysis of 7 different Ar-Sm and Ne-Sm spectra. We set baselines and integration limits “interactively” during analysis of the FTS spectra. A simple numerical integration routine was used to determine the un-

¹ Available at http://physics.nist.gov/cgi-bin/AtData/main_asd

calibrated intensities of Sm II lines and selected Ar II and Ar I lines used to establish a relative radiometric calibration of the spectra.

The procedure for determining branching fraction uncertainties was described in detail by Wickliffe et al. (2000). Branching fractions from a given upper level are defined to sum to unity, thus a dominant line from an upper level has small branching fraction uncertainty almost by definition. Branching fractions for weaker lines near the dominant line(s) tend to have uncertainties limited by their signal-to-noise ratios. Systematic uncertainties in the radiometric calibration are typically the most serious source of uncertainty for widely separated lines from a common upper level. We used a formula for estimating this systematic uncertainty that was presented and tested extensively by Wickliffe et al. (2000).

The problem of “residual” branches to currently unknown lower levels deserves some discussion because of the complexity of Sm II. All of the upper levels in this study have strong branches in the blue and/or near UV to the $4f^6(7F)6s$ sub-configuration. Observed weaker transitions in the yellow and/or red region to the $4f^6(7F)5d$ sub-configuration, some of which are listed in Table 2, account for 0% to 44% of the total decay. Typically, 15% to 25% of the total decay goes to the $4f^6(7F)5d$ sub-configuration. We know that the unknown even-parity levels start about 15470 cm^{-1} . The lack of assignment for the odd-parity levels makes it difficult to estimate the strength of branches to the unknown levels. Two transition probabilities with similar dipole matrix elements scale in proportion to their frequencies cubed. This frequency scaling suppresses lower frequency transitions to the unknown even-parity levels. We estimate that branches to unknown lower levels from upper levels below $25,000\text{ cm}^{-1}$ are negligible. A search of the near IR study of Sm II by Blaise et al. (1969) supports this assessment. We measured in our study most of the strong near IR lines listed by Blaise et al. (1969). There is increasing risk of missing branches to unknown even-parity levels for higher odd-parity upper levels. Errors from missing branches are likely still covered by our total uncertainties for odd-parity upper levels in the $25,000\text{ cm}^{-1}$ to $30,000\text{ cm}^{-1}$ range. The situation for odd-parity upper levels in the $30,000\text{ cm}^{-1}$ to $35,000\text{ cm}^{-1}$ range is less certain. Our transition probabilities from these upper levels could be too high by 10% or perhaps somewhat more due to missing branches to unknown even-parity lower levels. Only one level above $35,000\text{ cm}^{-1}$ was included in our branching fraction study. The decay of this level at $38,505.66\text{ cm}^{-1}$ is dominated by the near UV branch to the even-parity $J=8.5$ level at $12,045.10\text{ cm}^{-1}$.

The difficulty in assigning the odd-parity levels is apparent in comments by Xu et al. (2003b). They report, “...according to our HFR calculations, the average purity, in *LS* coupling, of odd-parity levels below $23,000\text{ cm}^{-1}$ is found to be equal to 77%, this value decreasing to 54% for the levels situated between $23,000\text{ cm}^{-1}$ and $25,000\text{ cm}^{-1}$ and to 32% for those located between $25,000\text{ cm}^{-1}$ and $35,000\text{ cm}^{-1}$ ”. Our experimental results on the lifetimes and branching fractions from the odd-parity levels up to $35,000\text{ cm}^{-1}$ should help in a more complete analysis and the eventual assignment of these levels. Cowan (1981) gave a lucid discussion of the difficulties in analysis and interpretation

of RE spectra. He concludes that one should use a battery of experimental and theoretical aids.

Branching fractions from the FTS spectra were combined with the radiative lifetime measurements described in §3 to determine absolute transition probabilities for 958 lines of Sm II in Table 2. Transition probabilities for the weakest lines which were observed with poor signal-to-noise ratios are not included in Table 2, however these lines are included in the branching fraction normalization. Weaker lines are also more susceptible to blending problems. The effect of weaker lines becomes apparent if one sums all transition probabilities in Table 2 from a chosen upper level, and compares the sum to the inverse of the upper level lifetime from Table 1. Typically the sum of the Table 2 transition probabilities is 75% to 95% of the inverse lifetime. Although there is significant fractional uncertainty in the branching fractions for these weaker lines, this does not have much effect on the uncertainty of the stronger lines which were kept in Table 2. Branching fraction uncertainties are combined in quadrature with lifetime uncertainties to determine the transition probability uncertainties in Table 2. This possible systematic error from missing branches to unknown even-parity lower levels is not included in the transition probability uncertainties listed in Table 2. Our estimates of such errors are very “rough” because of the lack of assignment of the odd-parity upper levels. We remind readers that any correction of errors from missing branches to unknown lower levels will always decrease tabulated transition probabilities. Such errors are: (1) thought to be negligible for upper levels below $25,000 \text{ cm}^{-1}$, (2) probably covered by our uncertainties for upper levels in the $25,000 \text{ cm}^{-1}$ to $30,000 \text{ cm}^{-1}$ range, and (3) may be 10% or perhaps somewhat more for upper levels above $30,000 \text{ cm}^{-1}$. Unknown branches do not affect the accuracy of the radiative lifetime measurements.

Although there have been a significant number of publications on Sm II radiative lifetime measurements, we found only two which report original laboratory intensity measurements and either branching fractions or absolute transition probabilities. Relative intensity measurements by Meggers et al. (1961) were converted to absolute transition probabilities by Corliss & Bozman (1962). Ward (1985) reported a formula for re-normalizing the Corliss & Bozman (1962) transition probabilities. Cowley & Corliss (1983) developed a formula for determining transition probabilities from line intensities published by Meggers et al. (1975) which are an updated version of the original Meggers et al. (1961) line intensities used by Corliss & Bozman (1962). Saffman & Whaling (1979) published a smaller, but high quality set of Sm II branching fraction measurements made with a grating spectrometer and a photoelectric detection system. Most of the authors who report radiative lifetime measurements have generated transition probabilities by combining their lifetimes with branching fractions deduced from the Corliss & Bozman (1962) transition probabilities or from measurements by Saffman & Whaling (1979). The recent work by Xu et al. (2003b) is an important exception. They made a serious attempt to determine branching fractions from a relativistic Hartree Fock calculation. It is clear that a large scale effort to measure Sm II branching fractions with an FTS is timely.

Our first comparison is to the recent theoretical work by Xu et al. (2003b).

Indeed, if the relativistic Hartree Fock method can be used with reliability to determine branching fractions in a spectrum as complex as Sm II, then the need for further work using a FTS is much reduced. The next comparison is to branching ratios measured by Saffman and Whaling (1979). We omit a comparison to the oldest measurements by Meggers et al. (1961). There are already numerous published discussions of the problems in the Corliss & Bozman (1962) transition probabilities (e.g. Obbarius & Kock 1983).

Figures 2, 3, and 4 show differences of $\log(gf)$ values from Xu et al. (2003b) and $\log(gf)$ values from our work, as functions of wavelength, transition probability, and upper transition energy, respectively. Xu et al. reported two sets of $\log(gf)$ values. One set is based entirely on relativistic Hartree Fock calculations and the second set is normalized using experimental radiative lifetimes. The branching fractions of the second set are from the relativistic Hartree Fock calculations. Our comparison uses the second set because it is thought to be more accurate. The level of agreement in Figures 2-4 is not as good as we hoped. The scatter in $\log(gf)$ differences for the blue and near UV transitions is larger than the scatter for the yellow and red transitions (Figure 2). Difficulties in establishing an unambiguous correspondence between energy levels from the relativistic Hartree Fock calculations and experimental energy levels may be responsible for some of the scatter in the blue and near UV region. Only the $\log(gf)$ differences plotted as a function of transition probability shown in Figure 3 shows a clear systematic trend. Our $\log(gf)$ values for weaker lines tend to be smaller than the $\log(gf)$ values from Xu et al. (2003b). The agreement “on average” in Figures 2 and 4 is from the use of experimental lifetimes to normalize both sets of transition probabilities. The use of slightly different radiative lifetimes from independent LIF measurements does not contribute much to the scatter as is shown below. The high density of odd-parity levels, the substantial breakdown of Russell-Saunders or *LS* coupling, and significant configuration mixing makes ab-initio calculations of Sm II transition probabilities a formidable task.

Figures 5, 6, and 7 show similar comparisons of $\log(gf)$ values from Saffman & Whaling (1979) to $\log(gf)$ values from our work. In order to make this a fair comparison we have normalized Saffman and Whaling’s branching fractions using our experimental lifetimes. Saffman and Whaling did not have access to the large sets of radiative lifetimes from LIF measurements which are now available. The ordinates of Figures 2 through 7 are identical in order to facilitate comparisons. The experimental branching fractions from Saffman and Whaling are in better agreement with our branching fractions than are branching fractions from the relativistic Hartree Fock calculations. Average and root-mean-squared (rms) values of $\log(gf_{Xu}) - \log(gf_{this_expt})$ for the 84 lines in Figures 2 through 4 are -0.006 and 0.41 respectively. If the comparison is limited to 11 lines listed in Table 3 of Xu et al. (2003) that are common to all three investigations, then the average and rms differences are -0.17 and 0.40 respectively. Similarly, average and root-mean-squared values of $\log(gf_{SW}) - \log(gf_{this_expt})$ for the 48 lines in Figures 5 through 7 are -0.001 and 0.17 respectively. Limiting the “SW” comparison to the 11 lines common to all three investigations yields average and rms differences of 0.005 and 0.21 respectively. In addition to generally bet-

ter agreement, no systematic trends with wavelength, transition probability, or upper transition energy can be discerned in the SW comparison of Figures 5 through 7. Differences between our branching fractions and those from Saffman & Whaling can, in many cases, be traced to line blends which were not resolved with Saffman & Whaling's grating spectrometer. Indeed, the high spectral resolving powers of the Kitt Peak 1.0 m FTS provided part of Prof. Whaling's motivation for pioneering its use in branching fraction measurements (Adams & Whaling 1981).

Figure 8 and 9 are comparisons of various sets of radiative lifetimes from LIF measurements to our measurements. The ordinate in Figure 8 has a similar logarithmic scale as Figures 2-7. Figure 8 clearly demonstrates that the absolute scale established using LIF lifetimes is not contributing much of the $\log(gf)$ scatter. Figure 9, with an expanded ordinate, reinforces our claim of 5% total uncertainty on our lifetime measurements. Most of the points in Figure 9 have ordinate values between -0.02 (-5%) and +0.02 (+5%). We conclude that for complex spectra such as Sm II, branching fraction uncertainties are greater than the lifetime uncertainties except for the dominant branches.

5. SOLAR AND STELLAR SAMARIUM ABUNDANCES

In this section we describe application of the new Sm II transition probability data to the solar spectrum and to the spectra of a few very metal-poor ($[\text{Fe}/\text{H}] < -2$)² stars. As in previous papers of this series, we chose for detailed investigation three metal-poor stars that are enriched in products of rapid n -capture (r -process) nucleosynthesis: HD 115444 ($[\text{Fe}/\text{H}] = -2.9$, $[\text{Eu}/\text{Fe}] = +0.8$, Westin et al. 2000); BD+17°3248 ($[\text{Fe}/\text{H}] = -2.1$, $[\text{Eu}/\text{Fe}] = +0.9$, Cowan et al. 2002), and CS 22892-052 ($[\text{Fe}/\text{H}] = -3.1$, $[\text{Eu}/\text{Fe}] = +1.5$, Sneden et al. 2003). Our Sm II abundance analysis followed the methods used in previous papers of this series, most closely resembling those employed for Nd II by Den Hartog et al. (2003).

5.1 Line Selection

The new laboratory study yielded nearly a thousand potentially useful Sm II lines. Selection of appropriate transitions for abundance analysis in the Sun and stars was the next task. We did not examine each of the Sm II lines of Table 2 in each of the program stars; more efficient means to the same end were adopted. Initial inspection of the solar and stellar spectra revealed that Sm II lines are usually very weak in all of our stars. For example consider 4424.35 Å, one of the strongest ($\chi = 0.48$ eV, $\log(gf) = +0.14$) relatively unblended lines of this species. Its measured equivalent width (EW) is 31 mÅ in CS 22892-052, 25 mÅ in BD+17°3248, 9 mÅ in HD 115444, and <15 mÅ (very contaminated by other absorption features) in the Sun. This implies that the reduced widths

²We adopt standard stellar spectroscopic notations that for elements A and B, $[\text{A}/\text{B}] = \log_{10}(\text{N}_A/\text{N}_B)_{\text{star}} - \log_{10}(\text{N}_A/\text{N}_B)_{\text{sun}}$, for abundances relative to solar ones, and $\log \varepsilon(\text{A}) = \log_{10}(\text{N}_A/\text{N}_H) + 12.0$, for absolute abundances. Overall metallicity is equated to the stellar $[\text{Fe}/\text{H}]$ value.

($RW = EW/\lambda$) for nearly all Sm II lines are small: $\log(RW) < -5.1$, placing these transitions on the linear part of the curve-of-growth. Therefore line saturation did not pose much difficulty in our abundance analysis.

In general, the absorption strengths of weak lines that arise from a single species (e.g., Sm II) vary directly with their transition probabilities modified by their Boltzmann factors. Thus for a given star, relative $\log(RW)$ is proportional to $\log(gf) - \theta\chi$, where χ is in units of eV and inverse temperature $\theta = 5040/T$. Adopting $T_{eff} = 5778$ K for the Sun (e.g. Cox 2000), 4650 K for HD 115444 (Westin et al. 2000), 5200 K for BD+17°3248 (Cowan et al. 2002), and 4800 K for CS 22892-052 (Sneden et al. 2003) yields $\theta_{eff} = 0.87, 1.08, 0.97$, and 1.05, respectively, or $\langle\theta\rangle = 0.99 \approx 1.0$ for our stars. Using this mean inverse temperature value, we computed relative strength factors for all Sm II lines. These are displayed in Figure 10.

For the strong 4424 Å line, $\log(gf) - \theta\chi = +0.14 - 0.48 = -0.34$. We assume that this relative strength corresponds to the largest reduced width of the line in our program stars: $\log(RW) = \log(0.031/4424) = -5.15$ in CS 22892-052. A reasonable lower limit for unambiguous detection of the 4424 Å line in the Sun or stars, given data of high resolution and signal-to-noise, would be ≈ 1.5 mÅ, or $\log(RW) \approx -6.45$. Then assuming that the 4424 Å line is unsaturated in all cases, the reduced width for detection implies a relative strength of $-0.34 + 5.15 - 6.45 = -1.64$, which should represent an approximate strength detection limit for Sm II features. This limit is denoted by a horizontal dashed line in Figure 10.

Of the total list of 958 lines, 410 of them are stronger than the detection limit relative strength value. Concentrating mainly on CS 22892-052 and BD+17°3248, which have larger n -capture elemental abundances than does HD 115444, we made many searches for lines somewhat below the strength detection limit in our spectra, but failed to recover any additional Sm II lines for abundance analyses. Therefore we discarded lines with $\log(gf) - \theta\chi < -1.64$, thus eliminating about 550 weaker transitions from further consideration. We caution the reader that our estimated Sm II line strength detection limit applies only to the present program stars. A more favorable situation can easily be imagined: in the spectra of cool, relatively metal-rich giant stars all Sm II lines will be much stronger, and thus the relative detection limit will be lower.

We examined the remaining 410 strongest lines. All of these transitions lie at wavelengths $\lambda < 5000$ Å, where blending with lines of other atomic and molecular features must be treated with care. Indeed, about 240 of these Sm II lines occur below $\lambda < 4000$ Å, where essentially no unblended line of interest can be detected in the solar spectrum. The majority of the 410 relatively strong lines were thus quickly discarded because they were totally masked or severely compromised by transitions of other species.

To give readers a better understanding of this process of elimination, we discuss here just the four Sm II lines with the largest relative strength factors: 3568.27, 3592.60, 3609.49, and 3634.27 Å, which are specially marked in Figure 10. All of these lines are identified as Sm II in the solar spectral atlas of Moore et al. (1966). The 3568 Å line appears to be relatively clean. Moore et al. list the

following transitions here: 3568.14 Å (Zr II, $\chi = 0.80$ eV: $EW = 6.5$ mÅ), 3568.25 Å (Sm II, 0.48 eV: 28 mÅ), and 3568.31 Å (unidentified: 12 mÅ). However, not only is the EW of the Sm II solar line large, but its measured wavelength is too blue to be attributed solely to the desired Sm II transition. This line is blended in the Sun, and examination of the current version of Kurucz's (1998) atomic and molecular line compendium³ reveals only one plausible contaminant: 3568.24 Å (Fe I, 2.48 eV). Lacking definitive identification, we assumed that Fe I is the correct blending agent, and retained this Sm II feature for abundance analyses. The 3592 Å line is a relatively minor part of a complex blend consisting mainly of 3592.48 Å (Fe I, 2.59 eV: 42 mÅ), 3592.60 Å (Sm II, 0.38 eV: 15 mÅ), 3592.68 Å (Fe I, 3.24 eV: 79 mÅ), and 3592.90 Å (Fe I, 2.20 eV, and Y I, 0.00 eV: 48 mÅ). The contaminants are too large in solar/stellar spectra to use this line. The 3609 Å transition lies in the wing of an extremely strong Fe I line (1.01 eV: 1046 mÅ), and is buried in a local complex blend: 3609.33 Å (Ni I, 0.11 eV: 69 mÅ), 3609.47 Å (Fe I, 2.86 eV, Cr I, 2.54 eV, Sm II, 0.28 eV: 42 mÅ), and 3609.56 Å (Pd I, 0.96 eV: 13 mÅ). It also had to be discarded. Finally, the 3634.27 Å (0.18 eV: 7.5 mÅ) line is sandwiched between 3634.20 Å (unidentified: 58 mÅ) and 3634.33 Å (Fe I, 2.94 eV: 136 mÅ), rendering it unusable. Therefore of the four strongest Sm II lines, only 3568 Å survived preliminary inspection to be employed in our abundance analyses. These line blending considerations eliminated all but ~ 100 Sm II lines. The remaining transitions were subjected to a more complete analysis.

5.2 The Solar Photospheric Samarium Abundances

The vast majority of Sm II transitions surviving the line selection process had residual blending and/or continuum placement concerns in the solar spectrum. Therefore we chose not to use equivalent width analyses for any lines. Instead we determined samarium abundances entirely from synthetic spectrum computations, in the same manner described in previous papers of this series.

Briefly, we assembled lists of atomic and molecular (CH and CN) lines in 4-6 Å surrounding each Sm II transition, using the Kurucz (1998) line database, and supplementing with some identifications in the Moore et al. (1966) solar atlas. We then used the current version of the LTE line analysis code MOOG (Sneden 1973) to generate synthetic spectra, adopting the Holweger & Müller (1974) empirical solar model atmosphere for these computations. Standard solar abundances (Grevesse & Sauval 1998, 2002; Lodders 2003) were assumed for most elements. Solar abundances of elements newly determined in this series (La, Nd, Eu, Tb, Ho, Pt) were taken from those papers listed in § 1. Transition probabilities of these elements were adopted without change from the respective laboratory analyses, as were those of Ce II (Palmeri et al. 2000) and of course Sm II (this study).

We took the observed solar photospheric spectra from the center-of-disk intensity spectral atlas of Delbouille et al. (1973)⁴. Iterative comparisons of syn-

³Available at <http://kurucz.harvard.edu/>

⁴Available at <http://mesola.obspm.fr/solar.spect.php>

thetic and observed center-of disk solar spectra yielded adjustments to the transition probabilities of contaminating spectral features. Molecular line strengths were altered as a group by varying abundances of the molecular constituent atoms. For absorptions present in the observed solar spectrum that have no plausible atomic or molecular identifications, we arbitrarily assumed that they were Fe I lines with excitation potentials $\chi = 3.5$ eV and transition probabilities arbitrarily set to match the observed features. These trial synthetic spectrum computations served also to eliminate ~ 20 more Sm II lines as unsuitable for both solar and stellar abundance computations for one or more of the reasons discussed above.

Final synthetic/observed matches to the approximately 80 potentially useful Sm II transitions yielded solar photospheric abundances for 36 of them. The lines not used in the solar analysis were retained for the stellar analysis described in the next section. The solar abundances for each line are listed in Table 3, and plotted as a function of wavelength in the top panel of Figure 11. From these 36 lines, we derived a mean abundance of $\log \varepsilon(\text{Sm})_{\text{Sun}} = +1.00 \pm 0.01$ ($\sigma = 0.05$). Abundance uncertainties for the solar Sm II lines are comprised of the effects of (internal) line profile fitting issues and (external) scale factors. Repeated matches of observed to synthetic spectra suggested that abundances for each could be estimated on average to ± 0.02 dex. For many photospheric Sm II lines, contamination by other features adds to this line profile fitting uncertainty, again estimated on the basis of repeated trial syntheses to be ± 0.02 dex. Adding these probable errors in quadrature to the estimated ± 0.02 dex typical $\log(gf)$ uncertainties for strong lines yields a total internal line-to-line scatter error of $\approx \pm 0.04$ dex, consistent with the observed $\sigma = 0.05$.

Overall scale errors can arise from other atomic data uncertainties and model atmosphere choices. Samarium, like all other rare earth elements, has a relatively small first ionization potential, 5.644 eV (e.g., Grigoriev & Melikhov 1997). Therefore it exists almost entirely as Sm II in the solar photosphere (and in the line-forming atmospheric layers of our metal-poor program giants), so that Saha-fraction corrections are negligible. Thus the derived Sm abundance varies almost linearly with the Sm II partition function (which enters through the Boltzmann equation). We employed the most recent atomic energy level data (Martin et al. 1978, Martin et al. 2000) to computed partition functions for Sm II, finding no change > 0.01 dex from the temperature-dependent polynomial representations of Irwin (1981). There are, however, many experimentally unknown levels of both parities above $20,000 \text{ cm}^{-1}$ as discussed in § 2. The existence of these levels is certain from counting angular momentum projections. The best approach to correcting a partition function for unknown levels is to perform a Cowan Code (Cowan 1981) calculation and to merge (eliminating duplicates) the resulting theoretical energy level list with the experimental list (eg. Bord & Cowley 2002). Prof. Don Bord (private communication 2005) has done such a calculation for Sm II and shared selected results with us. The Cowan code approach yields a partition function 2.2% (5.6%) larger than that from the Martin et al. energy levels at 5000K (6000K). Although we have not included this “unknown level” correction to the partition function in our abundance studies,

its effect is to increase Sm abundance for the Sun by 0.01 dex. The correction is similar for the warmest of the r-process rich stars, BD+17°3248, discussed in § 5.3.

To assess the influence of solar model atmosphere choice, we repeated the abundance computation for the 4424 Å line with Kurucz (1998) and Grevesse & Sauval (1999) models, finding abundance differences of -0.02 and -0.03 dex with respect to those derived with the Holweger & Müller (1974) model. These differences are nearly identical to those determined for other rare earth ions in the previous papers of this series. Therefore abundance scale errors appear to be very small, of order 0.03 dex. Considering internal line-to-line scatter uncertainties (negligible in the mean value, given the large number of lines used) and external scale uncertainties, we suggest that $\log \varepsilon(\text{Sm})_{\text{Sun}} = +1.00 \pm 0.03$ be adopted as the solar photospheric samarium abundance.

In recent compilations of solar-system data, Grevesse & Sauval (1998) have recommended a meteoritic abundance of $\log \varepsilon(\text{Sm})_{\text{Sun}} = +0.98 \pm 0.02$, while Lodders (2003) has recommended $+0.95 \pm 0.04$. Our new photospheric abundance is consistent with these meteoritic values to within the stated uncertainties.

Several previous studies over the last 30 years have discussed the solar photospheric Sm abundance. Line-by-line abundances from these papers are displayed in the lower panel of Figure 11. Most of the previous analyses employed very few Sm II transitions: Andersen et al. (1975), $\log \varepsilon(\text{Sm})_{\text{Sun}} = +0.72$ from one line; Saffman & Whaling (1979), $+0.80 \pm 0.11$ from four lines out of six attempted; Vogel et al. (1988), $+1.02 \pm 0.11$ from one line out of four; and Youssef & Khalil (1989), $+0.99 \pm 0.05$ from two lines out of three. They will not be considered further here. As discussed in previous sections, Biémont et al. (1989) combined their own lifetime measurements with branching fractions taken mainly from Corliss & Bozman (1962) to determine transition probabilities for nearly 40 Sm II lines, and derived a photospheric abundance of

$\log \varepsilon(\text{Sm})_{\text{Sun}} = +1.00 \pm 0.03$ ($\sigma = 0.14$) from an *EW* analysis of 26 of these lines. Our analysis is clearly in excellent agreement with the Biémont et al. study. The factor of three decrease between the line-to-line scatter of their study and the present one appears to arise from use of improved *gf* values and adoption of a synthetic-spectrum approach in the solar Sm analysis .

5.3 Samarium Abundances in *r*-Process-Rich Stars

We next analyzed Sm II lines in HD 115444, BD+17°3248, and CS 22892-052. We computed Sm abundances via synthetic spectrum computations with the line lists developed for the solar analysis. The combination of overall metal deficiency and relative *n*-capture-element enhancement in these stars produces many relatively unblended Sm II lines, allowing reliable abundances to be determined for many transitions that are hopelessly masked in the solar spectrum. In Table 3 we list the abundances from individual lines in the three stars, and in Table 4 we summarize previously-published and new mean Sm abundances. The line-to-line scatters are all small: $\sigma = 0.05 - 0.07$, decreased from the typical 0.15 values of the original studies. In Figure 12 we demonstrate this result

for BD+17°3248, as was done for Nd II lines in Figure 1 of Den Hartog et al. (2003). Repeating also the numerical experiments of that paper, we have computed line-by-line Sm abundance differences between the metal-poor giants and the Sun, between HD 115444 and BD+17°3248, and between CS 22892-052 and BD+17°3248. In all cases we found $\sigma \{ \Delta \log \varepsilon(\text{Sm}) \} \geq 0.07$. That is, no reduction in σ values was achieved by comparing abundances between stars on a line-by-line basis. This indicates that the abundance scatters are dominated by various factors in the stellar analyses; uncertainties in transition probabilities appear to be negligible contributors here.

6. ABUNDANCES OF n -CAPTURE ELEMENTS IN METAL-POOR HALO STARS

One of the main motivations of the new laboratory experiments is to provide increasingly more accurate determinations of the heavy n -capture element abundances in the metal-poor halo stars. Understanding these stellar distributions, and in particular comparing them to the (total and r -process only) solar system abundance distributions, also provides fresh new insights into the astrophysical conditions, the nuclear processes and the stellar sites for heavy element nucleosynthesis. Since the halo stars are so old and were formed so early, such abundance comparisons and analyses may also help to identify the earliest Galactic stellar generations.

In Figure 13 we summarize the n -capture abundances in the atomic number range $56 \leq Z \leq 68$ for the solar system and for the three very metal-poor ($[\text{Fe}/\text{H}] < -2$) halo giant stars CS 22892-052, HD 115444 and BD+17°3248. We have plotted the abundance differences ($\log \text{observed abundance} - \log \text{solar system } r\text{-process only value}$) for each element in each star. For this comparison we have normalized the abundance distributions of all three stars at the r -process element Eu. The solar system elemental r -process abundance distribution was obtained by summing the individual r -process isotopic abundance contributions, based upon the so-called standard model (see Simmerer et al. 2004 and discussion below in §7). Perfect agreement between the stellar and solar r -process values would result in a difference of zero, and thus would fall on the solid horizontal line in the figure. We also compare the abundance differences for Sm and the other n -capture elements in the top panel of the figure with the total Solar System meteoritic abundance values (dotted-line curve) recommended by Lodders (2003). The stellar abundances in this top panel are those of the original papers on these stars by our group (Westin et al. 2000, Cowan et al. 2002; Sneden et al. 2003). A large scatter, reflected in the large error bars, is seen especially for elements Nd, Sm, and Ho in the stellar data.

The bottom panel of Figure 13 reflects the recent efforts to obtain improved laboratory data for various elements of astrophysical interest. In this panel we have added the most recent solar photospheric abundances (black dots) in order to compare them with meteoritic values. The new laboratory transition probabilities for Nd (Den Hartog et al. 2003) and Ho (Lawler et al. 2004) have resulted in excellent agreement seen in this panel for the abundances (with

respect to the solar r -process values) for those elements in CS 22892-052, HD 115444 and BD+17°3248.⁵ For Sm the comparison between the top and bottom panels of Figure 13 indicates graphically the new concordance of the abundance data for this element - with very small uncertainties the differences between the stellar and solar r -values are identical in CS 22892-052, HD 115444 and BD+17°3248. It is clear now that the abundance ratio of Sm/Eu is the same for all three stars (see also Table 4). This strongly indicates that both Sm and Eu were synthesized in the r -process *only*, and with relative solar system values, in nucleosynthesis sites that ejected these elements into the interstellar medium early in the history of the Galaxy and are seen now in all three of these old halo stars. This is in contrast to Sm in solar system material, which has an r -process fraction of 67%. (Eu is always made almost entirely in the r -process.)

The data of Figure 13 demonstrate that the differences in the abundances for the elements below Sm ($Z < 62$) are not consistent with the total (dotted line curve) photospheric solar abundances (Lodders 2003), but instead fall mostly on the horizontal solid line, indicating an r -process only origin. This follows since in solar system material, elements such as Ba and La are predominantly synthesized in the s -process, not the r -process. For elements above Sm ($Z > 62$), the total solar system abundances are overwhelmingly from r -process nucleosynthesis - Eu, Tb and Ho are 97%, 93%, 94% r -process, respectively (Simmerer et al. 2004) - so not surprisingly the solar and r -process curves are almost coincident. The agreement between the abundance data of the heavier n -capture elements and both of these curves is again an indication of an r -process only synthesis history, and a further indication that the stellar and relative solar system r -process abundances are consistent. Previous abundance determinations of Sm in the three metal-poor halo stars (as shown in the upper panel of Figure 13) had large errors bars and were scattered from the r -process only up to and on the total solar system curve. With the new more accurate atomic physics data the Sm (relative to solar system r -process only) abundances for all three stars now clearly lie below the total solar system abundances and are consistent with the r -process only solar curve.

This agreement between the n -capture element abundances in many metal-poor halo stars and the solar system r -process abundance distribution has been noted for some time (see the reviews of Truran et al. 2002; Sneden & Cowan 2003; Cowan & Thielemann 2004). The s -process nuclei and elements that contribute to solar system matter are produced in low- and intermediate-mass stars that evolve over very long time periods (Busso et al. 1999). Thus, early in the history of the Galaxy, when the most metal-poor halo stars formed, the s -process could not have been responsible for major element formation. Therefore, the predominant early Galactic synthesis must have resulted from the r -process, and presumably from rapidly evolving sites such as core-collapse supernovae (Cowan & Thielemann 2004).

⁵Beyond the RE group, thus not shown in Figure 13, is the very heavy r-process-dominated element Pt, which is accessible to high resolution UV spectroscopy. A new laboratory analysis of Pt (Den Hartog et al. 2005) has resulted in a similar improvement of the abundance of this element in BD+17°3248.

While it has been clear that there is a general consistency between the n -capture elements in the metal-poor halo stars and the relative (or scaled) solar system r -process abundance distribution, this agreement has for some elements, and in some cases, been only approximate with fairly large abundance uncertainties. The new experimental atomic transition data for individual elements - in this case Sm - has now made that agreement much more precise. In fact the scatter has become so low and the agreement has become so good that the abundance data might now possibly be employed to constrain predictions for the solar system abundances. In the particular case of Sm it is seen in Figure 13 that the abundances of all three halo stars lie above the solar system r -process prediction - here the standard model value. This might suggest that the value for the solar system r -process (and likewise the s -process) contribution to Sm should be reassessed.

Finally, we note that there are a few exceptions to the excellent agreement for element-to-element abundances in these stars and with the solar system r -process abundances. Gd for example (in Figure 13) shows considerable abundance scatter suggesting a need for new experimental atomic data for that element. Likewise, there are several other cases where improved atomic laboratory data would make more precise the abundance determinations of certain n -capture elements in the metal-poor halo stars.

7. ISOTOPIC AND HYPERFINE SUBSTRUCTURE CONSIDERATIONS FOR SM II

Samarium has seven abundant naturally occurring isotopes: ^{144}Sm (3.1% of the solar-system elemental abundance), ^{147}Sm (15.0%), ^{148}Sm (11.2%), ^{149}Sm (13.8%), ^{150}Sm (7.4%), ^{152}Sm (26.8%), and ^{154}Sm (22.7%). Isotopes 147 and 149 can have complex hyperfine structures, and transition substructures must exist for all Sm II lines to some degree. However, for lines used in the present abundance analyses, the combined hyperfine and isotopic substructures are reasonably compact. On the FTS laboratory spectra, measured full-width-at-half-maxima of completely unresolved Sm II lines are $\approx 0.06 \text{ cm}^{-1}$, consistent with the 0.053 cm^{-1} spectral resolution limit given in §4. In wavelength units this corresponds to $\Delta\lambda \approx 0.01 \text{ \AA}$ for lines near 4000 \AA . As indicated by the “Comment” column in Table 3, most transitions used in our abundance analyses show no intrinsic broadening in excess of this value in our lab spectra. The Doppler smearing of lines in the stellar atmospheres of this study is $\sqrt{(2k_B T/M + v_t^2)} \geq 2 \text{ km s}^{-1}$ or $\Delta\lambda \geq 0.03 \text{ \AA}$, much larger than the intrinsic line broadening. Therefore for present purposes most Sm II lines can be treated as single transitions. Those lines with detectable intrinsic broadening in excess of 0.01 \AA are noted with “hfs” in the “Comment” column.

The relatively strong 4424 \AA line discussed earlier is one of the Sm II transitions that exhibits significant hyperfine/isotopic splitting on our lab spectra. Three obvious components of this line are blended together, with a total wavelength spread of $\approx 0.04 \text{ \AA}$. Comprising this blend are 21 components each of isotopes 147 and 149, and single components of the remaining five isotopes.

Using the isotopic and hyperfine structure data of Masterman et al. (2003) we synthesized the 4424 Å line in all four stellar spectra. As expected given the previous discussion about the intrinsic weakness of Sm II lines in our stars, we found little change to abundances determined with the single-line approximation to this feature. Since the 4424 Å line is one of the strongest of all Sm II transitions, further consideration of hyperfine/isotopic substructure seemed unwarranted here. More careful treatment would be required for accurate elemental abundance determinations in stars with deeper, more saturated Sm II lines.

Although these tests with the 4424 Å line indicate that it will be quite difficult to determine Sm isotopic abundances, the possibility still merits some discussion. Many 5d – 6p yellow-red lines of Sm II have appreciably wider structure than the 6s – 6p blue-UV lines. Continued improvements in telescopes and spectrometers or the discovery of a more favorable star might make it possible to determine a Sm isotopic abundance, and so we include here a summary of the *s*– and *r*–process contributions to Sm and some predictions of possibly observable effects.

We neglect the small (3% of the solar system) contribution to Sm from the *p*–process isotope ^{144}Sm in the following discussion. We show in Table 5 the individual breakdown of the contribution by process. The *s*–process additions to the solar system abundances were first determined based upon one of several approaches. The so-called standard or “classical” (empirical) model assumes a smooth fit (smooth behavior) of the “ $\sigma_n N_s$ ” curve (*i.e.* the product of the *n*–capture cross-section σ_n and *s*–process abundances N_s) to the solar system *s*–process abundances. Determinations of the neutron-capture cross sections (see e.g. Käppeler et al. 1989) then allows the direct determination of the N_s contributions to each isotope (see Burris et al. 2000; Simmerer et al. 2004). An alternative approach employs more detailed (low-mass AGB) stellar model and nucleosynthesis calculations to obtain the isotopic *s*–process solar system abundances (see Arlandini et al. 1999). Subtracting these *s*–process isotopic abundances from the total solar abundances determines the individual *r*–process contributions, or residuals. We note that experimental determinations of individual *r*–process abundance contributions are, in general, not possible at this time.

We have listed the values from both the standard and stellar models in Table 5. The abundances for the *s*– and *r*–process contributions are based upon the Si = 10^6 scale. We have also listed the percentage contribution by individual isotope to the total elemental *s*– and *r*–process abundances (*i.e.*, the vertical columns add up to 100% in those particular columns). It is clear from the table that both the standard and stellar models give very similar isotopic abundance predictions for the *s*- and *r*-process mixtures for Sm.

It may be possible to observe the isotopic mixture of Sm in a metal-poor halo star. Lambert & Allende Prieto (2002) observed the isotopic mixture for the element Ba in the halo star HD 140283. They found, specifically, that the fractional abundance of the odd isotopes

$$f_{odd} = [N(^{135}\text{Ba}) + N(^{137}\text{Ba})]/N(\text{Ba})$$

in this star was consistent with the solar system *r*-process isotopic ratio. Sm, like Ba, is an even-Z nucleus with one *p*-process isotope and six other stable (*s*- and *r*-process admixed) isotopes. Thus (similarly to Ba), we can define for Sm

$$f_{odd} = [N(^{147}\text{Sm}) + N(^{149}\text{Sm})]/N(\text{Sm})$$

For the pure *r*-process components of solar system isotopic abundances, we find that $f_{odd}^r = 0.36$ for both the standard model (Burris et al. 2000; Simmerer et al. 2004) and for the stellar model calculations given by Arlandini et al. (1999). For comparison, the Sm solar *s*-process values are $f_{odd}^s = 0.09$ and $f_{odd}^{s+} = 0.17$ for the standard and stellar models, respectively. It might be possible to observe this f_{odd}^r isotopic mixture for Sm in a halo star, similarly to what Lambert & Allende-Prieto did for Ba in HD 140283. Such an observation would provide a direct measure of the *r*-process isotopic contribution to the elemental Sm production in nucleosynthetic (e.g., supernovae) sites that were operating in the early Galaxy. Except for the one measurement of Ba and several Eu observations (Sneden et al. 2002, Aoki et al. 2003), there have been very few stellar isotopic abundance determinations. Sm (as noted above) has more of an *s*-process fraction than Eu, but less than Ba, in solar system material. Thus, any isotopic abundance observations of Sm would provide additional information about the early synthesis, and possible confirmation of the *r*-process only origin, for this element in halo stars.

8. SUMMARY

We report here the largest-scale laboratory study to date of Sm II transition probabilities using modern methods. Specifically we have measured radiative lifetimes, accurate to $\pm 5\%$, for 212 odd-parity levels of Sm II using laser-induced fluorescence. The lifetimes are combined with branching fractions measured using Fourier-transform spectrometry to determine transition probabilities for 958 lines of Sm II. This improved data set has been used to determine a new solar photospheric Sm abundance, $\log \varepsilon = 1.00 \pm 0.03$, from 26 lines. The spectra of three very metal-poor, neutron-capture-rich stars (CS 22892-052, HD 115444 and BD+17°3248) also have been reanalyzed, employing between 55 and 72 Sm II lines per star. We have compared the differences between the Sm abundances and the predicted solar system *r*-process only values in all three stars. We find with very small uncertainties that these ratios are the same. Utilizing additional recent experimental atomic data it was found that the abundance ratios of Sm relative to other rare earth elements in these stars are in agreement, and are consistent with ratios expected from rapid neutron-capture nucleosynthesis (the *r*-process). The newly determined abundance values for Sm, based upon the much more precise atomic data, might possibly be employed to constrain predictions for the solar system abundances. Thus, the slight disagreement between the stellar Sm values and the predicted *r*-process only value might suggest a minor reassessment of the solar system *r*- (and *s*-) process contributions to Sm synthesis. We finally note the possibility of observing the isotopic mixture of Sm, similarly to what has been accomplished for Ba, in a metal-poor halo star.

Such an observation would provide important additional information about the nature of nucleosynthesis early in the history of the Galaxy.

ACKNOWLEDGMENTS

This work is supported by the National Science Foundation under grants AST-0205124 and 0506324 (JEL and EADH), AST0307495 (CS), and AST-0307279 (JJC). J. E. Lawler is a guest observer at the National Solar Observatory and he is indebted to Mike Dulick and Detrick Branstrom for help with the 1 m Fourier transform spectrometer. Much of the solar/stellar abundance analysis was accomplished while CS was an Erskine Fellow at the University of Canterbury, Christchurch, New Zealand. Their Department of Physics and Astronomy is thanked for financial support and encouragement of this work. We are very grateful to Don Bord and J.-F. Wyart for sharing unpublished Cowan Code calculations with us.

REFERENCES

- Adams, D. L., & Whaling, W. 1981, J. Opt. Soc. Am., 71, 1036
- Anderson, H. M., Den Hartog, E. A., & Lawler, J. E. 1996, J. Opt. Soc. Am. B, 13, 2382
- Andersen, T., Poulsen, O., Ramanujam, P. S., & Petkov, A. P. 1975, Solar Physics 44, 257
- Aoki, W., Ryan, S. G., Iwamoto, N., Beers, T. C., Norris, J. E., Ando, H., Kajino, T., Mathews, G. J., Fujimoto, M. Y. 2003, ApJ, 582, L67
- Arlandini, C., Käppeler, F., Wissak, K., Gallino, R., Lugardo, M., Busso, M., & Straniero, O. 1999, ApJ, 525, 886
- Biémont, E., Grevesse, N., Hannaford, P., & Lowe, R. M. 1989, A&Ap, 222, 307
- Biémont, E., Baudoux, M., Kurucz, R. L., Ansbacher, W., & Pinnington, E. H. 1991, A&Ap, 249, 539
- Biémont, E., Dutrieux, J.-F., Martin, I., Quinet, P. 1998, J. Phys. B: At. Molec. Opt. Phys., 31, 3321
- Biémont, E., & Quinet P. 2003, Physica Scripta, T105, 38
- Blaise, J., Morillon, C., Schweighofer, M. G., & Verges, J. 1969, Spectrochim. Acta B, 24, 405
- Bord, D. J., Cowley, C. R., & Mirjianian, D. 1998, Solar Physics, 178, 221
- Bord, D. J., & Cowley, C. R. 2002, Solar Physics, 211, 3
- Brault, J. W. 1976, J. Opt. Soc. Am., 66, 1081
- Burris, D. L., Pilachowski, C. A., Armandroff, T. E., Sneden, C., Cowan, J. J., & Roe, H. 2000, ApJ, 544, 302
- Busso, M., Gallino, R., & Wasserburg, G.J. 1999, ARA&A, 37, 239
- Cayrel, R., Depagne, E., Spite, M., Hill, V., Spite, F., Francois, P., Plez, B., Beers, T., Primas, F., Andersen, J., Barbuy, B., Bonifacio, P., Molaro, P., & Nordstrom, B. 2004, A&A, 416, 1117
- Corliss, C. H., & Bozman, W. R. 1962, *Experimental Transition Probabilities for Spectral Lines of Seventy Elements*, U. S. Natl. Bur. Standards Monograph 53, (Washington: U. S. Government Printing Office)
- Cowan, J. J., Burris, D. L., Sneden, C., McWilliam, A., & Preston, G. W. 1995, ApJ, 439, L51
- Cowan, J. J., Sneden, C., Burles, S., Ivans, I. I., Beers, T. C., Truran, J. W., Lawler, J. E., Primas, F., Fuller, G. M., Pfeiffer, B., & Kratz, K.-L. 2002, ApJ., 572, 861
- Cowan, J. J., & Thielemann, F.-K. 2004, Phys. Today, 57, 47
- Cowan, R. D. 1981, *The Theory of Atomic Structure and Spectra* (Berkeley, Univ. of California Press)
- Cowley, C. R. & Corliss, C. H. 1983, MNRAS 203, 651
- Cox, A. N. 2000, *Allen's Astrophysical Quantities* (New York: AIP Press)
- Curry, J. J., Den Hartog, E. A., & Lawler, J. E. 1997, J. Opt. Soc. Am. B, 14, 2788
- Danzmann, K., & Kock, M. 1982, J. Opt. Soc. Am., 72, 1556

- Den Hartog, E. A., Curry, J. J., Wickliffe, M. E., & Lawler, J. E. 1998, Sol. Phys. 178, 239
- Den Hartog, E. A., Wiese, L. M. & Lawler, J. E. 1999, J. Opt. Soc. Am. B, 16, 2278
- Den Hartog, E. A., Fedchak, J. A., & Lawler, J. E. 2001, J. Opt. Soc. Am. B 18, 861
- Den Hartog, E. A., Wickliffe, M. E., & Lawler, J. E. 2002, ApJS, 141, 255
- Den Hartog, E. A., Lawler, J. E., Sneden, C., & Cowan, J. J. 2003, ApJS, 148, 543
- Den Hartog, E. A., Herd, M. T., Lawler, J. E., Sneden, C., Cowan, J. J., Beers, T. C. 2005, ApJ, 619, 639
- Delbouille, L, Roland, G., & Neven, L. 1973, *Photometric Atlas of the Solar Spectrum from lambda 3000 to lambda 10000*, (Liège, Inst. d'Ap., Univ. de Liège)
- Derkatch, A., Ilyinsky, L., Mannervik, S., Norlin, L.-O., Rostohar, D., Royen, P., Schef, P., & Biémont, E. 2002, Phys. Rev. A, 65, 062508
- Edlén, B. 1953, J. Opt. Soc. Am., 43, 339
- Edlén, B. 1966, Metrologia, 2, 71
- Fedchak, J. A., Den Hartog, E. A., Lawler, J. E., Palmeri, P., Quinet, P., & Biémont, E. 2000, ApJ, 542, 1109
- Gratton, R. G., & Sneden, C. 1994, A&Ap, 287, 927
- Grevesse, N., & Sauval, A. J. 1998, Space Sci. Rev., 85, 161
- Grevesse, N., & Sauval, A. J. 1999, A&Ap, 347, 348
- Grevesse, N., & Sauval, A. J. 2002, Adv. Space. Res., 30, 3
- Grigoriev, I. S., & Melikhov, E. Z. 1997, *Handbook of Physical Quantities*, (Boca Raton, CRC Press) p. 516
- Guo, B., Ansbacher, W., Pinnington, E. H., Ji, Q., & Berends, R. W. 1992, Phys. Rev. A, 46, 641
- Hashiguchi, S., & Hasikuni, M. 1985, J. Phys. Soc. Japan 54, 1290
- Holweger, H., & Müller, E. A. 1974, Sol. Phys., 39, 19
- Irwin, A. W. 1981, ApJS, 45, 621
- Ivarsson, S., Litzén, U., & Wahlgren, G. M. 2001, Physica Scripta, 64, 455
- Käppeler, F., Beer, H., & Wisshak, K. 1989, Rep. Prog. Phys., 52, 945
- Kono, A., & Hattori, S. 1984, Phys. Rev. A, 29, 2981
- Kurucz, R. L. 1998, in Fundamental Stellar Properties: *The Interaction between Observation and Theory*, IAU Symp. 189, ed T. R. Bedding, A. J. Booth and J. Davis (Dordrecht: Kluwer), p. 217
- Lambert, D.L., & Allende Prieto, C. 2002, MNRAS, 335, 325
- Lawler, J. E., Bonvallet, G., & Sneden, C. 2001a, ApJ, 556, 452
- Lawler, J. E., Wickliffe, M. E., Cowley, C. R., & Sneden, C. 2001b, ApJS, 137, 341
- Lawler, J. E., Wickliffe, M. E., Den Hartog, E. A., & Sneden, C. 2001c, ApJ, 563, 1075
- Lawler, J. E., Sneden, C., & Cowan, J. J. 2004, ApJ, 604, 850
- Li, Z. S., Svanberg, S., Quinet, P., Tordoir, X., & Biémont, E. 1999, J. Phys. B: At. Molec. Opt. Phys., 32, 1731

- Li, Z. S., & Zhankui J. 1999, Physica Scripta, 60, 414
- Lodders, K. 2003, ApJ, 591, 1220
- Martin, W.C., Zalubas, R., & Hagan, L. 1978, *Atomic Energy Levels The Rare Earth Elements*, NSRDSNBS 60 (Washington: U. S. G. P. O.) p. 174
- Martin, W. C., Sugar, J., & Musgrove, A. 2000, NIST Atomic Spectra Database, (<http://physics.nist.gov/cgi-bin/AtData/main.asd>)
- Masterman D., Rosner, S. D., Scholl, T. J., Sharikova, A., & Holt, R. A. 2003, Can J. Phys., 81, 1389
- McWilliam, A., Preston, G. W., Sneden, C., & Searle, L. 1995, ApJ, 109, 2757
- Meggers, W. F., Corliss, C. H., and Scribner, B. F. 1961, *Tables of Spectral Line Intensities*, U. S. Natl. Bur. Standards Monograph 32, (Washington: U.S. G.P.O.)
- Meggers, W. F., Corliss, C. H., and Scribner, B. F. 1975, *Tables of Spectral Line Intensities*, U. S. Natl. Bur. Standards Monograph 145, (Washington: U.S. G. P. O.)
- Moore, C. E., Minnaert, M. G. J., & Houtgast, J. 1966, *The Solar Spectrum 2934 Å to 8770 Å*, NBS Monograph 61 (Washington: U.S. G. P. O.)
- Obbarius H. U., & Kock, M. 1982, J. Phys. B: At. Mol. Opt. Phys., 15, 527
- Palmeri, P., Quinet, P., Wyart, J.-F., & Biémont, E. 2000, Physica Scripta, 61, 323
- Pinnington, E. H., Rieger, G., & Kernahan, J. A. 1997, Phys. Rev. A, 56, 2421
- Quinet, P., Palmeri, P., & Biémont, E. 1999a, J. Quant. Spectrosc. Radiat. Transfer, 62 625
- Quinet, P., Palmeri, P., Biémont, E., McCurdy, M. M., Rieger, G., Pinnington, E. H., Wickliffe, M. E., & Lawler, J. E. 1999b, MNRAS, 307, 934
- Rieger, G., McCurdy, M. M., & Pinnington E. H. 1999, Phys. Rev. A, 60, 4150
- Rostohar, D., Andersson, K., Derkatch, A., Hartman, H., Mannervik, S., Norlin, L.-O., Royen, P., Schmidtt, A., Tordoir, X. 2001, Physica Scripta, 64, 237
- Ryan, S. G., Norris, J. E., and Beers, T. C. 1996, ApJ, 471, 254
- Saffman L., & Whaling W. 1979, J. Quant. Spectrosc. Radiat. Transfer, 21, 93
- Scholl, T. J., Holt, R. A., Masterman, D., Rivest, R. C., Rosner, S. D., & Sharikova, A. 2002, Can. J. Phys., 80, 1621
- Simmerer, J., Sneden, C., Cowan, J. J., Collier, J., Woolf, V. M., & Lawler, J. E. 2004, ApJ, 617, 1091
- Sneden, C. 1973, ApJ, 184, 839
- Sneden, C., McWilliam, A., Preston, G. W., Cowan, J. J., Burris, D. L., and Armosky, B. J. 1996, ApJ, 467, 819
- Sneden, C., Cowan, J. J., Lawler, J. E., Burles, S., Beers, T. C., Fuller, G. M. 2002, 566, L25

- Sneden, C., Cowan, J. J., Lawler, J. E., Ivans, I. I., Burles, S., Beers, T. C., Primas, F., Hill, V., Truran, J. W., Fuller, G. M., Pfeiffer, B., & Kratz, K.-L. 2003, ApJ, 591, 936
 Sneden, C., & Cowan, J. J. 2003, Science, 299, 70
 Taylor, P., Roberts, M., Gateva-Kostova, S. V., Clarke, R. B. M., Barwood, G. P., Rowley, W. R. C., & Gill, P. 1997, Phys. Rev. A, 56, 2699
 Truran, J. W., Cowan, J. J., Pilachowski, C. A., & Sneden, C. 2002, PASP, 114, 1293
 Vogel, O., Edvardsson, B., W  nnstr  m, A., Arneson, A., & Hallin, R. 1988, Physica Scripta, 38, 567
 Volz, U., & Schmoranz, H. 1998, in AIP Conf. Proc. 434, *Atomic and Molecular Data and Their Applications*, ed. P. J. Mohr and W. L. Wiese (Woodbury, NY:AIP), p. 67
 Ward, L. 1985, Mon. Not. R. Astr. Soc. 213, 17
 Weiss, A. W. 1995, Phys. Rev. A, 51, 1067
 Westin, J., Sneden, C., Gustafsson, B., & Cowan, J.J. 2000, ApJ, 530, 783
 Whaling, W., Carle, M. T., & Pitt, M. L. 1993, J. Quant. Spectrosc. Radiat. Transfer 50, 7
 Wickliffe, M. E., & Lawler, J. E. 1997, J. Opt. Soc. Am. B, 14, 737
 Wickliffe, M. E., Lawler, J. E., & Nave, G. 2000, J. Quant. Spectrosc. Radiat. Transfer, 66, 363
 Wyart, J.-F., & Bauche-Arnoult, Cl. 1981, Physica Scripta, 22, 583
 Xu, H. L., Jiang, Z. K., & Svanberg, S. 2003a, J. Phys. B: At. Molec. Opt. Phys., 36, 411
 Xu, H. L., Svanberg, S., Quinet, P., Garnir, H. P., & Bi  mont, E. 2003b, J. Phys. B: At. Molec. Opt. Phys., 36, 4773
 Yan, Z-C, Tambasco, M., & Drake, G. W. F. 1998, Phys. Rev. A, 57, 1652
 Youssef, N. H., & Khalil, N. M. 1989, A&Ap, 215, 165
 Yu, N., & Maleki L. 2000, Phys. Rev. A, 61, 022507
 Zhang, Z. G., Li Z. S., Lundberg, H., Zhang, K. Y., Dai, Z. W., Jiang, Z. K., Svanberg, S. 2000, J. Phys. B: At. Molec. Opt. Phys., 33, 521
 Zhang, Z. G., Persson A., Li, Z. S., Svanberg, S., & Zhankui, J. 2001a, Eur. J. Phys. D, 13, 301
 Zhang, Z. G., Svanberg, S., Jiang, Z. K., Palmeri, P., Quinet, P., & Bi  mont, E. 2001b, Physica Scripta, 63, 122
 Zhao, R. C., Huang, W., Xu, X. Y., Tong, X. M., Qu, Y. Z., Xu, C. B., & Xue, P. 1996, Phys. Rev. A, 53, 3994
 Zhiguo, Z., Zhongshan, L., & Zhankui J. 1999, Eur. Phys. J. D, 7, 499

FIGURE CAPTIONS

Figure 1. Partial Grotrian diagram for singly ionized samarium.

Figure 2. Comparison of the $\log(gf)$ values from Xu et al. (2003b) to $\log(gf)$ values from this paper as a function of wavelength. Solid round symbols are for lines which Xu et al. gave a $\log(gf)$ uncertainty < 0.04 dex, open circle symbols are for lines which Xu et al. gave a $\log(gf)$ uncertainty of < 0.11 dex, and the “x” symbols are used for lines which Xu et al. gave a $\log(gf)$ uncertainty > 0.11 dex.

Figure 3. Comparison of the $\log(gf)$ values from Xu et al. (2003b) to $\log(gf)$ values from this paper as a function of our $\log(gf)$ value. The symbols have the same meaning as in Figure 2.

Figure 4. Comparison of the $\log(gf)$ values from Xu et al. (2003b) to $\log(gf)$ values from this paper as a function of upper level energy E_{upper} . The symbols have the same meaning as in Figure 2.

Figure 5. Comparison of the $\log(gf)$ values from Saffman & Whaling (1979), normalized to our experimental radiative lifetimes, to $\log(gf)$ values from this paper as a function of wavelength.

Figure 6. Comparison of the $\log(gf)$ values from Saffman & Whaling (1979), normalized to our experimental radiative lifetimes, to $\log(gf)$ values from this paper as a function of our $\log(gf)$ value.

Figure 7. Comparison of the $\log(gf)$ values from Saffman & Whaling (1979), normalized to our experimental radiative lifetimes, to $\log(gf)$ values from this paper as a function of upper level energy.

Figure 8. Comparison of radiative lifetimes τ_{other} measured using LIF by: Biémont et al. (1989) solid round symbol, Scholl et al. (2002) open circle symbol, Vogel et al. (1988) “x” symbol, and Xu et al. (2003b) “+” symbol to radiative lifetimes τ_{this_expt} measured in this experiment. The ordinate scale is designed to match the ordinate scale of Figures 2-7.

Figure 9. Same as Figure 8 except with an expanded ordinate.

Figure 10. Relative strength factors, defined as $\log(gf) - \theta\chi$, for Sm II transitions. Reduced widths of weak lines should be proportional to these factors. For these computations, $\theta = 1.0$, the mean of inverse effective temperature of the four program stars. The 4424.35 Å is specially noted in the plot, as it is the strongest yet reasonably unblended Sm II feature in our solar and stellar spectra. The text discusses this line and the four “strongest lines” that are noted in this figure with a large enclosing circle.

Figure 11. Individual Sm II line abundances in the solar photosphere derived in this work (upper panel) and in four previous studies (lower panel). In the upper panel, a dotted horizontal line denotes the mean abundance. In the lower panel, symbols as indicated in the plot denote the results of Andersen et al. (1975: And75 in the plot legend), Saffman & Whaling (1979: Saf79), Vogel et al. (1988: Vog88), Youssef & Khalil (1989: You89), and Biémont et al. (1989: Bie89).

Figure 12. Abundances of Sm in the very metal-poor, n -capture-rich giant star BD+17°3248. The upper panel contains our published results (Cowan et

al. 2002), and the lower panel shows the data of this paper.

Figure 13. The neutron-capture elemental abundance pattern in the Galactic halo stars CS 22892-052, HD 115444, and BD+17°3248 compared with the (scaled) Solar System *r*-process abundances (solid line) and the total Solar System meteoritic abundances recommended by Lodders (2003; dashed line). The abundances of all of the stars have been compared by normalizing the abundance distributions at the *r*-process element Eu. In the top panel, stellar abundances are those reported in the original papers on these stars (HD 115444, Westin et al. 2000; BD+17°3248, Cowan et al. 2002; CS 22892-052, Sneden et al. 2003). In the bottom panel the comparisons are repeated for these stars, but substituting in the abundances of Nd, Ho, and Sm derived in the most recent papers of this series (see text). Also shown are solar photospheric abundances, with values of La, Nd, Sm, Eu, Tb, and Ho taken from this series, otherwise from Lodders (2003).

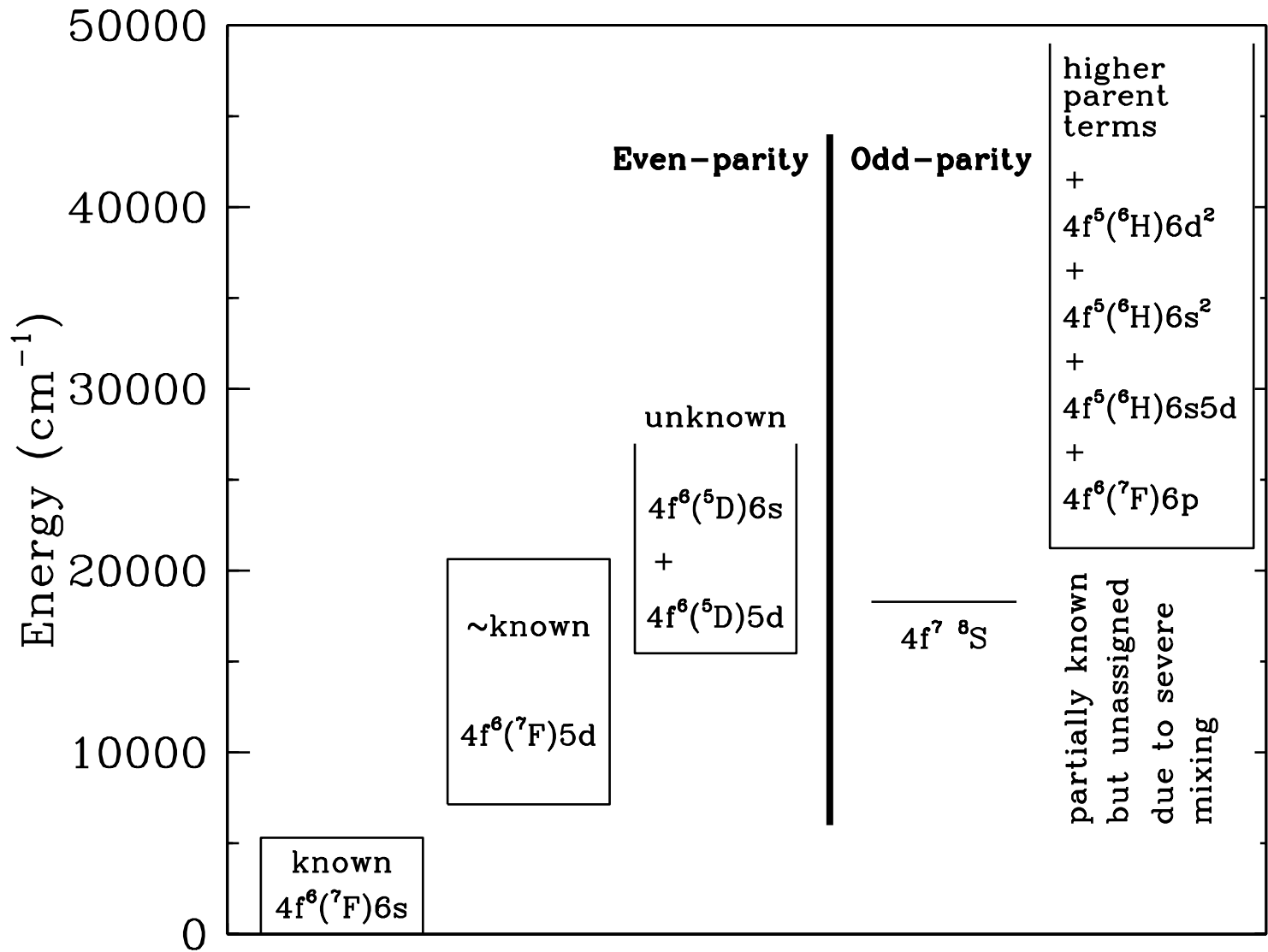


Table 1. Radiative lifetimes of Sm II from LIF measurements.

Level (cm ⁻¹)	J	Laser Wavelength (Å)	Lifetime (ns)		
			This Experiment	Other Experiment	References
21250.75	0.5	4704.40, 4777.84	28.0	28 ± 1	b
21507.87	1.5	4648.16, 4719.84	92.0	10.9 ± 0.5	b
21655.42	0.5	4616.49, 4687.19	49.4	51.9 ± 0.5	c
21702.33	1.5	4606.51, 4676.90	39.3	39 ± 2	b
				40.2 ± 0.2	c
				41 ± 3	d
21904.12	1.5	4564.07, 4745.68	67.7	70.8 ± 0.6	c
				65 ± 6	d
22039.98	2.5	4604.17, 4715.27	181		

-2

Table 1—Continued

Level (cm ⁻¹)	J	Laser Wavelength (Å)	Lifetime (ns)		
			This Experiment	Other Experiment	References
22248.32	2.5	4669.39, 4815.80	32.9	176 ± 2	c
22429.49	2.5	4630.20, 4774.14	78.4	33 ± 1	b
22788.68	3.5	4554.44, 4693.63	195	33.80 ± 0.09	c
22875.41	3.5	4536.51, 4674.59	39.1	79.4 ± 0.9	c
23177.49	1.5	4374.98, 4615.68	47.3	72 ± 7	d
				189 ± 2	c
				39.9 ± 0.1	c
				40 ± 3	d
				48.0 ± 0.4	c

|
c
|

Table 1—Continued

Level (cm ⁻¹)	J	Laser Wavelength (Å)	Lifetime (ns)		
			This Experiment	Other Experiment	References
23260.95	3.5	4458.51, 4591.81	53.4	48 ± 3	d
23352.41	0.5	4281.01, 4578.70	63.2	54 ± 2	b
23646.90	4.5	4511.83, 4669.64	42.0	53.8 ± 0.6	c
23659.99	0.5	4284.51, 4515.10	31.8	63.8 ± 0.3	c
23752.70	4.5	4646.68, 4829.56	155	42 ± 2	b
23842.20	2.5	4345.85, 4577.69	32.8	42.5 ± 0.1	c
				31.8 ± 0.5	c
				148 ± 1	c

Table 1—Continued

Level (cm ⁻¹)	J	Laser Wavelength (Å)	Lifetime (ns)		
			This Experiment	Other Experiment	References
23962.25	1.5	4229.71, 4323.29	22.3	34 ± 2	b
				33.6 ± 0.3	c
				35 ± 2	d
24013.56	1.5	4163.14, 4542.05	68.5	22.54 ± 0.06	c
				24.7 ± 1.5	d
24194.38	2.5	4280.32, 4505.04	169	69.1 ± 0.2	c
				162.8 ± 0.7	c
24221.81	0.5	4183.77, 4403.37	15.3	16.7 ± 0.9	b
				15.5 ± 0.2	c
24257.37	4.5	4390.86, 4540.18	45.5		

Table 1—Continued

Level (cm ⁻¹)	J	Laser Wavelength (Å)	Lifetime (ns)		
			This Experiment	Other Experiment	References
24429.52	1.5	4092.25, 4237.66	25.1	46.6 ± 0.3 47 ± 3	c d
24582.59	2.5	4210.34, 4329.02	19.1	24.7 ± 0.1 27.5 ± 1.5	c d
24588.00	5.5	4473.01, 4642.23	40.4	20.2 ± 1.0 19.6 ± 0.3	b c
24685.53	1.5	4049.81, 4104.12	53.6	41.5 ± 3 40.7 ± 0.5 42 ± 3	b c d
				55.1 ± 0.9	c

Table 1—Continued

Level (cm ⁻¹)	J	Laser Wavelength (Å)	Lifetime (ns)		
			This Experiment	Other Experiment	References
24689.84	3.5	4309.01, 4452.72	20.2	21.5 ± 1.0	b
24816.28	5.5	4427.79, 4593.53	116	20.5 ± 0.3	c
24848.47	2.5	4076.85, 4163.71	115	111 ± 1	c
24919.90	0.5	4011.72, 4272.01	196	112 ± 1	c
24928.80	2.5	4063.54, 4149.83	24.8	189 ± 2	c
25055.54	1.5	4042.71, 4469.65	34.3	24.7 ± 1.0	b
25055.54	1.5	4042.71, 4469.65	34.3	25.4 ± 0.9	c
25055.54	1.5	4042.71, 4469.65	34.3	34.9 ± 0.5	c

Table 1—Continued

Level (cm ⁻¹)	J	Laser Wavelength (Å)	Lifetime (ns)		
			This Experiment	Other Experiment	References
25175.32	2.5	4023.22, 4107.79	81.2	77 ± 5	b
				81 ± 3	c
25178.45	1.5	3970.53, 4107.27	23.1	23.5 ± 0.2	c
				25 ± 2	d
25304.09	3.5	4334.14, 4420.52	22.0	23.4 ± 1.0	b
				22.2 ± 0.6	c
25361.45	1.5	3941.88, 3993.31	16.6	17.3 ± 0.9	b
				16.8 ± 0.2	c
				16.6 ± 0.2	e
25385.36	5.5	4318.93, 4655.11	41.1		

|
 ∞
|

Table 1—Continued

Level (cm ⁻¹)	J	Laser Wavelength (Å)	Lifetime (ns)		
			This Experiment	Other Experiment	References
25546.03	2.5	4046.16	163	38.7 ± 2.0	b
25552.80	1.5	4045.05, 4245.17	80.4	42.2 ± 0.2	c
25565.97	3.5	4042.90, 4152.20	29.1	43 ± 3	d
25597.70	4.5	4434.32, 4523.91	14.0	42.0 ± 1.0	e
25664.97	6.5	4421.13, 4595.28	43.4	79 ± 1	c
				31.1 ± 0.5	c
				31 ± 2	d
				14.8 ± 0.6	b
				14.2 ± 0.1	c

Table 1—Continued

Level (cm ⁻¹)	J	Laser Wavelength (Å)	Lifetime (ns)		
			This Experiment	Other Experiment	References
25790.15	3.5	4113.90, 4244.70	56.9	42 ± 3	b
				44.4 ± 0.2	c
25939.87	6.5	4368.02, 4537.94	60.6	54 ± 3	b
				57.3 ± 0.3	c
25980.32	2.5	3896.97, 3976.27	19.0	28.4 ± 1.0	b
				62.4 ± 0.3	c
26046.35	4.5	4347.80, 4433.89	20.6	20.0 ± 1.5	b
				19.9 ± 0.4	c
				20.0 ± 1.0	d
				21.8 ± 1.0	b

| 10 |

Table 1—Continued

Level (cm ⁻¹)	J	Laser Wavelength (Å)	Lifetime (ns)		
			This Experiment	Other Experiment	References
26086.63	3.5	3959.52, 4191.93	68.9	20.9 ± 0.8	c
26159.60	3.5	3948.11, 4259.39	94.6	70 ± 2	c
26190.92	2.5	3943.24, 4047.15	38.6	93 ± 4	c
26214.05	2.5	4129.22, 4249.54	64.8	39.3 ± 0.3	c
26253.55	0.5	3855.90, 4041.67	12.7	66 ± 1	c
26357.90	2.5	3840.45, 3917.43	31.3	12.6 ± 0.3	c
				32.2 ± 0.3	c
				33 ± 2	d

| 11 |

Table 1—Continued

Level (cm ⁻¹)	J	Laser Wavelength (Å)	Lifetime (ns)		
			This Experiment	Other Experiment	References
26413.29	5.5	4442.47, 4538.56	247		
26442.18	0.5	3780.76, 3828.05	25.2		
26484.66	1.5	3774.70, 4083.58	55.8		
				54 ± 3	d
26505.53	5.5	4262.67, 4424.34	12.6		
				14.0 ± 0.7	b
				12.7 ± 0.3	c
				12.7 ± 0.2	e
26540.12	6.5	4256.39, 4417.57	33.3		
				33 ± 2	b
				34.0 ± 0.4	c
				34.4 ± 0.7	e
26565.61	4.5	3986.68, 4109.39	65.4		
				65.6 ± 0.4	c

Table 1—Continued

Level (cm ⁻¹)	J	Laser Wavelength (Å)	Lifetime (ns)		
			This Experiment	Other Experiment	References
26599.08	1.5	3758.46, 3880.76	17.9	64 ± 4	d
26690.30	0.5	3792.02, 4049.56	14.0	17.9 ± 0.2	c
26723.87	1.5	3787.20, 3862.05	51.4	20.0 ± 1.0	d
26820.81	4.5	3946.51, 4066.73	34.3	14.0	13 –
26828.29	5.5	4362.03, 4454.63	28.0	16.0 ± 1.0	d
				47.0 ± 1.4	c
				88 ± 5	b
				35.2 ± 0.3	c
				27.3 ± 0.4	c
				30 ± 2	d

Table 1—Continued

Level (cm ⁻¹)	J	Laser Wavelength (Å)	Lifetime (ns)		
			This Experiment	Other Experiment	References
26880.60	5.5	4352.10, 4444.27	46.3	27.6 ± 0.7	e
26889.18	7.5	4350.47	136	48.4 ± 0.6	c
26938.42	3.5	3830.30, 3928.28	35.9	131 ± 2	c
26974.67	2.5	4003.44, 4116.44	52.4	38 ± 2	d
27001.20	4.5	3918.61, 4037.10	190	36.4 ± 0.7	e
27063.30	1.5	3693.99, 3812.06	9.8	54.4 ± 0.7	c
				53 ± 4	d
				10.6 ± 0.5	d

Table 1—Continued

Level (cm ⁻¹)	J	Laser Wavelength (Å)	Lifetime (ns)		
			This Experiment	Other Experiment	References
27078.30	2.5	3986.90, 4098.95	101		
27107.62	3.5	4094.03, 4234.57	40.6		
				41.4 ± 0.2	c
27165.35	2.5	3797.28, 4084.37	60.2		
				64 ± 3	c
				60 ± 4	d
27188.30	3.5	3793.98, 3890.08	26.6		
				26.5 ± 2.0	b
				26.9 ± 0.4	c
27210.12	0.5	3891.19, 3966.05	20.0		
				22 ± 2	d
27263.25	7.5	4280.78	28.4		
				29.2 ± 0.2	c
				29.1 ± 0.6	e

Table 1—Continued

Level (cm ⁻¹)	J	Laser Wavelength (Å)	Lifetime (ns)		
			This Experiment	Other Experiment	References
27284.69	2.5	3875.54, 4203.05	16.9		
				17.6 ± 0.9	b
				17.3 ± 0.2	c
				18.4 ± 1.0	d
27309.73	4.5	3871.78, 3987.42	42.2	21.9 ± 1.4	e
				38 ± 2	c
				170 ± 4	c
27386.69	4.5	3975.22, 4108.31	172		
				35 ± 3	b
				36.9 ± 0.8	c
27464.20	3.5	4035.10, 4171.56	37.2	39 ± 3	d
27492.95	1.5	3922.04	56.6		

Table 1—Continued

Level (cm ⁻¹)	J	Laser Wavelength (Å)	Lifetime (ns)		
			This Experiment	Other Experiment	References
27552.45	3.5	3835.73, 4156.26	139		
27631.18	2.5	3661.35, 3824.17	9.2		
				9.3 ± 0.2	c
				9.36 ± 0.15	e
27638.83	5.5	3935.76, 4213.03	170		
27639.40	6.5	4478.66	80.8		
27695.96	6.5	4202.91, 4467.34	24.2		
				24.6 ± 0.5	c
				24 ± 2	d
				24.0 ± 0.6	e
27829.77	1.5	3799.54, 3976.43	18.5		
27849.30	4.5	3903.42	58.8		
27923.96	2.5	3622.51, 3690.93	194		
27942.33	1.5	3620.10, 3688.43	41.2		

Table 1—Continued

Level (cm ⁻¹)	J	Laser Wavelength (Å)	Lifetime (ns)		
			This Experiment	Other Experiment	References
27987.24	5.5	3882.5	196		
28011.88	1.5	3843.78, 3947.83	40.6		
28022.50	4.5	3767.77, 3877.20	95.4		
28072.33	3.5	4068.32, 4220.66	9.8		
				10.6 ± 0.8	b
				9.96 ± 0.09	c
				10.2 ± 0.3	e
28142.79	0.5	3552.29, 3754.87	28.9		
28151.40	5.5	3983.14, 4123.95	28.6		
				27.7 ± 2.0	b
				29.3 ± 0.4	c
				28.6 ± 0.6	e
28191.96	4.5	3851.88, 4048.61	35.4		
				37 ± 1	c

Table 1—Continued

Level (cm ⁻¹)	J	Laser Wavelength (Å)	Lifetime (ns)		
			This Experiment	Other Experiment	References
28239.54	1.5	3741.28, 3810.43	22.4		
28256.32	3.5	3842.35, 4188.13	34.8		
				35.7 ± 0.2	c
28314.18	4.5	3726.80, 3833.83	85.2		
28394.04	2.5	3627.96, 3788.12	28.5		
				27 ± 2	b
28429.38	2.5	3557.36, 3623.32	47.5		
28445.43	3.5	3708.66, 3881.38	12.3		
				12.5 ± 0.2	c
28540.12	5.5	3800.89, 3922.39	21.0		
				21.5 ± 0.7	c
				21.1 ± 0.3	e
28573.13	2.5	3762.59, 3862.23	47.8		
28672.08	2.5	3847.52, 3971.39	19.2		

Table 1—Continued

Level (cm ⁻¹)	J	Laser Wavelength (Å)	Lifetime (ns)		
			This Experiment	Other Experiment	References
28725.53	4.5	3894.06, 4107.39	37.9	38.1 ± 0.2	c
28730.14	3.5	3838.94, 4106.61	66.6		
28812.92	1.5	3662.68, 3728.93	72.2		
28850.60	5.5	3875.18, 4008.33	95.4		
28913.99	4.5	4075.83, 4236.74	14.6	14.9 ± 0.1	c
28929.72	2.5	3712.76, 3809.74	84.7	64 ± 5	b
28938.55	1.5	3645.90, 3808.46	28.9		
28997.14	4.5	3634.27, 5103.09	9.7	10.1 ± 0.7	b
				9.6 ± 0.5	c
				9.62 ± 0.15	e

Table 1—Continued

Level (cm ⁻¹)	J	Laser Wavelength (Å)	Lifetime (ns)		
			This Experiment	Other Experiment	References
29238.56	2.5	3670.66, 3765.43	81.5		
29246.00	3.5	3701.55, 3764.37	30.1		
29310.16	3.5	3755.30, 3873.21	36.5		
29314.23	5.5	3692.22, 3806.76	162		
29387.87	4.5	3583.37, 4153.32	57.4		
				59.0 ± 1.3	c
29391.38	2.5	3650.17	48.8		
29422.65	0.5	3397.77	48.2		
				52 ± 4	c
29493.71	5.5	3667.91, 3780.92	67.4		
				67 ± 3	c
29509.60	3.5	3843.51, 3979.20	21.6		
29591.12	4.5	3831.51, 4118.55	16.3		
				16.4 ± 0.4	c

Table 1—Continued

Level (cm ⁻¹)	J	Laser Wavelength (Å)	Lifetime (ns)		
			This Experiment	Other Experiment	References
29619.89	3.5	3712.11, 3961.81	118		
29640.51	6.5	3885.28, 4110.18	17.9		
				18.4 ± 0.2	e
29655.90	1.5	3615.26, 4517.27	60.8		
29801.08	5.5	3627.00, 3737.47	38.5		
29804.88	4.5	3800.37, 4082.59	56.2		
29913.42	6.5	3721.84	47.1		
29934.80	5.5	3609.49, 3912.97	9.4		
				9.38 ± 0.12	e
29986.54	2.5	3370.59, 3662.25	46.6		
29998.15	4.5	3772.65	166		
30031.47	2.5	3566.81, 3656.23	58.4		
30082.93	1.5	3499.83, 3560.27	75.0		
30104.78	4.5	3757.53, 3887.11	33.6		

Table 1—Continued

Level (cm ⁻¹)	J	Laser Wavelength (Å)	Lifetime (ns)		
			This Experiment	Other Experiment	References
30112.78	3.5	3645.39, 3885.90	37.4		
30123.89	6.5	3813.63	279		
30252.90	0.5	3304.52, 3340.59	10.6		
30345.63	4.5	3556.73, 3662.90	64.0		
30445.87	6.5	3649.50, 3767.36	46.4		
30511.73	3.5	3444.61, 3826.56	52.2		
30514.16	4.5	3826.21, 3967.67	22.3		
30539.73	1.5	3273.48, 3365.87	11.3		
30652.56	4.5	3427.97, 3681.73	140		
30710.03	5.5	3797.74, 3937.06	34.8		
30756.88	1.5	3250.37, 3341.43	79.2		
			75 ± 6	d	
30816.69	3.5	3554.16, 3659.61	83.4		
30879.74	6.5	3706.75, 3910.92	9.3		

Table 1—Continued

Level (cm ⁻¹)	J	Laser Wavelength (Å)	Lifetime (ns)		
			This Experiment	Other Experiment	References
			10.0 ± 0.7	b	
			9.42 ± 0.15	e	
30969.35	4.5	3391.13, 3479.52	78.4		
30970.56	6.5	3580.91, 3694.31	97.6		
30981.48	5.5	3758.97, 3895.42	70.9		
31045.47	2.5	3254.39, 3382.40	10.5		
			11.2 ± 0.8	d	
31052.45	1.5	3219.43, 3253.65	98.2		
31089.52	0.5	3249.73	25.0		
31122.17	5.5	3461.11, 3561.57	31.3		
31171.00	1.5	3241.15, 3295.81	16.2		
			17.9 ± 1.0	d	
31189.83	4.5	3729.75, 3864.05	67.0		
31255.90	5.5	3720.58, 3854.20	17.6		

Table 1—Continued

Level (cm ⁻¹)	J	Laser Wavelength (Å)	Lifetime (ns)		
			This Experiment	Other Experiment	References
31309.40	1.5	3193.01, 3280.84	32.1		
31352.93	4.5	3433.68, 3532.52	122		
31441.34	7.5	3631.14, 5154.20	47.4		
31521.61	5.5	3413.90, 3620.58	80.0		
31566.40	3.5	3253.40, 3408.68	21.8		
31599.63	2.5	3249.89, 3320.15	51.4		
31646.49	7.5	3604.28, 5100.26	25.2		
31669.82	2.5	3312.43, 3449.53	41.2		
31725.56	2.5	3183.90, 3236.64	16.9		
31768.14	5.5	3650.98, 3779.56	93.1		
31774.52	3.5	3231.52, 3300.97	23.8		
			25 ± 2	d	
31830.06	5.5	3642.74, 3770.73	87.2		
31902.10	0.5	3290.28, 3343.65	38.3		

Table 1—Continued

Level (cm ⁻¹)	J	Laser Wavelength (Å)	Lifetime (ns)		
			This Experiment	Other Experiment	References
31915.67	3.5	3216.84, 3368.57	26.6	29 ± 2	d
31926.40	7.5	3568.27, 5028.45	13.2	13.2 ± 0.3	e
31998.58	7.5	3559.10	107		
32067.40	0.5	3272.47, 3325.26	20.4		
32130.57	6.5	3438.05, 3728.47	25.8		
32204.31	3.5	3336.12, 3593.73	85.6		
32286.05	6.5	3419.76, 3706.98	53.2		
32299.89	4.5	3244.69, 3418.15	49.0		
32358.56	1.5	3241.58, 3369.45	15.4		
				16.6 ± 1.2	d
32380.78	3.5	3316.59	58.0		
32397.48	2.5	3459.41	80		

Table 1—Continued

Level (cm ⁻¹)	J	Laser Wavelength (Å)	Lifetime (ns)		
			This Experiment	Other Experiment	References
32434.70	4.5	3230.55, 3310.66	14.0	15.5 ± 0.9	d
32451.66	3.5	3162.30	100		
32549.64	3.5	3152.53, 3218.60	23.1		
32852.81	6.5	3354.72, 3630.67	77.8		27
32857.54	4.5	3187.00, 3264.94	38.0		
				41 ± 3	d
32935.43	2.5	3305.19, 3396.19	22.3	24 ± 2	d
32945.19	4.5	3255.62, 3344.35	40.1	42 ± 3	d
33107.10	2.5	3286.54, 3376.50	67.2	68 ± 6	d
33153.69	5.5	3233.67, 3321.19	17.9		

Table 1—Continued

Level (cm ⁻¹)	J	Laser Wavelength (Å)	Lifetime (ns)		
			This Experiment	Other Experiment	References
33286.30	5.5	3403.08, 3459.18	61.0		
33333.40	3.5	3262.27, 3350.89	36.0		
33364.81	4.5	3136.28, 3211.73	27.3		
33539.60	2.5	3327.88	65.0		
33598.70	5.5	3187.78, 3272.80	31.2		
				33 ± 2	d
33661.26	0.5	3110.20	38.6		
33763.45	7.5	3348.69	99.2		
33775.84	5.5	3169.87, 3253.93	32.1		
				35 ± 2	d
33809.85	6.5	3343.49	80.0		
33881.94	3.5	3204.90, 3389.33	26.7		
				29 ± 2	d
34066.75	2.5	3186.02, 3270.49	69.5		

Table 1—Continued

Level (cm ⁻¹)	J	Laser Wavelength (Å)	Lifetime (ns)		
			This Experiment	Other Experiment	References
34145.44	6.5	3215.25, 3306.38	14.6	16.0 ± 0.9	d
34188.47	5.5	3301.68	69.7		
34330.90	5.5	3196.19, 3286.23	35.7		
34374.70	4.5	3333.63, 3440.51	50.4	52 ± 4	d
34418.95	5.5	3187.21, 3276.74	35.5	38 ± 2	d
34745.47	6.5	3242.04	119		
34768.41	6.5	3152.09, 3239.63	30.2	32 ± 2	d
34890.85	6.5	3139.97, 3226.83	62.4		
35547.50	5.5	3208.16, 3307.03	16.2		
38505.66	9.5	3778.14	43.6		

Table 1—Continued

Level (cm ⁻¹)	J	Laser Wavelength (Å)	Lifetime (ns)		
			This Experiment	Other Experiment	References

Note. — ^aUncertainty $\pm 5\%$ except for upper levels 31902.10 cm^{-1} ($\pm 10\%$) and 32397.48 cm^{-1} ($\pm 7.5\%$).

^b Biémont et al. (1989)

^c Scholl et al. (2002)

^d Xu et al. (2003)

^e Vogel et al. (1988)

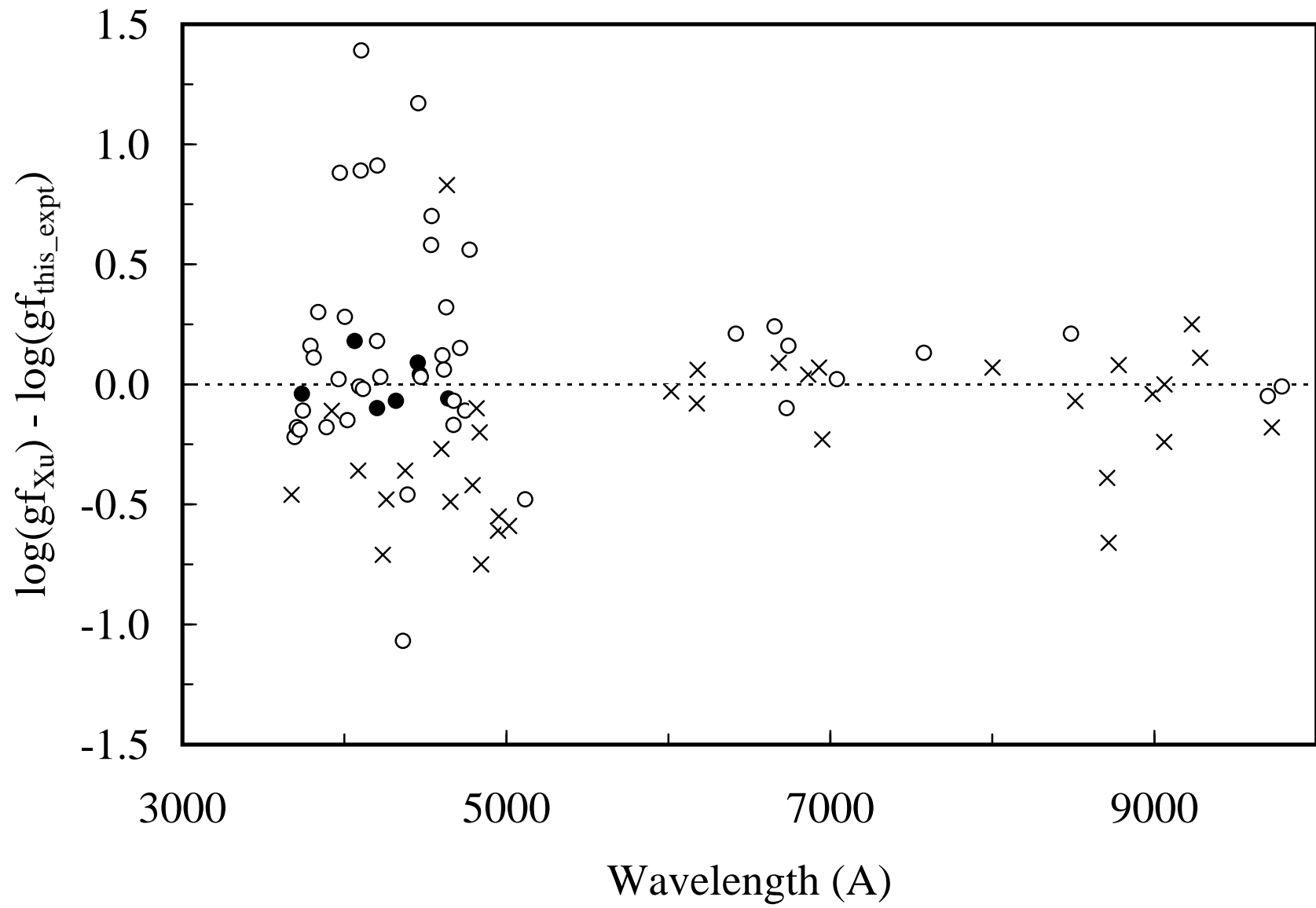


Table 2. Atomic transition probabilities for Sm II organized by increasing wavelength in air, λ_{air} .

λ_{air}	E_{upper}	J_{upp}	E_{lower}	J_{low}	A-value	$\log(gf)$
Å	(cm $^{-1}$)		(cm $^{-1}$)		(10 6 s $^{-1}$)	
3110.20	33661.26	0.5	1518.29	0.5	16.0 ± 1.5	-1.33
3115.05	34330.90	5.5	2237.97	4.5	1.18 ± 0.11	-1.69
3117.91	34066.75	2.5	2003.23	1.5	1.15 ± 0.16	-2.00
3136.28	33364.81	4.5	1489.16	3.5	5.2 ± 0.3	-1.12
3139.38	33333.40	3.5	1489.16	3.5	1.52 ± 0.25	-1.74
3152.09	34768.41	6.5	3052.65	5.5	3.53 ± 0.26	-1.13
3152.53	32549.64	3.5	838.22	2.5	9.4 ± 0.5	-0.95
3157.84	33661.26	0.5	2003.23	1.5	6.3 ± 0.7	-1.73
3169.87	33775.84	5.5	2237.97	4.5	5.6 ± 0.3	-1.00
3178.12	32945.19	4.5	1489.16	3.5	4.18 ± 0.26	-1.20
3183.90	31725.56	2.5	326.64	1.5	23.1 ± 1.2	-0.68
3186.02	34066.75	2.5	2688.69	2.5	5.6 ± 0.4	-1.29
3187.00	32857.54	4.5	1489.16	3.5	7.3 ± 0.4	-0.95
3187.78	33598.70	5.5	2237.97	4.5	8.6 ± 0.5	-0.80

Table 2—Continued

λ_{air}	E_{upper}	J_{upp}	E_{lower}	J_{low}	A-value	$\log(gf)$
Å	(cm $^{-1}$)		(cm $^{-1}$)		(10 6 s $^{-1}$)	
3189.56	31669.82	2.5	326.64	1.5	1.10 ± 0.19	-2.00
3193.01	31309.40	1.5	0.00	0.5	12.2 ± 0.7	-1.13
3196.19	34330.90	5.5	3052.65	5.5	7.8 ± 0.5	-0.84
3196.72	31599.63	2.5	326.64	1.5	0.29 ± 0.05	-2.58
3204.90	33881.94	3.5	2688.69	2.5	5.6 ± 0.7	-1.16
3207.18	31171.00	1.5	0.00	0.5	14.9 ± 0.8	-1.04
3210.81	34188.47	5.5	3052.65	5.5	1.05 ± 0.08	-1.71
3211.73	33364.81	4.5	2237.97	4.5	14.5 ± 0.8	-0.65
3215.25	34145.44	6.5	3052.65	5.5	6.3 ± 0.4	-0.87
3215.59	31089.52	0.5	0.00	0.5	7.9 ± 0.5	-1.61
3216.84	31915.67	3.5	838.22	2.5	12.6 ± 0.7	-0.81
3218.60	32549.64	3.5	1489.16	3.5	18.4 ± 1.0	-0.64
3219.43	31052.45	1.5	0.00	0.5	3.34 ± 0.21	-1.68
3230.55	32434.70	4.5	1489.16	3.5	19.5 ± 1.2	-0.52

|
e
|

Table 2—Continued

λ_{air}	E_{upper}	J_{upp}	E_{lower}	J_{low}	A-value	$\log(gf)$
Å	(cm ⁻¹)		(cm ⁻¹)		(10 ⁶ s ⁻¹)	
3231.94	32935.43	2.5	2003.23	1.5	8.3 ± 0.5	-1.11
3234.44	32397.48	2.5	1489.16	3.5	4.2 ± 0.4	-1.41
3236.19	32380.78	3.5	1489.16	3.5	0.43 ± 0.05	-2.27
3236.64	31725.56	2.5	838.22	2.5	24.9 ± 1.3	-0.63
3237.87	34374.70	4.5	3499.12	3.5	4.16 ± 0.28	-1.18
3239.63	34768.41	6.5	3909.62	6.5	20.8 ± 1.1	-0.34
3241.15	31171.00	1.5	326.64	1.5	23.9 ± 1.3	-0.82
3241.58	32358.56	1.5	1518.29	0.5	12.6 ± 0.8	-1.10
3242.49	31669.82	2.5	838.22	2.5	1.33 ± 0.20	-1.90
3244.69	32299.89	4.5	1489.16	3.5	2.99 ± 0.28	-1.33
3249.73	31089.52	0.5	326.64	1.5	21.2 ± 1.2	-1.17
3249.89	31599.63	2.5	838.22	2.5	2.17 ± 0.20	-1.69
3250.33	33809.85	6.5	3052.65	5.5	3.01 ± 0.21	-1.18
3250.37	30756.88	1.5	0.00	0.5	6.9 ± 0.4	-1.36

Table 2—Continued

λ_{air}	E_{upper}	J_{upp}	E_{lower}	J_{low}	A-value	$\log(gf)$
Å	(cm $^{-1}$)		(cm $^{-1}$)		(10 6 s $^{-1}$)	
3253.40	31566.40	3.5	838.22	2.5	13.3 ± 0.8	-0.77
3253.65	31052.45	1.5	326.64	1.5	1.90 ± 0.15	-1.92
3253.93	33775.84	5.5	3052.65	5.5	11.7 ± 0.6	-0.65
3254.78	32204.31	3.5	1489.16	3.5	1.07 ± 0.11	-1.87
3255.62	32945.19	4.5	2237.97	4.5	2.15 ± 0.17	-1.47
3262.27	33333.40	3.5	2688.69	2.5	4.88 ± 0.29	-1.21
3264.94	32857.54	4.5	2237.97	4.5	6.1 ± 0.3	-1.01
3270.49	34066.75	2.5	3499.12	3.5	5.4 ± 0.4	-1.28
3272.47	32067.40	0.5	1518.29	0.5	13.5 ± 0.9	-1.36
3272.80	33598.70	5.5	3052.65	5.5	12.9 ± 0.7	-0.61
3273.48	30539.73	1.5	0.00	0.5	27.4 ± 1.5	-0.75
3280.84	31309.40	1.5	838.22	2.5	9.1 ± 0.5	-1.23
3285.26	30756.88	1.5	326.64	1.5	1.01 ± 0.08	-2.19
3285.66	31915.67	3.5	1489.16	3.5	4.68 ± 0.28	-1.22

Table 2—Continued

λ_{air}	E_{upper}	J_{upp}	E_{lower}	J_{low}	A-value	$\log(gf)$
Å	(cm $^{-1}$)		(cm $^{-1}$)		(10 6 s $^{-1}$)	
3286.23	34330.90	5.5	3909.62	6.5	13.9 ± 0.8	-0.57
3289.15	32397.48	2.5	2003.23	1.5	0.83 ± 0.08	-2.09
3290.39	33881.94	3.5	3499.12	3.5	10.7 ± 0.6	-0.86
3293.37	32358.56	1.5	2003.23	1.5	15.7 ± 0.9	-0.99
3295.81	31171.00	1.5	838.22	2.5	18.1 ± 1.0	-0.93
3298.06	33364.81	4.5	3052.65	5.5	10.8 ± 0.6	-0.75
3298.11	32549.64	3.5	2237.97	4.5	7.5 ± 0.4	-1.01
3301.68	34188.47	5.5	3909.62	6.5	8.2 ± 0.4	-0.79
3305.19	32935.43	2.5	2688.69	2.5	13.2 ± 0.7	-0.89
3306.32	31725.56	2.5	1489.16	3.5	3.37 ± 0.25	-1.48
3306.38	34145.44	6.5	3909.62	6.5	52.6 ± 2.7	0.08
3310.66	32434.70	4.5	2237.97	4.5	18.8 ± 1.0	-0.51
3312.43	31669.82	2.5	1489.16	3.5	16.7 ± 0.9	-0.78
3316.59	32380.78	3.5	2237.97	4.5	10.1 ± 0.6	-0.88

Table 2—Continued

λ_{air}	E_{upper}	J_{upp}	E_{lower}	J_{low}	A-value	$\log(gf)$
Å	(cm ⁻¹)		(cm ⁻¹)		(10 ⁶ s ⁻¹)	
3320.15	31599.63	2.5	1489.16	3.5	9.0 ± 0.5	-1.05
3323.82	31566.40	3.5	1489.16	3.5	7.1 ± 0.4	-1.02
3325.26	32067.40	0.5	2003.23	1.5	35.5 ± 1.9	-0.93
3325.51	32299.89	4.5	2237.97	4.5	4.40 ± 0.28	-1.14
3333.63	34374.70	4.5	4386.03	4.5	6.1 ± 0.4	-0.99
3336.12	32204.31	3.5	2237.97	4.5	3.66 ± 0.20	-1.31
3341.43	30756.88	1.5	838.22	2.5	2.70 ± 0.29	-1.74
3343.49	33809.85	6.5	3909.62	6.5	7.4 ± 0.4	-0.76
3344.35	32945.19	4.5	3052.65	5.5	8.0 ± 0.4	-0.87
3347.30	33775.84	5.5	3909.62	6.5	6.2 ± 0.3	-0.90
3348.69	33763.45	7.5	3909.62	6.5	6.5 ± 0.4	-0.76
3350.89	33333.40	3.5	3499.12	3.5	9.9 ± 0.6	-0.87
3354.19	32857.54	4.5	3052.65	5.5	6.5 ± 0.4	-0.96
3354.72	32852.81	6.5	3052.65	5.5	2.96 ± 0.18	-1.16

Table 2—Continued

λ_{air}	E_{upper}	J_{upp}	E_{lower}	J_{low}	A-value	$\log(gf)$	
Å	(cm ⁻¹)		(cm ⁻¹)		(10 ⁶ s ⁻¹)		
3365.04	32397.48	2.5	2688.69	2.5	0.60 ± 0.08	-2.22	
3365.87	30539.73	1.5	838.22	2.5	46.5 ± 2.5	-0.50	
3365.96	31189.83	4.5	1489.16	3.5	2.15 ± 0.14	-1.44	
3366.93	32380.78	3.5	2688.69	2.5	0.32 ± 0.05	-2.36	
3367.27	33598.70	5.5	3909.62	6.5	4.9 ± 0.4	-1.00	
3368.57	31915.67	3.5	2237.97	4.5	10.0 ± 0.6	-0.87	∞
3369.04	30511.73	3.5	838.22	2.5	2.58 ± 0.20	-1.45	
3369.45	32358.56	1.5	2688.69	2.5	33.0 ± 1.7	-0.65	
3370.59	29986.54	2.5	326.64	1.5	3.92 ± 0.25	-1.40	
3371.04	29655.90	1.5	0.00	0.5	1.54 ± 0.16	-1.98	
3377.82	31599.63	2.5	2003.23	1.5	1.60 ± 0.10	-1.78	
3378.31	31830.06	5.5	2237.97	4.5	0.62 ± 0.04	-1.89	
3380.69	31089.52	0.5	1518.29	0.5	3.85 ± 0.27	-1.88	
3384.94	31052.45	1.5	1518.29	0.5	1.59 ± 0.15	-1.96	

Table 2—Continued

λ_{air}	E_{upper}	J_{upp}	E_{lower}	J_{low}	A-value	$\log(gf)$
Å	(cm $^{-1}$)		(cm $^{-1}$)		(10 6 s $^{-1}$)	
3385.40	31768.14	5.5	2237.97	4.5	1.18 ± 0.09	-1.61
3387.06	32204.31	3.5	2688.69	2.5	1.40 ± 0.10	-1.72
3389.33	33881.94	3.5	4386.03	4.5	17.7 ± 1.0	-0.61
3391.13	30969.35	4.5	1489.16	3.5	1.99 ± 0.19	-1.47
3396.19	32935.43	2.5	3499.12	3.5	19.9 ± 1.0	-0.68
3397.77	29422.65	0.5	0.00	0.5	5.0 ± 0.4	-1.76
3402.46	32434.70	4.5	3052.65	5.5	22.9 ± 1.2	-0.40
3408.59	29655.90	1.5	326.64	1.5	2.83 ± 0.21	-1.71
3408.68	31566.40	3.5	2237.97	4.5	20.4 ± 1.1	-0.55
3411.27	31309.40	1.5	2003.23	1.5	2.6 ± 0.3	-1.75
3413.90	31521.61	5.5	2237.97	4.5	1.02 ± 0.08	-1.67
3414.96	30112.78	3.5	838.22	2.5	1.03 ± 0.07	-1.84
3418.15	32299.89	4.5	3052.65	5.5	8.7 ± 0.5	-0.82
3419.76	32286.05	6.5	3052.65	5.5	3.46 ± 0.22	-1.07

Table 2—Continued

λ_{air}	E_{upper}	J_{upp}	E_{lower}	J_{low}	A-value	$\log(gf)$
Å	(cm ⁻¹)		(cm ⁻¹)		(10 ⁶ s ⁻¹)	
3420.52	31915.67	3.5	2688.69	2.5	1.24 ± 0.10	-1.76
3422.19	33598.70	5.5	4386.03	4.5	0.93 ± 0.10	-1.71
3427.97	30652.56	4.5	1489.16	3.5	0.71 ± 0.05	-1.90
3429.75	29986.54	2.5	838.22	2.5	1.84 ± 0.14	-1.71
3433.68	31352.93	4.5	2237.97	4.5	2.60 ± 0.17	-1.34
3438.05	32130.57	6.5	3052.65	5.5	3.12 ± 0.21	-1.11
3440.51	34374.70	4.5	5317.56	5.5	7.1 ± 0.4	-0.90
3444.32	30514.16	4.5	1489.16	3.5	0.29 ± 0.03	-2.28
3444.61	30511.73	3.5	1489.16	3.5	1.65 ± 0.14	-1.63
3445.16	31255.90	5.5	2237.97	4.5	0.49 ± 0.04	-1.98
3445.70	34330.90	5.5	5317.56	5.5	1.35 ± 0.14	-1.54
3449.53	31669.82	2.5	2688.69	2.5	1.23 ± 0.11	-1.88
3453.02	31189.83	4.5	2237.97	4.5	0.36 ± 0.05	-2.20
3453.56	33333.40	3.5	4386.03	4.5	6.6 ± 0.4	-1.03

Table 2—Continued

λ_{air}	E_{upper}	J_{upp}	E_{lower}	J_{low}	A-value	$\log(gf)$
Å	(cm $^{-1}$)		(cm $^{-1}$)		(10 6 s $^{-1}$)	
3454.96	32434.70	4.5	3499.12	3.5	2.81 ± 0.18	-1.30
3457.91	31599.63	2.5	2688.69	2.5	1.68 ± 0.10	-1.74
3459.41	32397.48	2.5	3499.12	3.5	4.1 ± 0.3	-1.36
3461.11	31122.17	5.5	2237.97	4.5	4.22 ± 0.24	-1.04
3461.41	32380.78	3.5	3499.12	3.5	1.33 ± 0.12	-1.72
3461.89	31566.40	3.5	2688.69	2.5	0.54 ± 0.08	-2.11
3462.70	34188.47	5.5	5317.56	5.5	2.40 ± 0.18	-1.28
3464.44	30345.63	4.5	1489.16	3.5	0.97 ± 0.07	-1.76
3467.87	34145.44	6.5	5317.56	5.5	3.91 ± 0.25	-1.01
3471.14	32299.89	4.5	3499.12	3.5	1.27 ± 0.12	-1.64
3473.95	31830.06	5.5	3052.65	5.5	1.17 ± 0.07	-1.60
3478.05	30981.48	5.5	2237.97	4.5	0.24 ± 0.04	-2.27
3479.52	30969.35	4.5	2237.97	4.5	1.80 ± 0.17	-1.49
3481.44	31768.14	5.5	3052.65	5.5	0.32 ± 0.04	-2.15

Table 2—Continued

λ_{air}	E_{upper}	J_{upp}	E_{lower}	J_{low}	A-value	$\log(gf)$
Å	(cm $^{-1}$)		(cm $^{-1}$)		(10 6 s $^{-1}$)	
3482.69	32204.31	3.5	3499.12	3.5	1.25 ± 0.07	-1.74
3492.62	30112.78	3.5	1489.16	3.5	0.91 ± 0.08	-1.87
3493.60	30104.78	4.5	1489.16	3.5	2.09 ± 0.15	-1.42
3498.11	30816.69	3.5	2237.97	4.5	0.19 ± 0.03	-2.55
3499.83	30082.93	1.5	1518.29	0.5	6.0 ± 0.4	-1.35
3500.50	32945.19	4.5	4386.03	4.5	4.07 ± 0.24	-1.13
3503.28	30539.73	1.5	2003.23	1.5	1.73 ± 0.18	-1.89
3508.72	33809.85	6.5	5317.56	5.5	0.69 ± 0.08	-1.75
3509.46	28812.92	1.5	326.64	1.5	0.64 ± 0.06	-2.33
3511.28	32857.54	4.5	4386.03	4.5	0.43 ± 0.07	-2.10
3511.59	31521.61	5.5	3052.65	5.5	0.69 ± 0.05	-1.81
3512.91	33775.84	5.5	5317.56	5.5	1.26 ± 0.18	-1.55
3518.07	31915.67	3.5	3499.12	3.5	1.04 ± 0.09	-1.81
3523.04	32286.05	6.5	3909.62	6.5	0.68 ± 0.09	-1.75

Table 2—Continued

λ_{air}	E_{upper}	J_{upp}	E_{lower}	J_{low}	A-value	$\log(gf)$
Å	(cm $^{-1}$)		(cm $^{-1}$)		(10 6 s $^{-1}$)	
3524.62	31052.45	1.5	2688.69	2.5	2.25 ± 0.14	-1.78
3526.90	28672.08	2.5	326.64	1.5	1.08 ± 0.12	-1.92
3530.60	29804.88	4.5	1489.16	3.5	2.97 ± 0.20	-1.25
3532.52	31352.93	4.5	3052.65	5.5	3.52 ± 0.21	-1.18
3534.92	33598.70	5.5	5317.56	5.5	0.82 ± 0.10	-1.74
3539.25	28573.13	2.5	326.64	1.5	0.56 ± 0.04	-2.20
3542.45	32130.57	6.5	3909.62	6.5	1.37 ± 0.08	-1.44
3548.77	31669.82	2.5	3499.12	3.5	0.80 ± 0.10	-2.04
3552.29	28142.79	0.5	0.00	0.5	4.48 ± 0.27	-1.77
3552.95	29655.90	1.5	1518.29	0.5	1.04 ± 0.08	-2.10
3553.00	31189.83	4.5	3052.65	5.5	0.30 ± 0.03	-2.24
3554.16	30816.69	3.5	2688.69	2.5	4.10 ± 0.25	-1.21
3556.73	30345.63	4.5	2237.97	4.5	2.63 ± 0.17	-1.30
3557.36	28429.38	2.5	326.64	1.5	2.27 ± 0.14	-1.59

Table 2—Continued

λ_{air}	E_{upper}	J_{upp}	E_{lower}	J_{low}	A-value	$\log(gf)$
Å	(cm $^{-1}$)		(cm $^{-1}$)		(10 6 s $^{-1}$)	
3557.64	31599.63	2.5	3499.12	3.5	1.10 ± 0.21	-1.90
3560.27	30082.93	1.5	2003.23	1.5	3.09 ± 0.22	-1.63
3561.57	31122.17	5.5	3052.65	5.5	3.14 ± 0.19	-1.14
3561.84	28394.04	2.5	326.64	1.5	0.19 ± 0.04	-2.66
3566.81	30031.47	2.5	2003.23	1.5	5.29 ± 0.30	-1.22
3568.27	31926.40	7.5	3909.62	6.5	63 ± 3	0.29
3568.89	28011.88	1.5	0.00	0.5	0.92 ± 0.09	-2.15
3571.08	32380.78	3.5	4386.03	4.5	1.20 ± 0.09	-1.73
3577.78	27942.33	1.5	0.00	0.5	6.5 ± 0.4	-1.30
3579.51	30981.48	5.5	3052.65	5.5	0.42 ± 0.04	-2.01
3580.58	31830.06	5.5	3909.62	6.5	0.96 ± 0.08	-1.65
3580.91	30970.56	6.5	3052.65	5.5	6.0 ± 0.3	-0.79
3581.06	30969.35	4.5	3052.65	5.5	0.41 ± 0.08	-2.11
3582.65	29422.65	0.5	1518.29	0.5	4.1 ± 0.3	-1.80

Table 2—Continued

λ_{air}	E_{upper}	J_{upp}	E_{lower}	J_{low}	A-value	$\log(gf)$
Å	(cm $^{-1}$)		(cm $^{-1}$)		(10 6 s $^{-1}$)	
3583.37	29387.87	4.5	1489.16	3.5	4.05 ± 0.29	-1.11
3584.24	28730.14	3.5	838.22	2.5	2.72 ± 0.15	-1.38
3587.47	30104.78	4.5	2237.97	4.5	1.96 ± 0.12	-1.42
3588.54	31768.14	5.5	3909.62	6.5	0.28 ± 0.04	-2.18
3589.51	30539.73	1.5	2688.69	2.5	2.03 ± 0.19	-1.80
3591.72	28672.08	2.5	838.22	2.5	0.37 ± 0.05	-2.37
3592.60	30879.74	6.5	3052.65	5.5	80 ± 4	0.33
3593.38	29310.16	3.5	1489.16	3.5	0.62 ± 0.05	-2.02
3593.73	32204.31	3.5	4386.03	4.5	2.81 ± 0.17	-1.36
3601.25	29998.15	4.5	2237.97	4.5	0.52 ± 0.05	-2.00
3601.69	29246.00	3.5	1489.16	3.5	6.7 ± 0.4	-0.98
3604.28	31646.49	7.5	3909.62	6.5	29.8 ± 1.6	-0.03
3609.49	29934.80	5.5	2237.97	4.5	61 ± 3	0.16
3610.29	31189.83	4.5	3499.12	3.5	0.66 ± 0.07	-1.89

Table 2—Continued

λ_{air}	E_{upper}	J_{upp}	E_{lower}	J_{low}	A-value	$\log(gf)$
Å	(cm ⁻¹)		(cm ⁻¹)		(10 ⁶ s ⁻¹)	
3615.26	29655.90	1.5	2003.23	1.5	2.73 ± 0.19	-1.67
3620.10	27942.33	1.5	326.64	1.5	3.65 ± 0.22	-1.54
3620.58	31521.61	5.5	3909.62	6.5	3.46 ± 0.23	-1.09
3621.21	28445.43	3.5	838.22	2.5	19.9 ± 1.1	-0.51
3622.51	27923.96	2.5	326.64	1.5	2.15 ± 0.13	-1.60
3623.32	28429.38	2.5	838.22	2.5	4.80 ± 0.28	-1.25
3626.50	29804.88	4.5	2237.97	4.5	0.78 ± 0.06	-1.81
3627.00	29801.08	5.5	2237.97	4.5	13.1 ± 0.7	-0.51
3627.96	28394.04	2.5	838.22	2.5	3.54 ± 0.21	-1.38
3630.67	32852.81	6.5	5317.56	5.5	5.17 ± 0.29	-0.84
3631.14	31441.34	7.5	3909.62	6.5	14.9 ± 0.8	-0.33
3634.27	28997.14	4.5	1489.16	3.5	52.8 ± 2.7	0.02
3634.91	27829.77	1.5	326.64	1.5	6.8 ± 0.4	-1.27
3639.27	30969.35	4.5	3499.12	3.5	2.04 ± 0.20	-1.39

Table 2—Continued

λ_{air}	E _{upper}	J _{upp}	E _{lower}	J _{low}	A-value	log(gf)
Å	(cm ⁻¹)		(cm ⁻¹)		(10 ⁶ s ⁻¹)	
3640.42	30514.16	4.5	3052.65	5.5	0.41 ± 0.03	-2.09
3642.74	31830.06	5.5	4386.03	4.5	3.75 ± 0.21	-1.05
3645.29	28913.99	4.5	1489.16	3.5	8.9 ± 0.6	-0.75
3645.39	30112.78	3.5	2688.69	2.5	9.3 ± 0.5	-0.83
3645.90	28938.55	1.5	1518.29	0.5	5.27 ± 0.30	-1.38
3646.01	29422.65	0.5	2003.23	1.5	4.07 ± 0.30	-1.79
3646.19	28256.32	3.5	838.22	2.5	0.190 ± 0.019	-2.52
3649.36	30082.93	1.5	2688.69	2.5	0.64 ± 0.07	-2.29
3649.50	30445.87	6.5	3052.65	5.5	8.8 ± 0.5	-0.61
3650.98	31768.14	5.5	4386.03	4.5	4.9 ± 0.3	-0.93
3654.84	29591.12	4.5	2237.97	4.5	1.31 ± 0.08	-1.58
3655.76	31255.90	5.5	3909.62	6.5	0.92 ± 0.06	-1.66
3656.23	30031.47	2.5	2688.69	2.5	5.8 ± 0.3	-1.16
3659.61	30816.69	3.5	3499.12	3.5	3.53 ± 0.22	-1.25

Table 2—Continued

λ_{air}	E_{upper}	J_{upp}	E_{lower}	J_{low}	A-value	$\log(gf)$
Å	(cm $^{-1}$)		(cm $^{-1}$)		(10 6 s $^{-1}$)	
3661.35	27631.18	2.5	326.64	1.5	36.4 ± 1.9	-0.36
3662.25	29986.54	2.5	2688.69	2.5	4.35 ± 0.25	-1.28
3662.68	28812.92	1.5	1518.29	0.5	7.6 ± 0.4	-1.21
3662.90	30345.63	4.5	3052.65	5.5	3.90 ± 0.24	-1.11
3669.89	28730.14	3.5	1489.16	3.5	0.53 ± 0.05	-2.07
3670.52	28725.53	4.5	1489.16	3.5	1.19 ± 0.11	-1.62
3670.82	28072.33	3.5	838.22	2.5	35.2 ± 1.8	-0.24
3674.06	27210.12	0.5	0.00	0.5	5.9 ± 0.5	-1.62
3678.08	31566.40	3.5	4386.03	4.5	1.35 ± 0.13	-1.66
3678.99	28011.88	1.5	838.22	2.5	0.42 ± 0.05	-2.46
3681.73	30652.56	4.5	3499.12	3.5	2.91 ± 0.18	-1.23
3682.21	29387.87	4.5	2237.97	4.5	1.05 ± 0.08	-1.67
3684.15	31521.61	5.5	4386.03	4.5	0.53 ± 0.04	-1.89
3688.43	27942.33	1.5	838.22	2.5	2.75 ± 0.16	-1.65

Table 2—Continued

λ_{air}	E_{upper}	J_{upp}	E_{lower}	J_{low}	A-value	$\log(gf)$
Å	(cm $^{-1}$)		(cm $^{-1}$)		(10 6 s $^{-1}$)	
3690.93	27923.96	2.5	838.22	2.5	1.02 ± 0.07	-1.90
3692.22	29314.23	5.5	2237.97	4.5	1.87 ± 0.11	-1.34
3692.78	29310.16	3.5	2237.97	4.5	1.97 ± 0.13	-1.49
3692.91	30123.89	6.5	3052.65	5.5	0.64 ± 0.06	-1.74
3693.99	27063.30	1.5	0.00	0.5	28.3 ± 1.5	-0.64
3694.31	30970.56	6.5	3909.62	6.5	2.40 ± 0.17	-1.16
3700.59	30514.16	4.5	3499.12	3.5	3.22 ± 0.18	-1.18
3700.92	30511.73	3.5	3499.12	3.5	4.88 ± 0.29	-1.10
3701.55	29246.00	3.5	2237.97	4.5	1.84 ± 0.11	-1.52
3705.07	32299.89	4.5	5317.56	5.5	1.20 ± 0.08	-1.61
3706.75	30879.74	6.5	3909.62	6.5	8.6 ± 0.5	-0.60
3706.98	32286.05	6.5	5317.56	5.5	11.4 ± 0.6	-0.48
3707.15	29655.90	1.5	2688.69	2.5	2.92 ± 0.22	-1.62
3708.41	27284.69	2.5	326.64	1.5	7.9 ± 0.5	-1.01

Table 2—Continued

λ_{air}	E_{upper}	J_{upp}	E_{lower}	J_{low}	A-value	$\log(gf)$
Å	(cm ⁻¹)		(cm ⁻¹)		(10 ⁶ s ⁻¹)	
3708.66	28445.43	3.5	1489.16	3.5	14.2 ± 0.8	-0.63
3710.87	28429.38	2.5	1489.16	3.5	2.55 ± 0.16	-1.50
3711.54	28938.55	1.5	2003.23	1.5	15.9 ± 0.8	-0.88
3712.11	29619.89	3.5	2688.69	2.5	3.83 ± 0.23	-1.20
3712.76	28929.72	2.5	2003.23	1.5	6.7 ± 0.4	-1.08
3718.70	27210.12	0.5	326.64	1.5	1.81 ± 0.13	-2.12
3718.88	29934.80	5.5	3052.65	5.5	19.8 ± 1.1	-0.31
3720.58	31255.90	5.5	4386.03	4.5	2.77 ± 0.17	-1.16
3723.82	30345.63	4.5	3499.12	3.5	0.46 ± 0.05	-2.02
3724.90	27165.35	2.5	326.64	1.5	4.38 ± 0.25	-1.26
3726.80	28314.18	4.5	1489.16	3.5	1.65 ± 0.11	-1.46
3727.37	29509.60	3.5	2688.69	2.5	0.97 ± 0.06	-1.79
3728.47	32130.57	6.5	5317.56	5.5	31.1 ± 1.6	-0.04
3728.93	28812.92	1.5	2003.23	1.5	3.75 ± 0.23	-1.50

Table 2—Continued

λ_{air}	E_{upper}	J_{upp}	E_{lower}	J_{low}	A-value	$\log(gf)$
Å	(cm ⁻¹)		(cm ⁻¹)		(10 ⁶ s ⁻¹)	
3729.75	31189.83	4.5	4386.03	4.5	6.4 ± 0.4	-0.88
3731.26	27631.18	2.5	838.22	2.5	37.2 ± 1.9	-0.33
3734.86	28256.32	3.5	1489.16	3.5	0.91 ± 0.08	-1.82
3735.97	28997.14	4.5	2237.97	4.5	24.8 ± 1.3	-0.28
3737.02	27078.30	2.5	326.64	1.5	0.68 ± 0.05	-2.07
3737.47	29801.08	5.5	3052.65	5.5	5.5 ± 0.3	-0.86
3739.12	27063.30	1.5	326.64	1.5	44.4 ± 2.3	-0.43
3739.19	31122.17	5.5	4386.03	4.5	21.4 ± 1.1	-0.27
3741.28	28239.54	1.5	1518.29	0.5	30.4 ± 1.6	-0.59
3743.86	28191.96	4.5	1489.16	3.5	13.6 ± 0.7	-0.55
3745.61	26690.30	0.5	0.00	0.5	44.9 ± 2.4	-0.72
3747.62	28913.99	4.5	2237.97	4.5	7.8 ± 0.5	-0.78
3748.63	28672.08	2.5	2003.23	1.5	2.55 ± 0.15	-1.49
3751.56	26974.67	2.5	326.64	1.5	2.17 ± 0.12	-1.56

Table 2—Continued

λ_{air}	E_{upper}	J_{upp}	E_{lower}	J_{low}	A-value	$\log(gf)$
Å	(cm $^{-1}$)		(cm $^{-1}$)		(10 6 s $^{-1}$)	
3754.87	28142.79	0.5	1518.29	0.5	10.0 ± 0.6	-1.37
3755.30	29310.16	3.5	2688.69	2.5	13.3 ± 0.7	-0.65
3756.40	30112.78	3.5	3499.12	3.5	10.1 ± 0.6	-0.77
3756.55	28850.60	5.5	2237.97	4.5	3.79 ± 0.21	-1.02
3757.53	30104.78	4.5	3499.12	3.5	21.0 ± 1.1	-0.35
3758.97	30981.48	5.5	4386.03	4.5	11.6 ± 0.6	-0.53
3760.05	29640.51	6.5	3052.65	5.5	3.83 ± 0.21	-0.94
3760.71	28072.33	3.5	1489.16	3.5	23.3 ± 1.2	-0.40
3762.59	28573.13	2.5	2003.23	1.5	11.0 ± 0.6	-0.85
3764.37	29246.00	3.5	2688.69	2.5	16.6 ± 0.9	-0.55
3767.36	30445.87	6.5	3909.62	6.5	6.7 ± 0.4	-0.70
3767.77	28022.50	4.5	1489.16	3.5	5.72 ± 0.30	-0.91
3767.91	30031.47	2.5	3499.12	3.5	2.50 ± 0.15	-1.50
3770.73	31830.06	5.5	5317.56	5.5	1.70 ± 0.13	-1.36

Table 2—Continued

λ_{air}	E_{upper}	J_{upp}	E_{lower}	J_{low}	A-value	$\log(gf)$
Å	(cm ⁻¹)		(cm ⁻¹)		(10 ⁶ s ⁻¹)	
3772.65	29998.15	4.5	3499.12	3.5	3.35 ± 0.19	-1.15
3773.43	28011.88	1.5	1518.29	0.5	3.76 ± 0.22	-1.49
3774.31	29986.54	2.5	3499.12	3.5	5.21 ± 0.29	-1.17
3774.70	26484.66	1.5	0.00	0.5	3.55 ± 0.20	-1.52
3778.14	38505.66	9.5	12045.10	8.5	22.9 ± 1.2	-0.01
3779.56	31768.14	5.5	5317.56	5.5	2.82 ± 0.20	-1.14
3780.15	27284.69	2.5	838.22	2.5	0.60 ± 0.04	-2.11
3780.76	26442.18	0.5	0.00	0.5	24.1 ± 1.3	-0.99
3783.06	28429.38	2.5	2003.23	1.5	1.03 ± 0.07	-1.88
3783.36	27942.33	1.5	1518.29	0.5	3.80 ± 0.25	-1.49
3787.20	26723.87	1.5	326.64	1.5	3.03 ± 0.17	-1.58
3788.12	28394.04	2.5	2003.23	1.5	22.5 ± 1.2	-0.54
3792.02	26690.30	0.5	326.64	1.5	8.3 ± 0.5	-1.45
3793.98	27188.30	3.5	838.22	2.5	12.3 ± 0.6	-0.67

Table 2—Continued

λ_{air}	E_{upper}	J_{upp}	E_{lower}	J_{low}	A-value	$\log(gf)$
Å	(cm $^{-1}$)		(cm $^{-1}$)		(10 6 s $^{-1}$)	
3797.28	27165.35	2.5	838.22	2.5	3.10 ± 0.17	-1.40
3797.74	30710.03	5.5	4386.03	4.5	21.3 ± 1.1	-0.26
3799.54	27829.77	1.5	1518.29	0.5	13.8 ± 0.7	-0.92
3800.37	29804.88	4.5	3499.12	3.5	3.00 ± 0.17	-1.19
3800.89	28540.12	5.5	2237.97	4.5	8.7 ± 0.5	-0.65
3805.63	27107.62	3.5	838.22	2.5	3.63 ± 0.22	-1.20
3806.05	30652.56	4.5	4386.03	4.5	0.84 ± 0.11	-1.74
3806.76	29314.23	5.5	3052.65	5.5	1.53 ± 0.10	-1.40
3807.93	26253.55	0.5	0.00	0.5	5.9 ± 0.3	-1.59
3808.46	28938.55	1.5	2688.69	2.5	9.2 ± 0.5	-1.10
3809.74	28929.72	2.5	2688.69	2.5	3.19 ± 0.21	-1.38
3809.88	27078.30	2.5	838.22	2.5	2.01 ± 0.13	-1.58
3810.43	28239.54	1.5	2003.23	1.5	9.4 ± 0.5	-1.09
3812.06	27063.30	1.5	838.22	2.5	8.5 ± 0.5	-1.13

Table 2—Continued

λ_{air}	E_{upper}	J_{upp}	E_{lower}	J_{low}	A-value	$\log(gf)$
Å	(cm $^{-1}$)		(cm $^{-1}$)		(10 6 s $^{-1}$)	
3813.63	30123.89	6.5	3909.62	6.5	2.51 ± 0.18	-1.12
3814.62	28445.43	3.5	2237.97	4.5	3.79 ± 0.24	-1.18
3821.83	26484.66	1.5	326.64	1.5	3.27 ± 0.19	-1.54
3824.17	27631.18	2.5	1489.16	3.5	8.7 ± 0.5	-0.94
3824.53	28142.79	0.5	2003.23	1.5	16.2 ± 0.9	-1.15
3824.99	26974.67	2.5	838.22	2.5	1.85 ± 0.13	-1.61
3826.21	30514.16	4.5	4386.03	4.5	29.3 ± 1.5	-0.19
3826.56	30511.73	3.5	4386.03	4.5	3.52 ± 0.22	-1.21
3827.29	29619.89	3.5	3499.12	3.5	0.67 ± 0.05	-1.93
3828.05	26442.18	0.5	326.64	1.5	8.6 ± 0.5	-1.42
3830.30	26938.42	3.5	838.22	2.5	4.28 ± 0.23	-1.12
3831.51	29591.12	4.5	3499.12	3.5	17.0 ± 0.9	-0.43
3833.83	28314.18	4.5	2237.97	4.5	5.13 ± 0.29	-0.95
3835.73	27552.45	3.5	1489.16	3.5	2.72 ± 0.15	-1.32

Table 2—Continued

λ_{air}	E_{upper}	J_{upp}	E_{lower}	J_{low}	A-value	$\log(gf)$
Å	(cm ⁻¹)		(cm ⁻¹)		(10 ⁶ s ⁻¹)	
3838.94	28730.14	3.5	2688.69	2.5	7.1 ± 0.4	-0.90
3839.84	31352.93	4.5	5317.56	5.5	0.54 ± 0.11	-1.93
3840.45	26357.90	2.5	326.64	1.5	6.3 ± 0.4	-1.08
3841.34	29934.80	5.5	3909.62	6.5	0.27 ± 0.05	-2.15
3842.35	28256.32	3.5	2237.97	4.5	3.12 ± 0.20	-1.26
3843.51	29509.60	3.5	3499.12	3.5	20.2 ± 1.0	-0.45
3843.78	28011.88	1.5	2003.23	1.5	9.4 ± 0.5	-1.08
3847.52	28672.08	2.5	2688.69	2.5	12.3 ± 0.7	-0.78
3851.05	30345.63	4.5	4386.03	4.5	0.166 ± 0.022	-2.43
3851.88	28191.96	4.5	2237.97	4.5	4.17 ± 0.22	-1.03
3854.20	31255.90	5.5	5317.56	5.5	51.5 ± 2.6	0.14
3855.90	26253.55	0.5	326.64	1.5	26.8 ± 1.4	-0.92
3857.91	28151.40	5.5	2237.97	4.5	3.67 ± 0.20	-1.01
3860.28	27386.69	4.5	1489.16	3.5	1.41 ± 0.09	-1.50

Table 2—Continued

λ_{air}	E_{upper}	J_{upp}	E_{lower}	J_{low}	A-value	$\log(gf)$
Å	(cm $^{-1}$)		(cm $^{-1}$)		(10 6 s $^{-1}$)	
3861.59	29387.87	4.5	3499.12	3.5	0.85 ± 0.07	-1.72
3862.05	26723.87	1.5	838.22	2.5	7.6 ± 0.4	-1.17
3862.23	28573.13	2.5	2688.69	2.5	5.9 ± 0.3	-1.10
3864.05	31189.83	4.5	5317.56	5.5	1.45 ± 0.09	-1.49
3865.24	26190.92	2.5	326.64	1.5	2.67 ± 0.14	-1.45
3865.68	28913.99	4.5	3052.65	5.5	0.92 ± 0.07	-1.69
3871.78	27309.73	4.5	1489.16	3.5	8.1 ± 0.4	-0.74
3873.21	29310.16	3.5	3499.12	3.5	2.86 ± 0.17	-1.29
3875.18	28850.60	5.5	3052.65	5.5	3.17 ± 0.18	-1.07
3875.54	27284.69	2.5	1489.16	3.5	8.2 ± 0.5	-0.96
3877.20	28022.50	4.5	2237.97	4.5	2.12 ± 0.14	-1.32
3881.38	28445.43	3.5	2688.69	2.5	6.0 ± 0.4	-0.96
3882.50	27987.24	5.5	2237.97	4.5	2.16 ± 0.12	-1.23
3882.87	29246.00	3.5	3499.12	3.5	0.96 ± 0.08	-1.76

Table 2—Continued

λ_{air}	E_{upper}	J_{upp}	E_{lower}	J_{low}	A-value	$\log(gf)$
Å	(cm $^{-1}$)		(cm $^{-1}$)		(10 6 s $^{-1}$)	
3883.80	28429.38	2.5	2688.69	2.5	1.00 ± 0.08	-1.87
3885.28	29640.51	6.5	3909.62	6.5	36.0 ± 1.9	0.06
3885.90	30112.78	3.5	4386.03	4.5	3.54 ± 0.21	-1.19
3887.11	30104.78	4.5	4386.03	4.5	1.47 ± 0.13	-1.48
3889.14	28394.04	2.5	2688.69	2.5	3.18 ± 0.17	-1.36
3890.08	27188.30	3.5	1489.16	3.5	6.2 ± 0.3	-0.95
3891.19	27210.12	0.5	1518.29	0.5	10.6 ± 0.6	-1.32
3894.06	28725.53	4.5	3052.65	5.5	4.37 ± 0.24	-1.00
3895.42	30981.48	5.5	5317.56	5.5	0.84 ± 0.09	-1.64
3896.97	25980.32	2.5	326.64	1.5	15.7 ± 0.8	-0.67
3897.26	30969.35	4.5	5317.56	5.5	2.01 ± 0.22	-1.34
3900.88	27631.18	2.5	2003.23	1.5	3.37 ± 0.22	-1.34
3902.33	27107.62	3.5	1489.16	3.5	0.51 ± 0.04	-2.03
3906.80	27078.30	2.5	1489.16	3.5	0.63 ± 0.04	-2.06

Table 2—Continued

λ_{air}	E_{upper}	J_{upp}	E_{lower}	J_{low}	A-value	$\log(gf)$
Å	(cm ⁻¹)		(cm ⁻¹)		(10 ⁶ s ⁻¹)	
3910.09	28256.32	3.5	2688.69	2.5	1.29 ± 0.08	-1.63
3910.92	30879.74	6.5	5317.56	5.5	0.88 ± 0.08	-1.55
3912.97	29934.80	5.5	4386.03	4.5	1.28 ± 0.15	-1.45
3913.55	27063.30	1.5	1518.29	0.5	1.18 ± 0.10	-1.97
3917.43	26357.90	2.5	838.22	2.5	7.2 ± 0.4	-1.00
3918.61	27001.20	4.5	1489.16	3.5	1.30 ± 0.07	-1.52
3920.76	28997.14	4.5	3499.12	3.5	0.277 ± 0.029	-2.20
3922.39	28540.12	5.5	3052.65	5.5	19.9 ± 1.0	-0.26
3922.69	26974.67	2.5	1489.16	3.5	1.51 ± 0.10	-1.68
3928.28	26938.42	3.5	1489.16	3.5	15.3 ± 0.8	-0.55
3931.16	28929.72	2.5	3499.12	3.5	0.75 ± 0.08	-1.98
3932.97	29804.88	4.5	4386.03	4.5	1.54 ± 0.10	-1.45
3933.59	28913.99	4.5	3499.12	3.5	5.2 ± 0.3	-0.91
3935.18	29314.23	5.5	3909.62	6.5	0.42 ± 0.03	-1.93

Table 2—Continued

λ_{air}	E _{upper}	J _{upp}	E _{lower}	J _{low}	A-value	log(gf)
Å	(cm ⁻¹)		(cm ⁻¹)		(10 ⁶ s ⁻¹)	
3935.76	27638.83	5.5	2237.97	4.5	3.20 ± 0.17	-1.05
3937.06	30710.03	5.5	5317.56	5.5	4.29 ± 0.24	-0.92
3938.43	28072.33	3.5	2688.69	2.5	0.46 ± 0.06	-2.07
3941.88	25361.45	1.5	0.00	0.5	14.9 ± 0.8	-0.86
3943.24	26190.92	2.5	838.22	2.5	7.1 ± 0.4	-1.01
3945.99	30652.56	4.5	5317.56	5.5	0.195 ± 0.029	-2.34
3946.51	26820.81	4.5	1489.16	3.5	4.95 ± 0.27	-0.94
3947.83	28011.88	1.5	2688.69	2.5	8.7 ± 0.5	-1.09
3948.11	26159.60	3.5	838.22	2.5	7.7 ± 0.4	-0.84
3954.35	27284.69	2.5	2003.23	1.5	0.32 ± 0.05	-2.34
3957.47	28314.18	4.5	3052.65	5.5	0.42 ± 0.03	-2.01
3958.70	27942.33	1.5	2688.69	2.5	2.36 ± 0.20	-1.65
3959.52	26086.63	3.5	838.22	2.5	2.96 ± 0.17	-1.25
3961.81	29619.89	3.5	4386.03	4.5	2.74 ± 0.18	-1.29

Table 2—Continued

λ_{air}	E_{upper}	J_{upp}	E_{lower}	J_{low}	A-value	$\log(gf)$
Å	(cm ⁻¹)		(cm ⁻¹)		(10 ⁶ s ⁻¹)	
3962.25	28730.14	3.5	3499.12	3.5	1.46 ± 0.10	-1.56
3962.98	28725.53	4.5	3499.12	3.5	3.75 ± 0.21	-1.05
3964.08	25546.03	2.5	326.64	1.5	0.392 ± 0.029	-2.26
3966.05	27210.12	0.5	2003.23	1.5	26.7 ± 1.4	-0.90
3966.33	29591.12	4.5	4386.03	4.5	1.50 ± 0.09	-1.45
3967.67	30514.16	4.5	5317.56	5.5	8.1 ± 0.5	-0.72
3970.53	25178.45	1.5	0.00	0.5	10.7 ± 0.6	-1.00
3971.39	28672.08	2.5	3499.12	3.5	32.6 ± 1.7	-0.34
3973.10	27165.35	2.5	2003.23	1.5	0.52 ± 0.04	-2.13
3975.22	27386.69	4.5	2237.97	4.5	1.10 ± 0.07	-1.58
3976.27	25980.32	2.5	838.22	2.5	8.8 ± 0.5	-0.90
3976.43	27829.77	1.5	2688.69	2.5	27.4 ± 1.4	-0.58
3976.71	28191.96	4.5	3052.65	5.5	0.228 ± 0.029	-2.27
3979.20	29509.60	3.5	4386.03	4.5	17.8 ± 0.9	-0.47

Table 2—Continued

λ_{air}	E_{upper}	J_{upp}	E_{lower}	J_{low}	A-value	$\log(gf)$
Å	(cm $^{-1}$)		(cm $^{-1}$)		(10 6 s $^{-1}$)	
3983.14	28151.40	5.5	3052.65	5.5	8.7 ± 0.5	-0.61
3986.68	26565.61	4.5	1489.16	3.5	5.9 ± 0.3	-0.85
3986.90	27078.30	2.5	2003.23	1.5	2.71 ± 0.16	-1.41
3987.07	28573.13	2.5	3499.12	3.5	0.91 ± 0.07	-1.89
3987.42	27309.73	4.5	2237.97	4.5	3.10 ± 0.17	-1.13
3990.01	25055.54	1.5	0.00	0.5	9.2 ± 1.0	-1.06
3993.31	25361.45	1.5	326.64	1.5	12.3 ± 0.6	-0.93
4003.44	26974.67	2.5	2003.23	1.5	4.57 ± 0.24	-1.18
4003.70	28022.50	4.5	3052.65	5.5	1.22 ± 0.07	-1.53
4004.26	26484.66	1.5	1518.29	0.5	0.96 ± 0.06	-2.03
4006.57	25790.15	3.5	838.22	2.5	1.66 ± 0.11	-1.50
4006.83	27188.30	3.5	2237.97	4.5	0.88 ± 0.05	-1.77
4007.48	28445.43	3.5	3499.12	3.5	4.43 ± 0.28	-1.07
4008.09	27631.18	2.5	2688.69	2.5	1.59 ± 0.13	-1.64

Table 2—Continued

λ_{air}	E_{upper}	J_{upp}	E_{lower}	J_{low}	A-value	$\log(gf)$
Å	(cm ⁻¹)		(cm ⁻¹)		(10 ⁶ s ⁻¹)	
4008.33	28850.60	5.5	3909.62	6.5	0.83 ± 0.06	-1.62
4009.36	27987.24	5.5	3052.65	5.5	0.182 ± 0.016	-2.28
4011.72	24919.90	0.5	0.00	0.5	1.02 ± 0.07	-2.31
4015.75	28394.04	2.5	3499.12	3.5	1.35 ± 0.10	-1.71
4019.83	27107.62	3.5	2237.97	4.5	1.52 ± 0.09	-1.53
4019.98	26357.90	2.5	1489.16	3.5	3.91 ± 0.23	-1.25
4020.78	27552.45	3.5	2688.69	2.5	0.302 ± 0.027	-2.23
4021.39	29246.00	3.5	4386.03	4.5	0.52 ± 0.04	-1.99
4022.71	25178.45	1.5	326.64	1.5	0.98 ± 0.08	-2.02
4023.22	25175.32	2.5	326.64	1.5	8.0 ± 0.4	-0.93
4037.10	27001.20	4.5	2237.97	4.5	1.44 ± 0.08	-1.45
4038.09	28256.32	3.5	3499.12	3.5	2.03 ± 0.11	-1.40
4041.67	26253.55	0.5	1518.29	0.5	21.0 ± 1.1	-0.99
4042.71	25055.54	1.5	326.64	1.5	10.5 ± 0.7	-0.99

Table 2—Continued

λ_{air}	E _{upper}	J _{upp}	E _{lower}	J _{low}	A-value	log(gf)
Å	(cm ⁻¹)		(cm ⁻¹)		(10 ⁶ s ⁻¹)	
4042.90	25565.97	3.5	838.22	2.5	9.8 ± 0.5	-0.72
4044.06	26723.87	1.5	2003.23	1.5	3.28 ± 0.20	-1.49
4045.05	25552.80	1.5	838.22	2.5	4.2 ± 0.3	-1.38
4046.16	25546.03	2.5	838.22	2.5	3.66 ± 0.22	-1.27
4047.15	26190.92	2.5	1489.16	3.5	8.2 ± 0.4	-0.92
4047.37	26938.42	3.5	2237.97	4.5	1.63 ± 0.09	-1.50
4049.56	26690.30	0.5	2003.23	1.5	3.5 ± 0.4	-1.76
4050.62	29998.15	4.5	5317.56	5.5	1.12 ± 0.08	-1.56
4052.29	26159.60	3.5	1489.16	3.5	0.164 ± 0.013	-2.49
4056.75	27695.96	6.5	3052.65	5.5	0.062 ± 0.008	-2.67
4058.86	28540.12	5.5	3909.62	6.5	4.68 ± 0.25	-0.86
4061.05	29934.80	5.5	5317.56	5.5	1.53 ± 0.12	-1.34
4062.06	28997.14	4.5	4386.03	4.5	0.29 ± 0.03	-2.15
4063.54	24928.80	2.5	326.64	1.5	10.8 ± 0.6	-0.79

Table 2—Continued

λ_{air}	E_{upper}	J_{upp}	E_{lower}	J_{low}	A-value	$\log(gf)$
Å	(cm ⁻¹)		(cm ⁻¹)		(10 ⁶ s ⁻¹)	
4064.31	26086.63	3.5	1489.16	3.5	2.68 ± 0.14	-1.28
4064.55	27284.69	2.5	2688.69	2.5	14.3 ± 0.7	-0.67
4065.01	24919.90	0.5	326.64	1.5	0.92 ± 0.08	-2.34
4065.49	26828.29	5.5	2237.97	4.5	0.108 ± 0.015	-2.49
4066.18	27638.83	5.5	3052.65	5.5	0.55 ± 0.03	-1.79
4066.73	26820.81	4.5	2237.97	4.5	7.3 ± 0.4	-0.74
4068.32	28072.33	3.5	3499.12	3.5	8.8 ± 0.5	-0.76
4070.98	26046.35	4.5	1489.16	3.5	0.370 ± 0.024	-2.04
4075.83	28913.99	4.5	4386.03	4.5	15.0 ± 0.8	-0.43
4076.62	25361.45	1.5	838.22	2.5	4.67 ± 0.26	-1.33
4076.85	24848.47	2.5	326.64	1.5	1.07 ± 0.06	-1.79
4080.55	27188.30	3.5	2688.69	2.5	3.58 ± 0.20	-1.15
4081.95	25980.32	2.5	1489.16	3.5	1.28 ± 0.07	-1.72
4082.59	29804.88	4.5	5317.56	5.5	7.6 ± 0.4	-0.72

Table 2—Continued

λ_{air}	E_{upper}	J_{upp}	E_{lower}	J_{low}	A-value	$\log(gf)$
Å	(cm ⁻¹)		(cm ⁻¹)		(10 ⁶ s ⁻¹)	
4083.23	29801.08	5.5	5317.56	5.5	1.27 ± 0.09	-1.42
4083.58	26484.66	1.5	2003.23	1.5	6.0 ± 0.3	-1.22
4084.37	27165.35	2.5	2688.69	2.5	3.06 ± 0.20	-1.34
4092.25	24429.52	1.5	0.00	0.5	13.5 ± 0.7	-0.87
4093.04	27923.96	2.5	3499.12	3.5	0.90 ± 0.11	-1.87
4094.03	27107.62	3.5	2688.69	2.5	3.51 ± 0.20	-1.15
4098.95	27078.30	2.5	2688.69	2.5	1.10 ± 0.07	-1.78
4101.47	27063.30	1.5	2688.69	2.5	0.43 ± 0.05	-2.36
4104.83	26357.90	2.5	2003.23	1.5	0.086 ± 0.010	-2.89
4106.61	28730.14	3.5	4386.03	4.5	1.31 ± 0.13	-1.58
4107.27	25178.45	1.5	838.22	2.5	3.72 ± 0.20	-1.42
4107.39	28725.53	4.5	4386.03	4.5	11.4 ± 0.6	-0.54
4107.79	25175.32	2.5	838.22	2.5	0.46 ± 0.03	-2.16
4108.31	27386.69	4.5	3052.65	5.5	1.39 ± 0.08	-1.45

Table 2—Continued

λ_{air}	E_{upper}	J_{upp}	E_{lower}	J_{low}	A-value	$\log(gf)$
Å	(cm $^{-1}$)		(cm $^{-1}$)		(10 6 s $^{-1}$)	
4109.39	26565.61	4.5	2237.97	4.5	3.64 ± 0.19	-1.04
4110.18	29640.51	6.5	5317.56	5.5	2.98 ± 0.18	-0.98
4113.90	25790.15	3.5	1489.16	3.5	4.15 ± 0.22	-1.07
4116.44	26974.67	2.5	2688.69	2.5	3.42 ± 0.19	-1.28
4118.55	29591.12	4.5	5317.56	5.5	33.3 ± 1.7	-0.07
4119.57	26505.53	5.5	2237.97	4.5	1.21 ± 0.08	-1.43
4121.34	27309.73	4.5	3052.65	5.5	4.72 ± 0.26	-0.92
4121.54	24582.59	2.5	326.64	1.5	1.42 ± 0.09	-1.66
4122.49	26253.55	0.5	2003.23	1.5	11.1 ± 0.6	-1.25
4123.95	28151.40	5.5	3909.62	6.5	6.6 ± 0.3	-0.69
4128.11	25055.54	1.5	838.22	2.5	0.43 ± 0.05	-2.35
4133.17	26190.92	2.5	2003.23	1.5	1.41 ± 0.08	-1.67
4138.92	28540.12	5.5	4386.03	4.5	0.77 ± 0.07	-1.62
4142.70	27631.18	2.5	3499.12	3.5	1.28 ± 0.08	-1.70

Table 2—Continued

λ_{air}	E_{upper}	J_{upp}	E_{lower}	J_{low}	A-value	$\log(gf)$
Å	(cm ⁻¹)		(cm ⁻¹)		(10 ⁶ s ⁻¹)	
4146.74	25597.70	4.5	1489.16	3.5	1.11 ± 0.07	-1.54
4147.71	24429.52	1.5	326.64	1.5	3.94 ± 0.21	-1.39
4149.83	24928.80	2.5	838.22	2.5	8.0 ± 0.4	-0.91
4152.06	27987.24	5.5	3909.62	6.5	1.54 ± 0.09	-1.32
4152.20	25565.97	3.5	1489.16	3.5	9.3 ± 0.5	-0.72
4153.32	29387.87	4.5	5317.56	5.5	9.6 ± 0.5	-0.61
4155.21	28445.43	3.5	4386.03	4.5	9.0 ± 0.6	-0.73
4155.65	25546.03	2.5	1489.16	3.5	0.309 ± 0.025	-2.32
4156.26	27552.45	3.5	3499.12	3.5	2.17 ± 0.12	-1.35
4159.40	26723.87	1.5	2688.69	2.5	2.53 ± 0.17	-1.58
4159.51	25552.80	1.5	1518.29	0.5	1.55 ± 0.13	-1.79
4163.14	24013.56	1.5	0.00	0.5	2.38 ± 0.15	-1.61
4163.71	24848.47	2.5	838.22	2.5	1.15 ± 0.07	-1.74
4169.47	25980.32	2.5	2003.23	1.5	11.2 ± 0.6	-0.76

Table 2—Continued

λ_{air}	E _{upper}	J _{upp}	E _{lower}	J _{low}	A-value	log(gf)
Å	(cm ⁻¹)		(cm ⁻¹)		(10 ⁶ s ⁻¹)	
4174.44	27001.20	4.5	3052.65	5.5	2.07 ± 0.11	-1.27
4179.14	26159.60	3.5	2237.97	4.5	0.124 ± 0.017	-2.59
4183.77	24221.81	0.5	326.64	1.5	17.0 ± 0.9	-1.05
4185.10	27386.69	4.5	3499.12	3.5	0.146 ± 0.014	-2.42
4188.13	28256.32	3.5	4386.03	4.5	17.3 ± 0.9	-0.44
4191.41	24689.84	3.5	838.22	2.5	0.125 ± 0.015	-2.58
4191.93	26086.63	3.5	2237.97	4.5	4.31 ± 0.23	-1.04
4192.89	25361.45	1.5	1518.29	0.5	0.366 ± 0.025	-2.41
4195.57	26880.60	5.5	3052.65	5.5	0.206 ± 0.024	-2.19
4197.86	25304.09	3.5	1489.16	3.5	0.49 ± 0.04	-1.98
4199.02	26046.35	4.5	2237.97	4.5	0.191 ± 0.018	-2.30
4199.45	28191.96	4.5	4386.03	4.5	3.33 ± 0.22	-1.06
4201.21	26484.66	1.5	2688.69	2.5	0.76 ± 0.06	-2.09
4202.91	27695.96	6.5	3909.62	6.5	2.82 ± 0.17	-0.98

Table 2—Continued

λ_{air}	E _{upper}	J _{upp}	E _{lower}	J _{low}	A-value	log(gf)
Å	(cm ⁻¹)		(cm ⁻¹)		(10 ⁶ s ⁻¹)	
4203.05	27284.69	2.5	3499.12	3.5	19.7 ± 1.0	-0.51
4204.80	26828.29	5.5	3052.65	5.5	0.358 ± 0.027	-1.94
4206.12	26820.81	4.5	3052.65	5.5	7.1 ± 0.4	-0.72
4206.62	28151.40	5.5	4386.03	4.5	4.68 ± 0.25	-0.83
4210.34	24582.59	2.5	838.22	2.5	6.9 ± 0.4	-0.96
4212.93	27639.40	6.5	3909.62	6.5	0.64 ± 0.06	-1.62
4213.03	27638.83	5.5	3909.62	6.5	0.48 ± 0.04	-1.81
4220.15	27188.30	3.5	3499.12	3.5	3.14 ± 0.18	-1.17
4220.55	24013.56	1.5	326.64	1.5	0.48 ± 0.04	-2.29
4220.66	28072.33	3.5	4386.03	4.5	16.8 ± 1.0	-0.44
4220.69	25175.32	2.5	1489.16	3.5	0.316 ± 0.027	-2.29
4221.86	28997.14	4.5	5317.56	5.5	0.59 ± 0.07	-1.80
4223.71	26357.90	2.5	2688.69	2.5	3.33 ± 0.18	-1.27
4224.24	27165.35	2.5	3499.12	3.5	0.96 ± 0.07	-1.81

Table 2—Continued

λ_{air}	E _{upper}	J _{upp}	E _{lower}	J _{low}	A-value	log(gf)
Å	(cm ⁻¹)		(cm ⁻¹)		(10 ⁶ s ⁻¹)	
4225.32	25178.45	1.5	1518.29	0.5	22.5 ± 1.2	-0.62
4229.56	28022.50	4.5	4386.03	4.5	0.315 ± 0.029	-2.07
4229.71	23962.25	1.5	326.64	1.5	12.6 ± 0.7	-0.87
4234.57	27107.62	3.5	3499.12	3.5	10.7 ± 0.6	-0.64
4235.88	27987.24	5.5	4386.03	4.5	0.32 ± 0.03	-1.98
4236.74	28913.99	4.5	5317.56	5.5	22.9 ± 1.2	-0.21
4237.66	24429.52	1.5	838.22	2.5	9.0 ± 0.5	-1.01
4244.70	25790.15	3.5	2237.97	4.5	7.2 ± 0.4	-0.81
4245.17	25552.80	1.5	2003.23	1.5	3.11 ± 0.24	-1.47
4246.39	25546.03	2.5	2003.23	1.5	0.142 ± 0.021	-2.64
4247.39	25055.54	1.5	1518.29	0.5	1.02 ± 0.08	-1.96
4248.15	28850.60	5.5	5317.56	5.5	0.190 ± 0.027	-2.21
4251.31	23842.20	2.5	326.64	1.5	0.135 ± 0.016	-2.66
4251.78	26565.61	4.5	3052.65	5.5	2.88 ± 0.16	-1.11

Table 2—Continued

λ_{air}	E_{upper}	J_{upp}	E_{lower}	J_{low}	A-value	$\log(gf)$
Å	(cm ⁻¹)		(cm ⁻¹)		(10 ⁶ s ⁻¹)	
4253.72	26190.92	2.5	2688.69	2.5	1.11 ± 0.07	-1.74
4256.39	26540.12	6.5	3052.65	5.5	18.5 ± 1.0	-0.15
4258.55	26974.67	2.5	3499.12	3.5	4.35 ± 0.24	-1.15
4259.39	26159.60	3.5	2688.69	2.5	0.309 ± 0.025	-2.17
4262.67	26505.53	5.5	3052.65	5.5	9.9 ± 0.5	-0.49
4265.08	24928.80	2.5	1489.16	3.5	5.5 ± 0.3	-1.04
4270.85	28725.53	4.5	5317.56	5.5	4.93 ± 0.27	-0.87
4272.01	24919.90	0.5	1518.29	0.5	1.97 ± 0.12	-1.97
4279.50	26413.29	5.5	3052.65	5.5	0.336 ± 0.022	-1.96
4279.67	25597.70	4.5	2237.97	4.5	11.0 ± 0.6	-0.52
4279.74	24848.47	2.5	1489.16	3.5	3.48 ± 0.19	-1.24
4279.94	25361.45	1.5	2003.23	1.5	9.1 ± 0.5	-1.00
4280.32	24194.38	2.5	838.22	2.5	1.11 ± 0.09	-1.74
4280.78	27263.25	7.5	3909.62	6.5	26.2 ± 1.5	0.06

Table 2—Continued

λ_{air}	E _{upper}	J _{upp}	E _{lower}	J _{low}	A-value	log(gf)
Å	(cm ⁻¹)		(cm ⁻¹)		(10 ⁶ s ⁻¹)	
4281.01	23352.41	0.5	0.00	0.5	11.2 ± 0.6	-1.21
4284.51	23659.99	0.5	326.64	1.5	1.13 ± 0.07	-2.21
4285.49	25565.97	3.5	2237.97	4.5	6.4 ± 0.4	-0.85
4286.65	26820.81	4.5	3499.12	3.5	3.92 ± 0.23	-0.97
4292.18	25980.32	2.5	2688.69	2.5	7.4 ± 0.4	-0.91
4299.35	27638.83	5.5	4386.03	4.5	0.94 ± 0.06	-1.51
4304.95	28540.12	5.5	5317.56	5.5	4.02 ± 0.26	-0.87
4309.01	24689.84	3.5	1489.16	3.5	8.1 ± 0.4	-0.74
4313.32	23177.49	1.5	0.00	0.5	0.52 ± 0.05	-2.24
4313.72	24013.56	1.5	838.22	2.5	1.72 ± 0.10	-1.72
4313.74	25178.45	1.5	2003.23	1.5	1.01 ± 0.08	-1.95
4314.32	25175.32	2.5	2003.23	1.5	0.235 ± 0.016	-2.40
4315.38	27552.45	3.5	4386.03	4.5	1.16 ± 0.09	-1.59
4318.93	25385.36	5.5	2237.97	4.5	16.9 ± 0.9	-0.25

Table 2—Continued

λ_{air}	E_{upper}	J_{upp}	E_{lower}	J_{low}	A-value	$\log(gf)$
Å	(cm ⁻¹)		(cm ⁻¹)		(10 ⁶ s ⁻¹)	
4323.29	23962.25	1.5	838.22	2.5	10.6 ± 0.6	-0.92
4327.51	25790.15	3.5	2688.69	2.5	0.77 ± 0.05	-1.76
4329.02	24582.59	2.5	1489.16	3.5	18.4 ± 0.9	-0.51
4334.07	26565.61	4.5	3499.12	3.5	0.279 ± 0.026	-2.10
4334.14	25304.09	3.5	2237.97	4.5	14.0 ± 0.7	-0.50
4336.74	25055.54	1.5	2003.23	1.5	0.99 ± 0.08	-1.95
4345.85	23842.20	2.5	838.22	2.5	5.20 ± 0.27	-1.05
4346.48	27386.69	4.5	4386.03	4.5	0.61 ± 0.05	-1.77
4347.24	28314.18	4.5	5317.56	5.5	0.58 ± 0.05	-1.79
4347.80	26046.35	4.5	3052.65	5.5	13.3 ± 0.7	-0.42
4350.47	26889.18	7.5	3909.62	6.5	5.6 ± 0.4	-0.59
4352.10	26880.60	5.5	3909.62	6.5	7.4 ± 0.4	-0.60
4360.72	24928.80	2.5	2003.23	1.5	7.9 ± 0.4	-0.87
4361.07	27309.73	4.5	4386.03	4.5	2.93 ± 0.20	-1.08

Table 2—Continued

λ_{air}	E_{upper}	J_{upp}	E_{lower}	J_{low}	A-value	$\log(gf)$
Å	(cm ⁻¹)		(cm ⁻¹)		(10 ⁶ s ⁻¹)	
4362.03	26828.29	5.5	3909.62	6.5	9.9 ± 0.5	-0.47
4362.41	24919.90	0.5	2003.23	1.5	0.66 ± 0.06	-2.43
4363.45	24429.52	1.5	1518.29	0.5	4.32 ± 0.25	-1.31
4368.02	25939.87	6.5	3052.65	5.5	2.97 ± 0.16	-0.93
4369.92	25565.97	3.5	2688.69	2.5	2.36 ± 0.14	-1.27
4370.47	28191.96	4.5	5317.56	5.5	0.89 ± 0.09	-1.59
4372.44	25552.80	1.5	2688.69	2.5	0.29 ± 0.05	-2.47
4373.46	26357.90	2.5	3499.12	3.5	7.9 ± 0.4	-0.87
4373.73	25546.03	2.5	2688.69	2.5	0.47 ± 0.04	-2.09
4374.98	23177.49	1.5	326.64	1.5	3.69 ± 0.20	-1.37
4376.05	24848.47	2.5	2003.23	1.5	0.244 ± 0.029	-2.38
4378.23	28151.40	5.5	5317.56	5.5	7.1 ± 0.4	-0.61
4384.30	27188.30	3.5	4386.03	4.5	4.13 ± 0.27	-1.02
4390.86	24257.37	4.5	1489.16	3.5	12.4 ± 0.7	-0.45

Table 2—Continued

λ_{air}	E_{upper}	J_{upp}	E_{lower}	J_{low}	A-value	$\log(gf)$
Å	(cm ⁻¹)		(cm ⁻¹)		(10 ⁶ s ⁻¹)	
4399.86	27107.62	3.5	4386.03	4.5	1.25 ± 0.07	-1.54
4403.04	24194.38	2.5	1489.16	3.5	1.18 ± 0.10	-1.69
4403.37	24221.81	0.5	1518.29	0.5	15.1 ± 0.8	-1.06
4405.64	26190.92	2.5	3499.12	3.5	0.81 ± 0.05	-1.85
4409.34	25361.45	1.5	2688.69	2.5	10.9 ± 0.7	-0.89
4409.94	27987.24	5.5	5317.56	5.5	0.100 ± 0.012	-2.46
4411.73	26159.60	3.5	3499.12	3.5	0.38 ± 0.03	-2.05
4417.57	26540.12	6.5	3909.62	6.5	3.29 ± 0.18	-0.87
4420.52	25304.09	3.5	2688.69	2.5	15.8 ± 0.8	-0.43
4421.13	25664.97	6.5	3052.65	5.5	7.9 ± 0.5	-0.49
4424.34	26505.53	5.5	3909.62	6.5	39.2 ± 2.0	0.14
4425.98	26086.63	3.5	3499.12	3.5	0.51 ± 0.05	-1.92
4427.58	24582.59	2.5	2003.23	1.5	2.89 ± 0.16	-1.29
4427.79	24816.28	5.5	2237.97	4.5	0.436 ± 0.027	-1.81

Table 2—Continued

λ_{air}	E_{upper}	J_{upp}	E_{lower}	J_{low}	A-value	$\log(gf)$
Å	(cm $^{-1}$)		(cm $^{-1}$)		(10 6 s $^{-1}$)	
4433.89	26046.35	4.5	3499.12	3.5	22.1 ± 1.1	-0.19
4434.32	25597.70	4.5	3052.65	5.5	28.6 ± 1.5	-0.07
4442.47	26413.29	5.5	3909.62	6.5	1.14 ± 0.07	-1.39
4444.27	26880.60	5.5	4386.03	4.5	9.6 ± 0.5	-0.47
4446.91	25980.32	2.5	3499.12	3.5	0.92 ± 0.07	-1.79
4449.97	30511.73	3.5	8046.00	3.5	0.55 ± 0.06	-1.88
4452.72	24689.84	3.5	2237.97	4.5	16.2 ± 0.8	-0.41
4454.63	26828.29	5.5	4386.03	4.5	17.6 ± 0.9	-0.20
4456.11	26820.81	4.5	4386.03	4.5	1.27 ± 0.08	-1.42
4457.80	24429.52	1.5	2003.23	1.5	0.45 ± 0.06	-2.27
4458.51	23260.95	3.5	838.22	2.5	9.1 ± 0.5	-0.66
4467.34	27695.96	6.5	5317.56	5.5	34.0 ± 1.7	0.15
4469.65	25055.54	1.5	2688.69	2.5	2.04 ± 0.16	-1.61
4472.41	23842.20	2.5	1489.16	3.5	6.0 ± 0.3	-0.96

Table 2—Continued

λ_{air}	E _{upper}	J _{upp}	E _{lower}	J _{low}	A-value	log(gf)
Å	(cm ⁻¹)		(cm ⁻¹)		(10 ⁶ s ⁻¹)	
4473.01	24588.00	5.5	2237.97	4.5	6.2 ± 0.3	-0.65
4475.17	23177.49	1.5	838.22	2.5	1.23 ± 0.07	-1.83
4478.66	27639.40	6.5	5317.56	5.5	10.4 ± 0.5	-0.36
4495.12	24928.80	2.5	2688.69	2.5	0.42 ± 0.03	-2.12
4499.48	24221.81	0.5	2003.23	1.5	22.0 ± 1.2	-0.87
4505.04	24194.38	2.5	2003.23	1.5	2.08 ± 0.15	-1.42
4507.39	26565.61	4.5	4386.03	4.5	0.141 ± 0.014	-2.37
4511.83	23646.90	4.5	1489.16	3.5	4.99 ± 0.27	-0.82
4515.10	23659.99	0.5	1518.29	0.5	21.9 ± 1.1	-0.87
4517.27	29655.90	1.5	7524.86	2.5	3.47 ± 0.29	-1.37
4519.63	26505.53	5.5	4386.03	4.5	12.1 ± 0.6	-0.35
4523.03	22429.49	2.5	326.64	1.5	5.5 ± 0.3	-0.99
4523.91	25597.70	4.5	3499.12	3.5	13.2 ± 0.7	-0.39
4529.95	27386.69	4.5	5317.56	5.5	0.195 ± 0.019	-2.22

Table 2—Continued

λ_{air}	E_{upper}	J_{upp}	E_{lower}	J_{low}	A-value	$\log(gf)$
Å	(cm $^{-1}$)		(cm $^{-1}$)		(10 6 s $^{-1}$)	
4536.51	22875.41	3.5	838.22	2.5	2.14 ± 0.12	-1.28
4537.94	25939.87	6.5	3909.62	6.5	7.7 ± 0.4	-0.48
4538.56	26413.29	5.5	4386.03	4.5	1.57 ± 0.09	-1.23
4540.18	24257.37	4.5	2237.97	4.5	1.68 ± 0.10	-1.28
4542.05	24013.56	1.5	2003.23	1.5	7.3 ± 0.4	-1.04
4543.94	24689.84	3.5	2688.69	2.5	13.0 ± 0.7	-0.49
4545.80	27309.73	4.5	5317.56	5.5	0.63 ± 0.05	-1.71
4552.66	23962.25	1.5	2003.23	1.5	12.1 ± 0.6	-0.82
4554.44	22788.68	3.5	838.22	2.5	2.24 ± 0.12	-1.25
4556.50	29986.54	2.5	8046.00	3.5	4.4 ± 0.3	-1.09
4560.42	22248.32	2.5	326.64	1.5	3.10 ± 0.16	-1.24
4564.07	21904.12	1.5	0.00	0.5	1.08 ± 0.07	-1.87
4566.20	24582.59	2.5	2688.69	2.5	13.8 ± 0.7	-0.59
4577.69	23842.20	2.5	2003.23	1.5	11.8 ± 0.6	-0.65

Table 2—Continued

λ_{air}	E_{upper}	J_{upp}	E_{lower}	J_{low}	A-value	$\log(gf)$
Å	(cm ⁻¹)		(cm ⁻¹)		(10 ⁶ s ⁻¹)	
4578.70	23352.41	0.5	1518.29	0.5	1.91 ± 0.11	-1.92
4579.04	30511.73	3.5	8679.23	4.5	3.78 ± 0.28	-1.02
4584.83	25304.09	3.5	3499.12	3.5	8.9 ± 0.5	-0.65
4589.41	31189.83	4.5	9406.63	5.5	2.62 ± 0.22	-1.08
4591.44	26159.60	3.5	4386.03	4.5	0.087 ± 0.013	-2.66
4591.81	23260.95	3.5	1489.16	3.5	3.00 ± 0.17	-1.12
4593.53	24816.28	5.5	3052.65	5.5	3.89 ± 0.21	-0.83
4594.57	32852.81	6.5	11094.06	7.5	2.90 ± 0.23	-0.89
4595.28	25664.97	6.5	3909.62	6.5	7.2 ± 0.4	-0.50
4598.35	24429.52	1.5	2688.69	2.5	2.90 ± 0.18	-1.43
4603.11	33763.45	7.5	12045.10	8.5	3.60 ± 0.30	-0.74
4604.17	22039.98	2.5	326.64	1.5	2.13 ± 0.12	-1.39
4606.51	21702.33	1.5	0.00	0.5	4.32 ± 0.24	-1.26
4606.88	26086.63	3.5	4386.03	4.5	1.29 ± 0.09	-1.49

Table 2—Continued

λ_{air}	E_{upper}	J_{upp}	E_{lower}	J_{low}	A-value	$\log(gf)$
Å	(cm ⁻¹)		(cm ⁻¹)		(10 ⁶ s ⁻¹)	
4610.48	27001.20	4.5	5317.56	5.5	0.120 ± 0.011	-2.42
4612.06	25175.32	2.5	3499.12	3.5	0.141 ± 0.014	-2.57
4615.44	26046.35	4.5	4386.03	4.5	6.3 ± 0.3	-0.69
4615.68	23177.49	1.5	1518.29	0.5	11.2 ± 0.6	-0.84
4616.49	21655.42	0.5	0.00	0.5	1.06 ± 0.07	-2.17
4624.98	31830.06	5.5	10214.38	6.5	1.03 ± 0.10	-1.40
4630.20	22429.49	2.5	838.22	2.5	1.80 ± 0.10	-1.46
4630.59	32549.64	3.5	10960.16	4.5	1.75 ± 0.22	-1.35
4633.16	21904.12	1.5	326.64	1.5	0.205 ± 0.013	-2.58
4636.27	26880.60	5.5	5317.56	5.5	1.80 ± 0.09	-1.16
4642.23	24588.00	5.5	3052.65	5.5	8.9 ± 0.5	-0.46
4646.68	23752.70	4.5	2237.97	4.5	2.86 ± 0.16	-1.03
4647.54	26828.29	5.5	5317.56	5.5	2.83 ± 0.16	-0.96
4648.16	21507.87	1.5	0.00	0.5	2.36 ± 0.13	-1.51

Table 2—Continued

λ_{air}	E _{upper}	J _{upp}	E _{lower}	J _{low}	A-value	log(gf)
Å	(cm ⁻¹)		(cm ⁻¹)		(10 ⁶ s ⁻¹)	
4648.63	24194.38	2.5	2688.69	2.5	0.229 ± 0.023	-2.35
4649.16	26820.81	4.5	5317.56	5.5	0.37 ± 0.06	-1.92
4655.11	25385.36	5.5	3909.62	6.5	1.82 ± 0.11	-1.15
4665.12	24928.80	2.5	3499.12	3.5	1.92 ± 0.13	-1.42
4669.39	22248.32	2.5	838.22	2.5	12.7 ± 0.7	-0.60
4669.64	23646.90	4.5	2237.97	4.5	9.1 ± 0.5	-0.53
4670.69	25790.15	3.5	4386.03	4.5	0.99 ± 0.07	-1.59
4674.59	22875.41	3.5	1489.16	3.5	10.5 ± 0.6	-0.56
4676.90	21702.33	1.5	326.64	1.5	10.3 ± 0.6	-0.87
4682.67	24848.47	2.5	3499.12	3.5	1.40 ± 0.08	-1.56
4682.71	23352.41	0.5	2003.23	1.5	1.07 ± 0.08	-2.15
4687.19	21655.42	0.5	326.64	1.5	10.8 ± 0.6	-1.15
4693.63	22788.68	3.5	1489.16	3.5	1.25 ± 0.07	-1.48
4699.36	23962.25	1.5	2688.69	2.5	2.72 ± 0.16	-1.44

Table 2—Continued

λ_{air}	E_{upper}	J_{upp}	E_{lower}	J_{low}	A-value	$\log(gf)$
Å	(cm ⁻¹)		(cm ⁻¹)		(10 ⁶ s ⁻¹)	
4704.40	21250.75	0.5	0.00	0.5	20.6 ± 1.1	-0.86
4705.00	26565.61	4.5	5317.56	5.5	0.171 ± 0.020	-2.25
4713.07	25597.70	4.5	4386.03	4.5	4.76 ± 0.25	-0.80
4714.61	24257.37	4.5	3052.65	5.5	0.98 ± 0.06	-1.49
4715.27	22039.98	2.5	838.22	2.5	1.75 ± 0.10	-1.46
4717.73	24689.84	3.5	3499.12	3.5	4.65 ± 0.26	-0.91
4718.34	26505.53	5.5	5317.56	5.5	3.81 ± 0.20	-0.82
4719.84	21507.87	1.5	326.64	1.5	4.31 ± 0.23	-1.24
4720.13	25565.97	3.5	4386.03	4.5	0.89 ± 0.07	-1.62
4721.39	23177.49	1.5	2003.23	1.5	0.78 ± 0.05	-1.98
4726.03	23842.20	2.5	2688.69	2.5	2.80 ± 0.15	-1.25
4741.73	24582.59	2.5	3499.12	3.5	1.27 ± 0.09	-1.59
4745.68	21904.12	1.5	838.22	2.5	8.6 ± 0.5	-0.93
4755.37	23260.95	3.5	2237.97	4.5	0.52 ± 0.03	-1.85

Table 2—Continued

λ_{air}	E_{upper}	J_{upp}	E_{lower}	J_{low}	A-value	$\log(gf)$
Å	(cm ⁻¹)		(cm ⁻¹)		(10 ⁶ s ⁻¹)	
4760.73	25385.36	5.5	4386.03	4.5	0.241 ± 0.018	-2.01
4774.14	22429.49	2.5	1489.16	3.5	1.20 ± 0.07	-1.61
4775.53	33775.84	5.5	12841.60	4.5	1.41 ± 0.17	-1.24
4777.84	21250.75	0.5	326.64	1.5	5.5 ± 0.3	-1.42
4779.22	25304.09	3.5	4386.03	4.5	0.270 ± 0.017	-2.13
4781.83	24816.28	5.5	3909.62	6.5	0.83 ± 0.05	-1.47
4791.58	21702.33	1.5	838.22	2.5	2.61 ± 0.15	-1.44
4808.45	31309.40	1.5	10518.50	1.5	0.79 ± 0.14	-1.96
4815.80	22248.32	2.5	1489.16	3.5	7.2 ± 0.4	-0.82
4816.02	24257.37	4.5	3499.12	3.5	0.91 ± 0.06	-1.50
4824.68	32380.78	3.5	11659.80	2.5	1.10 ± 0.14	-1.51
4826.57	32945.19	4.5	12232.34	3.5	1.05 ± 0.13	-1.43
4829.56	23752.70	4.5	3052.65	5.5	1.51 ± 0.08	-1.28
4830.67	24194.38	2.5	3499.12	3.5	0.174 ± 0.020	-2.44

Table 2—Continued

λ_{air}	E_{upper}	J_{upp}	E_{lower}	J_{low}	A-value	$\log(gf)$
Å	(cm ⁻¹)		(cm ⁻¹)		(10 ⁶ s ⁻¹)	
4834.62	24588.00	5.5	3909.62	6.5	0.84 ± 0.05	-1.45
4836.66	21507.87	1.5	838.22	2.5	0.459 ± 0.028	-2.19
4837.66	30879.74	6.5	10214.38	6.5	1.97 ± 0.20	-1.01
4844.21	22875.41	3.5	2237.97	4.5	4.59 ± 0.25	-0.89
4847.08	32857.54	4.5	12232.34	3.5	0.82 ± 0.13	-1.54
4847.76	25939.87	6.5	5317.56	5.5	2.64 ± 0.15	-0.89
4854.37	23646.90	4.5	3052.65	5.5	1.60 ± 0.09	-1.25
4859.56	23260.95	3.5	2688.69	2.5	1.08 ± 0.07	-1.51
4865.42	28072.33	3.5	7524.86	2.5	0.33 ± 0.05	-2.03
4869.99	29934.80	5.5	9406.63	5.5	2.6 ± 0.3	-0.95
4879.35	23177.49	1.5	2688.69	2.5	0.207 ± 0.025	-2.53
4891.94	31309.40	1.5	10873.30	2.5	3.5 ± 0.4	-1.30
4893.34	24816.28	5.5	4386.03	4.5	1.10 ± 0.07	-1.32
4894.29	22429.49	2.5	2003.23	1.5	0.55 ± 0.03	-1.92

Table 2—Continued

λ_{air}	E_{upper}	J_{upp}	E_{lower}	J_{low}	A-value	$\log(gf)$
Å	(cm ⁻¹)		(cm ⁻¹)		(10 ⁶ s ⁻¹)	
4900.73	28445.43	3.5	8046.00	3.5	1.76 ± 0.17	-1.30
4913.26	25664.97	6.5	5317.56	5.5	2.29 ± 0.14	-0.93
4914.30	23842.20	2.5	3499.12	3.5	0.340 ± 0.020	-2.13
4916.11	32380.78	3.5	12045.17	4.5	0.71 ± 0.12	-1.69
4920.39	28997.14	4.5	8679.23	4.5	3.4 ± 0.3	-0.90
4922.47	33775.84	5.5	13466.50	5.5	2.28 ± 0.29	-1.00
4923.81	24689.84	3.5	4386.03	4.5	0.82 ± 0.05	-1.62
4929.56	25597.70	4.5	5317.56	5.5	0.61 ± 0.05	-1.65
4935.46	31915.67	3.5	11659.80	2.5	0.98 ± 0.15	-1.54
4936.02	23752.70	4.5	3499.12	3.5	0.54 ± 0.04	-1.71
4938.09	22248.32	2.5	2003.23	1.5	1.66 ± 0.10	-1.44
4948.63	24588.00	5.5	4386.03	4.5	2.56 ± 0.15	-0.95
4952.37	22875.41	3.5	2688.69	2.5	1.89 ± 0.11	-1.25
4953.03	21702.33	1.5	1518.29	0.5	0.85 ± 0.06	-1.90

Table 2—Continued

λ_{air}	E_{upper}	J_{upp}	E_{lower}	J_{low}	A-value	$\log(gf)$
Å	(cm ⁻¹)		(cm ⁻¹)		(10 ⁶ s ⁻¹)	
4961.94	23646.90	4.5	3499.12	3.5	2.19 ± 0.13	-1.09
4964.57	21655.42	0.5	1518.29	0.5	1.86 ± 0.11	-1.86
4965.78	33598.70	5.5	13466.50	5.5	1.41 ± 0.25	-1.20
4972.17	27631.18	2.5	7524.86	2.5	5.1 ± 0.4	-0.94
4973.74	22788.68	3.5	2688.69	2.5	0.362 ± 0.026	-1.97
4989.44	22039.98	2.5	2003.23	1.5	0.384 ± 0.026	-2.06
4992.03	28072.33	3.5	8046.00	3.5	3.14 ± 0.29	-1.03
4994.62	32857.54	4.5	12841.60	4.5	1.25 ± 0.22	-1.33
5001.21	21507.87	1.5	1518.29	0.5	0.65 ± 0.04	-2.01
5016.61	27063.30	1.5	7135.06	1.5	4.2 ± 0.4	-1.19
5023.50	21904.12	1.5	2003.23	1.5	1.03 ± 0.09	-1.81
5029.66	30970.56	6.5	11094.06	7.5	0.50 ± 0.13	-1.57
5030.97	24257.37	4.5	4386.03	4.5	0.140 ± 0.018	-2.27
5031.18	31915.67	3.5	12045.17	4.5	2.7 ± 0.4	-1.09

Table 2—Continued

λ_{air}	E_{upper}	J_{upp}	E_{lower}	J_{low}	A-value	$\log(gf)$
Å	(cm ⁻¹)		(cm ⁻¹)		(10 ⁶ s ⁻¹)	
5039.93	29246.00	3.5	9410.00	2.5	0.71 ± 0.14	-1.66
5052.75	30879.74	6.5	11094.06	7.5	12.9 ± 1.2	-0.16
5057.73	28445.43	3.5	8679.23	4.5	3.2 ± 0.3	-1.00
5058.85	23260.95	3.5	3499.12	3.5	0.207 ± 0.019	-2.20
5064.24	22429.49	2.5	2688.69	2.5	0.415 ± 0.030	-2.02
5066.38	21250.75	0.5	1518.29	0.5	0.63 ± 0.04	-2.31
5069.47	29934.80	5.5	10214.38	6.5	10.5 ± 1.0	-0.31
5087.07	21655.42	0.5	2003.23	1.5	1.02 ± 0.08	-2.10
5100.26	31646.49	7.5	12045.10	8.5	5.1 ± 0.5	-0.49
5103.09	28997.14	4.5	9406.63	5.5	11.5 ± 1.0	-0.35
5104.08	29801.08	5.5	10214.38	6.5	2.15 ± 0.22	-1.00
5104.48	27631.18	2.5	8046.00	3.5	9.5 ± 0.8	-0.65
5111.15	22248.32	2.5	2688.69	2.5	0.201 ± 0.021	-2.33
5116.69	27063.30	1.5	7524.86	2.5	12.1 ± 1.0	-0.72

Table 2—Continued

λ_{air}	E_{upper}	J_{upp}	E_{lower}	J_{low}	A-value	$\log(gf)$
Å	(cm ⁻¹)		(cm ⁻¹)		(10 ⁶ s ⁻¹)	
5124.84	28913.99	4.5	9406.63	5.5	2.16 ± 0.24	-1.07
5125.56	21507.87	1.5	2003.23	1.5	0.040 ± 0.006	-3.20
5127.11	24816.28	5.5	5317.56	5.5	0.66 ± 0.07	-1.51
5154.20	31441.34	7.5	12045.10	8.5	3.20 ± 0.30	-0.69
5155.04	28072.33	3.5	8679.23	4.5	7.8 ± 0.7	-0.60
5157.07	30345.63	4.5	10960.16	4.5	1.05 ± 0.14	-1.38
5162.88	27942.33	1.5	8578.70	1.5	1.31 ± 0.15	-1.68
5166.04	30445.87	6.5	11094.06	7.5	2.82 ± 0.28	-0.80
5190.43	23646.90	4.5	4386.03	4.5	0.093 ± 0.011	-2.42
5202.70	21904.12	1.5	2688.69	2.5	0.36 ± 0.03	-2.23
5234.19	29314.23	5.5	10214.38	6.5	1.09 ± 0.11	-1.27
5257.92	21702.33	1.5	2688.69	2.5	0.096 ± 0.013	-2.80
5272.85	26484.66	1.5	7524.86	2.5	1.34 ± 0.16	-1.65
5364.38	29509.60	3.5	10873.30	2.5	1.54 ± 0.15	-1.28

Table 2—Continued

λ_{air}	E_{upper}	J_{upp}	E_{lower}	J_{low}	A-value	$\log(gf)$
Å	(cm ⁻¹)		(cm ⁻¹)		(10 ⁶ s ⁻¹)	
5478.33	28429.38	2.5	10180.70	3.5	1.87 ± 0.21	-1.30
5600.86	29640.51	6.5	11791.05	5.5	2.4 ± 0.3	-0.80
5637.30	26413.29	5.5	8679.23	4.5	0.59 ± 0.05	-1.47
5743.35	31521.61	5.5	14115.00	4.5	3.5 ± 0.4	-0.68
5830.99	29934.80	5.5	12789.81	5.5	2.6 ± 0.4	-0.79
5831.73	31646.49	7.5	14503.67	7.5	1.56 ± 0.28	-0.89
5836.33	25175.32	2.5	8046.00	3.5	1.25 ± 0.16	-1.42
5848.66	29934.80	5.5	12841.60	4.5	1.36 ± 0.22	-1.08
5878.10	27188.30	3.5	10180.70	3.5	0.67 ± 0.11	-1.56
5878.42	26413.29	5.5	9406.63	5.5	0.24 ± 0.03	-1.83
5889.70	25552.80	1.5	8578.70	1.5	0.58 ± 0.07	-1.92
5897.38	28997.14	4.5	12045.17	4.5	2.11 ± 0.30	-0.96
5902.36	31441.34	7.5	14503.67	7.5	1.47 ± 0.22	-0.91
5955.83	28445.43	3.5	11659.80	2.5	0.89 ± 0.17	-1.42

Table 2—Continued

λ_{air}	E_{upper}	J_{upp}	E_{lower}	J_{low}	A-value	$\log(gf)$
Å	(cm ⁻¹)		(cm ⁻¹)		(10 ⁶ s ⁻¹)	
5957.50	26190.92	2.5	9410.00	2.5	0.90 ± 0.11	-1.54
5963.23	28997.14	4.5	12232.34	3.5	1.25 ± 0.24	-1.18
5968.83	28540.12	5.5	11791.05	5.5	1.10 ± 0.16	-1.15
5994.65	28072.33	3.5	11395.40	3.5	1.33 ± 0.26	-1.24
6017.39	26828.29	5.5	10214.38	6.5	0.61 ± 0.08	-1.40
6149.06	29246.00	3.5	12987.86	3.5	1.82 ± 0.26	-1.08
6160.43	27188.30	3.5	10960.16	4.5	1.18 ± 0.17	-1.27
6164.53	23352.41	0.5	7135.06	1.5	1.00 ± 0.13	-1.94
6174.94	27063.30	1.5	10873.30	2.5	1.88 ± 0.25	-1.37
6179.83	26357.90	2.5	10180.70	3.5	1.21 ± 0.14	-1.38
6181.05	29640.51	6.5	13466.50	5.5	1.09 ± 0.19	-1.06
6182.89	27263.25	7.5	11094.06	7.5	0.79 ± 0.08	-1.14
6267.29	25361.45	1.5	9410.00	2.5	4.2 ± 0.6	-1.01
6289.91	25304.09	3.5	9410.00	2.5	0.73 ± 0.09	-1.46

Table 2—Continued

λ_{air}	E_{upper}	J_{upp}	E_{lower}	J_{low}	A-value	$\log(gf)$
Å	(cm ⁻¹)		(cm ⁻¹)		(10 ⁶ s ⁻¹)	
6294.68	26253.55	0.5	10371.51	0.5	4.6 ± 0.6	-1.26
6302.40	28429.38	2.5	12566.80	2.5	2.4 ± 0.3	-1.07
6303.17	26820.81	4.5	10960.16	4.5	1.03 ± 0.12	-1.21
6307.08	24429.52	1.5	8578.70	1.5	2.12 ± 0.26	-1.30
6327.52	25980.32	2.5	10180.70	3.5	3.7 ± 0.5	-0.88
6406.25	26565.61	4.5	10960.16	4.5	0.74 ± 0.10	-1.34
6417.48	24257.37	4.5	8679.23	4.5	0.90 ± 0.12	-1.26
6431.01	26505.53	5.5	10960.16	4.5	0.95 ± 0.10	-1.15
6431.98	26938.42	3.5	11395.40	3.5	0.69 ± 0.11	-1.47
6472.35	26540.12	6.5	11094.06	7.5	1.96 ± 0.23	-0.76
6477.05	24013.56	1.5	8578.70	1.5	0.57 ± 0.10	-1.84
6490.81	28191.96	4.5	12789.81	5.5	2.3 ± 0.4	-0.84
6498.65	23962.25	1.5	8578.70	1.5	2.8 ± 0.4	-1.15
6549.77	23842.20	2.5	8578.70	1.5	0.79 ± 0.13	-1.52

Table 2—Continued

λ_{air}	E_{upper}	J_{upp}	E_{lower}	J_{low}	A-value	$\log(gf)$
Å	(cm ⁻¹)		(cm ⁻¹)		(10 ⁶ s ⁻¹)	
6569.29	27263.25	7.5	12045.10	8.5	6.4 ± 0.8	-0.18
6570.67	23260.95	3.5	8046.00	3.5	0.81 ± 0.13	-1.38
6601.83	27188.30	3.5	12045.17	4.5	2.4 ± 0.3	-0.90
6628.90	23659.99	0.5	8578.70	1.5	1.36 ± 0.25	-1.75
6630.62	27309.73	4.5	12232.34	3.5	0.70 ± 0.13	-1.33
6651.63	26820.81	4.5	11791.05	5.5	0.97 ± 0.14	-1.19
6656.16	24429.52	1.5	9410.00	2.5	1.15 ± 0.18	-1.51
6681.53	26357.90	2.5	11395.40	3.5	1.13 ± 0.19	-1.34
6731.81	24257.37	4.5	9406.63	5.5	2.7 ± 0.4	-0.74
6734.83	26889.18	7.5	12045.10	8.5	1.47 ± 0.26	-0.80
6735.35	25361.45	1.5	10518.50	1.5	1.65 ± 0.25	-1.35
6741.50	22875.41	3.5	8046.00	3.5	1.13 ± 0.15	-1.21
6778.22	26540.12	6.5	11791.05	5.5	0.80 ± 0.10	-1.11
6778.66	24928.80	2.5	10180.70	3.5	2.4 ± 0.3	-1.00

Table 2—Continued

λ_{air}	E_{upper}	J_{upp}	E_{lower}	J_{low}	A-value	$\log(gf)$
Å	(cm ⁻¹)		(cm ⁻¹)		(10 ⁶ s ⁻¹)	
6780.03	28938.55	1.5	14193.43	2.5	2.4 ± 0.4	-1.18
6783.00	32130.57	6.5	17391.89	7.5	2.0 ± 0.4	-0.71
6794.15	26505.53	5.5	11791.05	5.5	3.7 ± 0.5	-0.51
6829.86	25597.70	4.5	10960.16	4.5	0.90 ± 0.11	-1.20
6846.53	24816.28	5.5	10214.38	6.5	0.60 ± 0.07	-1.30
6854.51	25980.32	2.5	11395.40	3.5	1.16 ± 0.22	-1.31
6856.01	23260.95	3.5	8679.23	4.5	2.2 ± 0.3	-0.90
6862.81	21702.33	1.5	7135.06	1.5	1.34 ± 0.15	-1.42
6909.84	27309.73	4.5	12841.60	4.5	0.96 ± 0.21	-1.16
6929.62	26086.63	3.5	11659.80	2.5	0.65 ± 0.12	-1.43
6930.40	25385.36	5.5	10960.16	4.5	0.43 ± 0.08	-1.43
6941.62	24582.59	2.5	10180.70	3.5	0.99 ± 0.16	-1.37
6950.50	22429.49	2.5	8046.00	3.5	0.96 ± 0.10	-1.38
6955.66	21507.87	1.5	7135.06	1.5	0.73 ± 0.10	-1.67

Table 2—Continued

λ_{air}	E_{upper}	J_{upp}	E_{lower}	J_{low}	A-value	$\log(gf)$
Å	(cm ⁻¹)		(cm ⁻¹)		(10 ⁶ s ⁻¹)	
7020.40	23646.90	4.5	9406.63	5.5	3.3 ± 0.3	-0.62
7036.72	30104.78	4.5	15897.54	5.5	1.59 ± 0.30	-0.93
7042.21	22875.41	3.5	8679.23	4.5	2.9 ± 0.3	-0.76
7082.36	21250.75	0.5	7135.06	1.5	7.4 ± 0.7	-0.95
7085.50	22788.68	3.5	8679.23	4.5	0.77 ± 0.09	-1.33
7119.80	26086.63	3.5	12045.17	4.5	1.24 ± 0.16	-1.12
7125.11	26820.81	4.5	12789.81	5.5	0.98 ± 0.16	-1.13
7143.96	22039.98	2.5	8046.00	3.5	0.80 ± 0.11	-1.44
7149.57	21507.87	1.5	7524.86	2.5	1.88 ± 0.18	-1.24
7240.89	25597.70	4.5	11791.05	5.5	1.46 ± 0.16	-0.94
7281.48	24689.84	3.5	10960.16	4.5	0.90 ± 0.12	-1.24
7283.39	28394.04	2.5	14667.96	3.5	2.3 ± 0.4	-0.96
7327.05	25304.09	3.5	11659.80	2.5	0.56 ± 0.11	-1.45
7481.97	26828.29	5.5	13466.50	5.5	0.72 ± 0.12	-1.14

Table 2—Continued

λ_{air}	E_{upper}	J_{upp}	E_{lower}	J_{low}	A-value	$\log(gf)$
Å	(cm ⁻¹)		(cm ⁻¹)			(10 ⁶ s ⁻¹)
7502.39	21904.12	1.5	8578.70	1.5	0.60 ± 0.10	-1.69
7578.10	27695.96	6.5	14503.67	7.5	0.71 ± 0.11	-1.07
7637.93	23962.25	1.5	10873.30	2.5	1.00 ± 0.16	-1.46
7645.07	21655.42	0.5	8578.70	1.5	1.98 ± 0.27	-1.46
7647.98	25304.09	3.5	12232.34	3.5	0.83 ± 0.15	-1.24
7749.19	26505.53	5.5	13604.50	6.5	0.81 ± 0.11	-1.06
7820.13	24582.59	2.5	11798.60	2.5	0.79 ± 0.14	-1.36
7835.09	27263.25	7.5	14503.67	7.5	1.23 ± 0.16	-0.74
7837.23	25597.70	4.5	12841.60	4.5	0.85 ± 0.13	-1.10
7928.13	25597.70	4.5	12987.86	3.5	2.1 ± 0.3	-0.70
7937.13	25385.36	5.5	12789.81	5.5	0.52 ± 0.09	-1.23
8001.56	21904.12	1.5	9410.00	2.5	0.51 ± 0.11	-1.71
8031.99	23842.20	2.5	11395.40	3.5	0.52 ± 0.10	-1.52
8068.46	26505.53	5.5	14115.00	4.5	3.6 ± 0.5	-0.37

Table 2—Continued

λ_{air}	E_{upper}	J_{upp}	E_{lower}	J_{low}	A-value	$\log(gf)$
Å	(cm ⁻¹)		(cm ⁻¹)		(10 ⁶ s ⁻¹)	
8161.94	29640.51	6.5	17391.89	7.5	1.6 ± 0.3	-0.66
8195.50	25664.97	6.5	13466.50	5.5	0.69 ± 0.11	-1.01
8218.96	23962.25	1.5	11798.60	2.5	1.20 ± 0.19	-1.31
8305.82	26540.12	6.5	14503.67	7.5	2.4 ± 0.4	-0.47
8387.76	25385.36	5.5	13466.50	5.5	0.58 ± 0.09	-1.13
8486.01	25385.36	5.5	13604.50	6.5	1.16 ± 0.17	-0.82
8510.91	24588.00	5.5	12841.60	4.5	0.78 ± 0.12	-0.99
8543.22	24689.84	3.5	12987.86	3.5	0.84 ± 0.16	-1.13
8617.04	23646.90	4.5	12045.17	4.5	0.50 ± 0.08	-1.26
8677.90	23752.70	4.5	12232.34	3.5	0.30 ± 0.05	-1.46
8706.36	25597.70	4.5	14115.00	4.5	0.49 ± 0.11	-1.25
8708.40	22875.41	3.5	11395.40	3.5	0.76 ± 0.15	-1.16
8717.86	24257.37	4.5	12789.81	5.5	0.80 ± 0.14	-1.04
8758.34	23646.90	4.5	12232.34	3.5	0.61 ± 0.10	-1.16

Table 2—Continued

λ_{air}	E_{upper}	J_{upp}	E_{lower}	J_{low}	A-value	$\log(gf)$
Å	(cm ⁻¹)		(cm ⁻¹)		(10 ⁶ s ⁻¹)	
8780.60	21904.12	1.5	10518.50	1.5	0.77 ± 0.15	-1.45
8788.78	22248.32	2.5	10873.30	2.5	0.88 ± 0.16	-1.21
8808.33	24816.28	5.5	13466.50	5.5	0.33 ± 0.06	-1.34
8859.74	21655.42	0.5	10371.51	0.5	1.84 ± 0.27	-1.36
8939.03	21702.33	1.5	10518.50	1.5	0.27 ± 0.05	-1.89
8976.68	21655.42	0.5	10518.50	1.5	1.29 ± 0.23	-1.51
8989.13	24588.00	5.5	13466.50	5.5	0.41 ± 0.08	-1.22
9012.20	22248.32	2.5	11155.30	1.5	1.05 ± 0.25	-1.11
9060.34	22429.49	2.5	11395.40	3.5	1.04 ± 0.25	-1.12
9063.02	21904.12	1.5	10873.30	2.5	0.84 ± 0.15	-1.38
9100.81	25178.45	1.5	14193.43	2.5	1.12 ± 0.19	-1.26
9119.18	23752.70	4.5	12789.81	5.5	0.25 ± 0.05	-1.50
9189.30	21250.75	0.5	10371.51	0.5	0.48 ± 0.07	-1.92
9231.90	21702.33	1.5	10873.30	2.5	0.25 ± 0.05	-1.89

Table 2—Continued

λ_{air}	E_{upper}	J_{upp}	E_{lower}	J_{low}	A-value	$\log(gf)$
Å	(cm $^{-1}$)		(cm $^{-1}$)		(10 6 s $^{-1}$)	
9282.77	22429.49	2.5	11659.80	2.5	0.19 ± 0.04	-1.84
9315.15	21250.75	0.5	10518.50	1.5	0.71 ± 0.12	-1.73
9393.21	22875.41	3.5	12232.34	3.5	0.30 ± 0.04	-1.49
9441.60	22248.32	2.5	11659.80	2.5	0.16 ± 0.03	-1.89
9702.24	27695.96	6.5	17391.89	7.5	3.0 ± 0.4	-0.23
9725.54	27284.69	2.5	17005.30	3.5	0.78 ± 0.12	-1.18
9739.08	26880.60	5.5	16615.50	6.5	0.91 ± 0.12	-0.81
9743.12	24928.80	2.5	14667.96	3.5	0.96 ± 0.15	-1.09
9755.79	27639.40	6.5	17391.89	7.5	0.98 ± 0.15	-0.71
9766.68	24429.52	1.5	14193.43	2.5	0.44 ± 0.08	-1.59
9788.96	26828.29	5.5	16615.50	6.5	1.78 ± 0.25	-0.51
9850.67	26046.35	4.5	15897.54	5.5	2.4 ± 0.4	-0.46
9936.51	25304.09	3.5	15242.95	4.5	2.1 ± 0.3	-0.61
10083.34	24582.59	2.5	14667.96	3.5	1.09 ± 0.22	-1.00

Table 2—Continued

λ_{air}	E_{upper}	J_{upp}	E_{lower}	J_{low}	A-value	$\log(gf)$
Å	(cm $^{-1}$)		(cm $^{-1}$)		(10 6 s $^{-1}$)	
10108.42	26505.53	5.5	16615.50	6.5	0.59 ± 0.09	-0.96
10116.94	29509.60	3.5	19627.90	3.5	1.11 ± 0.23	-0.87
10233.85	23962.25	1.5	14193.43	2.5	0.35 ± 0.07	-1.66
10289.15	27284.69	2.5	17568.38	1.5	0.69 ± 0.14	-1.18
10306.28	25597.70	4.5	15897.54	5.5	0.55 ± 0.08	-1.05
10582.60	24689.84	3.5	15242.95	4.5	0.33 ± 0.06	-1.36

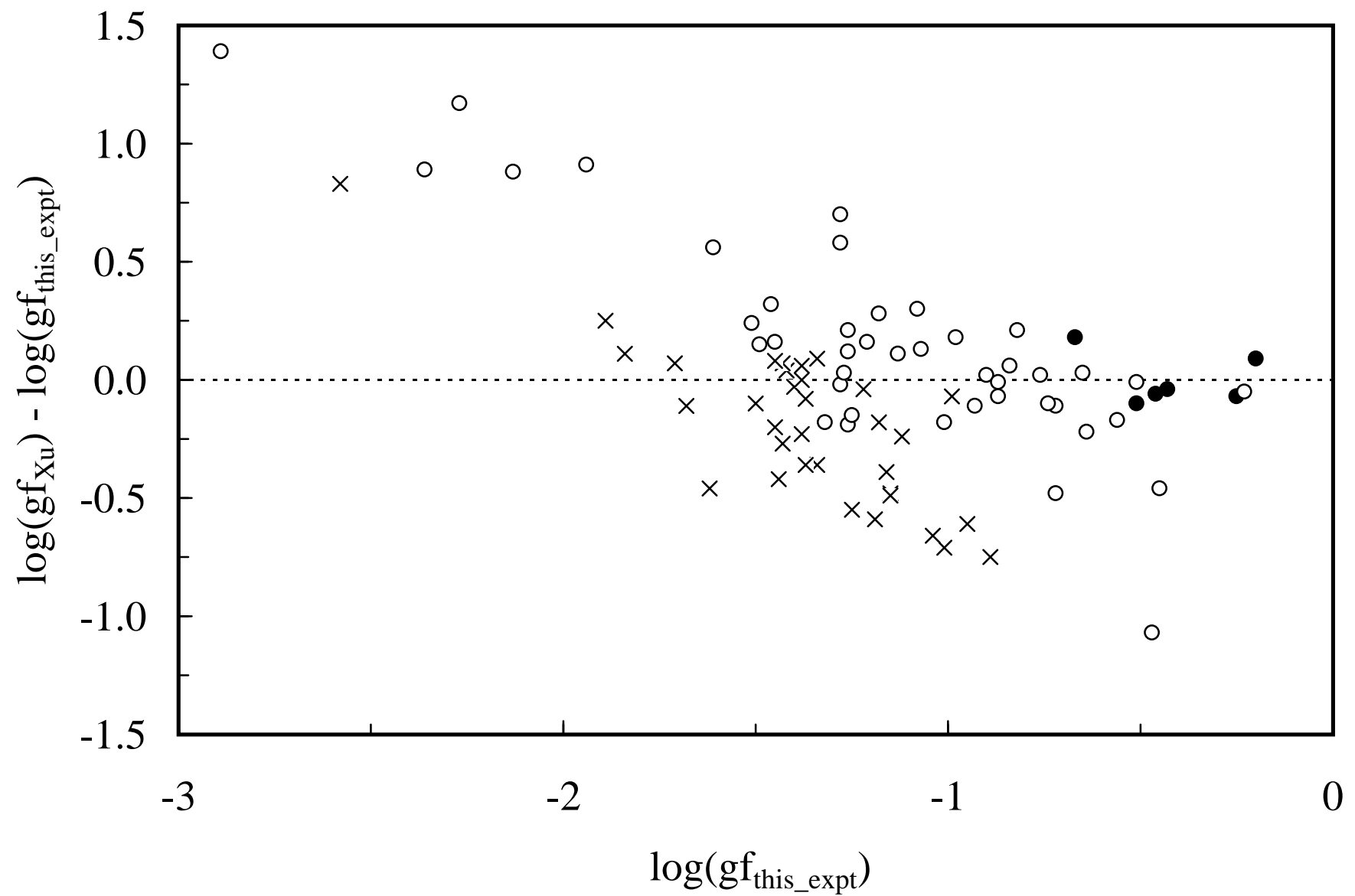


Table 3. Samarium abundance determinations in the Sun, BD+17°3248, HD 115444 and CS 22892-052.

λ_{air}	E.P.	log(gf)	Comment	Sun	BD	HD	CS
Å	(eV)			log(ε)	log(ε)	log(ε)	log(ε)
3568.260	0.484	0.29	hfs	...	-0.37	-1.38	-0.61
3626.995	0.277	-0.51	hfs	...	-0.34	-1.38 :	...
3706.750	0.484	-0.60	Single	...	-0.42	-1.23 :	-0.61
3708.410	0.040	-1.01	Single	1.00	-0.55	-1.38 :	-0.56
3708.659	0.184	-0.63	Single	...	-0.34	-1.20	-0.56
3755.281	0.333	-0.65	Single	1.15	-0.22 :	-1.18 :	-0.48
3764.379	0.333	-0.55	Single	...	-0.30	-1.18	-0.63
3831.505	0.434	-0.43	Single	...	-0.27	...	-0.58
3847.521	0.333	-0.78	Single	...	-0.37	-1.28	-0.58
3896.970	0.040	-0.67	Single	0.94	-0.37	-1.33	-0.68
3922.386	0.378	-0.26	Single	...	-0.37	-1.30	-0.61
3946.503	0.184	-0.94	Single	...	-0.30	-1.25	-0.56
3976.265	0.104	-0.90	Single	...	-0.29	-1.18	-0.64
3976.429	0.333	-0.58	Single	...	-0.42	-1.13	-0.66

Table 3—Continued

λ_{air}	E.P.	log(gf)	Comment	Sun	BD	HD	CS
Å	(eV)			log(ε)	log(ε)	log(ε)	log(ε)
3979.195	0.543	-0.47	Single	...	-0.37	-1.28	-0.56
3993.301	0.040	-0.93	Single	...	-0.42	-1.28	-0.63
4023.224	0.040	-0.93	Single	1.00	-0.29	-1.21	-0.57
4047.151	0.184	-0.92	Single	...	-0.33	-1.08	...
4064.565	0.184	-1.28	hfs	...	-0.42	-1.41	-0.68
4068.324	0.434	-0.76	Single	0.98	-0.32	-1.23	-0.61
4094.025	0.333	-1.15	Single	...	-0.30	...	-0.43
4113.898	0.184	-1.07	Single	-0.56 :
4155.211	0.543	-0.73	Single	-0.53
4169.472	0.248	-0.76	Single	...	-0.32	-1.23	-0.63 :
4188.125	0.543	-0.44	Single	...	-0.30	-1.18	-0.53
4206.121	0.378	-0.72	Single	...	-0.37	-1.25	-0.66
4220.658	0.543	-0.44	Single	...	-0.33	-1.31	-0.63
4244.696	0.277	-0.81	Single	1.04	-0.42	-1.28	-0.63

Table 3—Continued

λ_{air}	E.P.	log(gf)	Comment	Sun log(ε)	BD log(ε)	HD log(ε)	CS log(ε)
Å	(eV)						
4256.394	0.378	-0.15	Single	0.98	-0.34	-1.23	-0.65
4265.071	0.184	-1.04	Single	0.92	-0.37	-1.25	...
4318.936	0.277	-0.25	Single	0.97	-0.33	-1.25	-0.65
4329.019	0.184	-0.51	Single	1.05	-0.32	-1.30	-0.73
4334.150	0.280	-0.50	Single	...	-0.34	-1.13	...
4360.713	0.248	-0.87	Single	...	-0.34	-1.33	...
4362.023	0.484	-0.47	Single	...	-0.39	-1.28	...
4420.528	0.333	-0.43	Single	1.02	-0.31	-1.23	-0.63
4421.133	0.378	-0.49	Single	...	-0.36	-1.23	...
4424.321	0.484	0.14	Single	0.95	-0.35	-1.35	-0.66
4433.887	0.434	-0.19	Single	...	-0.33	-1.24	...
4452.722	0.277	-0.41	Single	1.10 :	-0.37	-1.25	...
4467.341	0.659	0.15	Single	1.02	-0.38	-1.38	-0.61
4472.406	0.184	-0.96	Single	1.02	-0.37	-1.28	-0.53

Table 3—Continued

λ_{air}	E.P.	log(gf)	Comment	Sun	BD	HD	CS
Å	(eV)			log(ε)	log(ε)	log(ε)	log(ε)
4478.654	0.659	-0.36	Single	...	-0.33	-1.18	...
4499.475	0.248	-0.87	Single	1.00	-0.35	-1.28	...
4511.830	0.184	-0.82	hfs	...	-0.32	-1.25	...
4515.092	0.188	-0.87	Single	1.04	-0.29	-1.18	-0.58
4519.630	0.543	-0.35	hfs	0.98	-0.34	-1.28	-0.58
4523.909	0.434	-0.39	Single	...	-0.35	-1.28	-0.68
4536.512	0.104	-1.28	Single	...	-0.31	-1.22	...
4537.951	0.484	-0.48	hfs	1.02	-0.36	-1.30	...
4540.184	0.277	-1.28	hfs	...	-0.35 :	-1.30	...
4542.048	0.248	-1.04	Single	1.00	-0.32	-1.28	-0.58
4552.654	0.248	-0.82	Single	...	-0.34	-1.20	-0.53
4554.437	0.104	-1.25	hfs	...	-0.34	-1.23	-0.56
4560.419	0.040	-1.24	Single	1.00	-0.34	-1.23	...
4566.202	0.333	-0.59	Single	1.00 :	-0.37	-1.23	-0.66

|
G
|

Table 3—Continued

λ_{air}	E.P.	log(gf)	Comment	Sun	BD	HD	CS
Å	(eV)			log(ε)	log(ε)	log(ε)	log(ε)
4577.688	0.248	-0.65	Single	1.03	-0.39	-1.26	-0.63
4584.833	0.434	-0.65	Single	...	-0.37 :	-1.33	-0.66
4591.820	0.184	-1.12	hfs	1.02	-0.33	-1.26	-0.58
4593.545	0.378	-0.83	hfs	...	-0.32	-1.25	-0.58
4595.290	0.484	-0.50	hfs	...	-0.31	-1.23	...
4604.174	0.040	-1.39	hfs	0.95	-0.32 :	-1.20	...
4606.510	0.000	-1.26	hfs	1.07 :	-0.26 :	-1.23	-0.53
4615.437	0.543	-0.69	Single	0.94	-0.30	-1.50	...
4615.683	0.188	-0.84	hfs	0.96	-0.29	-1.25	...
4642.228	0.378	-0.46	Single	1.05 :	-0.30	-1.23	-0.71
4669.389	0.104	-0.60	Single	1.00	-0.30	...	-0.65
4669.641	0.277	-0.53	hfs	...	-0.30	...	-0.67
4676.902	0.040	-0.87	hfs	1.00 :	...	-1.25	-0.58
4687.178	0.040	-1.15	hfs	...	-0.24 :	...	-0.63

Table 3—Continued

λ_{air}	E.P.	log(gf)	Comment	Sun	BD	HD	CS
Å	(eV)			log(ε)	log(ε)	log(ε)	log(ε)
4719.844	0.040	-1.24	hfs	...	-0.32	-1.28	-0.43
4745.674	0.104	-0.93	hfs	...	-0.42	-1.25	-0.73
4777.844	0.040	-1.42	Single	0.96	-0.29	...	-0.73
4815.808	0.184	-0.82	Single	0.95	-0.37	-1.34	-0.68
4844.209	0.277	-0.89	Single	1.00	...	-1.36	-0.60
4854.372	0.378	-1.25	Single	0.98
4913.258	0.659	-0.93	hfs	...	-0.27 : :
4948.627	0.543	-0.95	hfs	1.00 :

Note. — Colons denote less certain abundances.

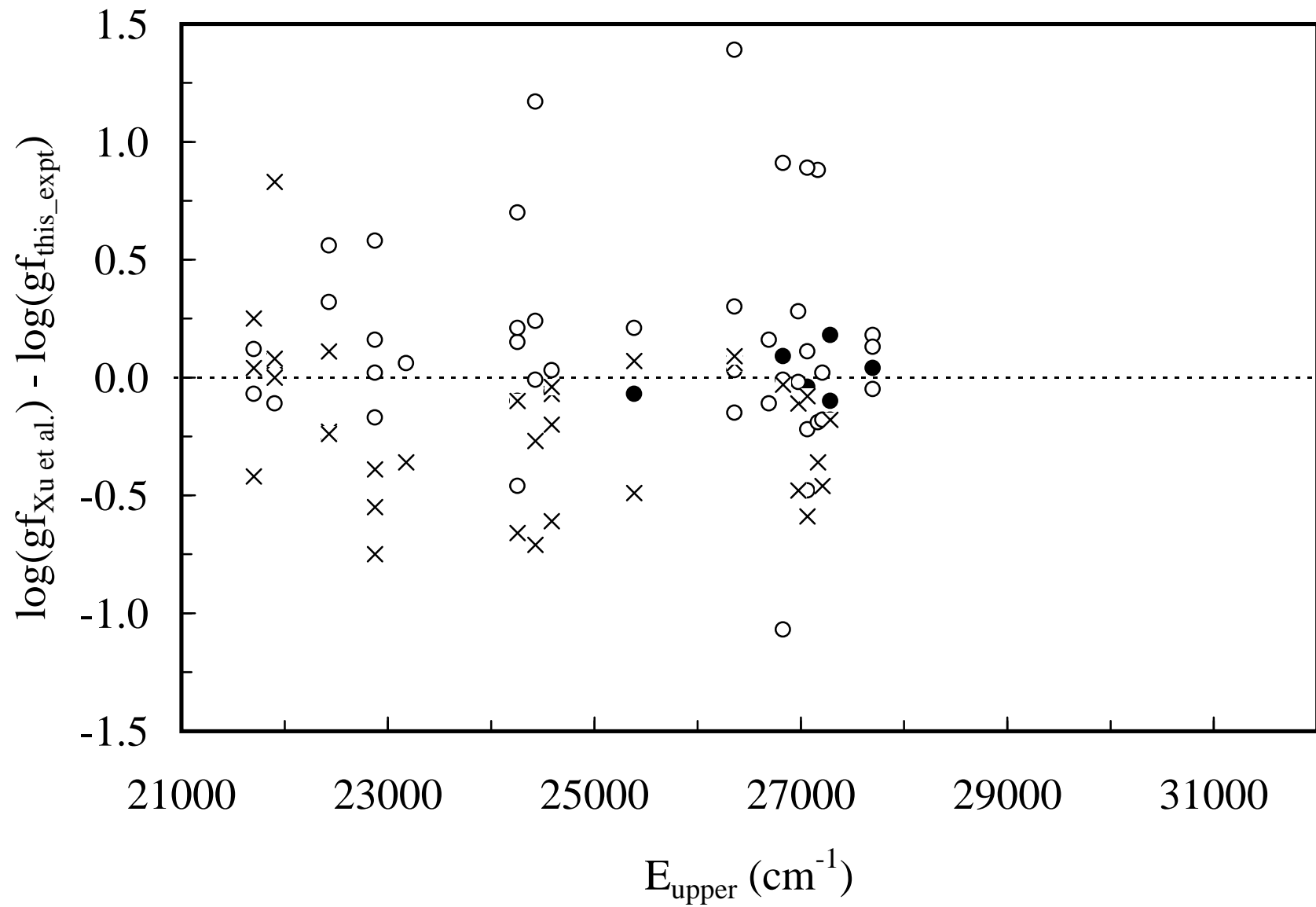


Table 4. Samarium abundance determinations in the Sun, BD+17°3248, HD 115444 and CS 22892-052.

Star	$\log \varepsilon(\text{Sm}) \pm \sigma$	# of published lines	$\log \varepsilon (\text{Sm}) \pm \sigma$	# of new lines	$\log \varepsilon (\text{Eu}) \pm \sigma$	# of lines	$\log \varepsilon (\text{Sm/Eu})$	Notes
Sun	+1.00 ± 0.14	26	+1.00 ± 0.05	36	+0.52 ± 0.04	14	0.48	1
HD 115444	-1.18 ± 0.16	4	-1.26 ± 0.07	67	-1.64 ± 0.02	5	0.38	2
BD+17°3248	-0.42 ± 0.14	17	-0.34 ± 0.05	72	-0.67 ± 0.05	9	0.33	3
CS 22892-052	-0.54 ± 0.13	15	-0.61 ± 0.07	55	-0.95 ± 0.03	8	0.35	4

- Note. — 1. Published Sm is from Biémont et al. (1989), Eu is from Lawler et al. (2001).
 2. Published Sm is from Westin et al. (2000), Eu is from Den Hartog et al. (2003).
 3. Published Sm is from Cowan et al. (2002), as is Eu.
 4. Published Sm is from Sneden et al. (2003), as is Eu.

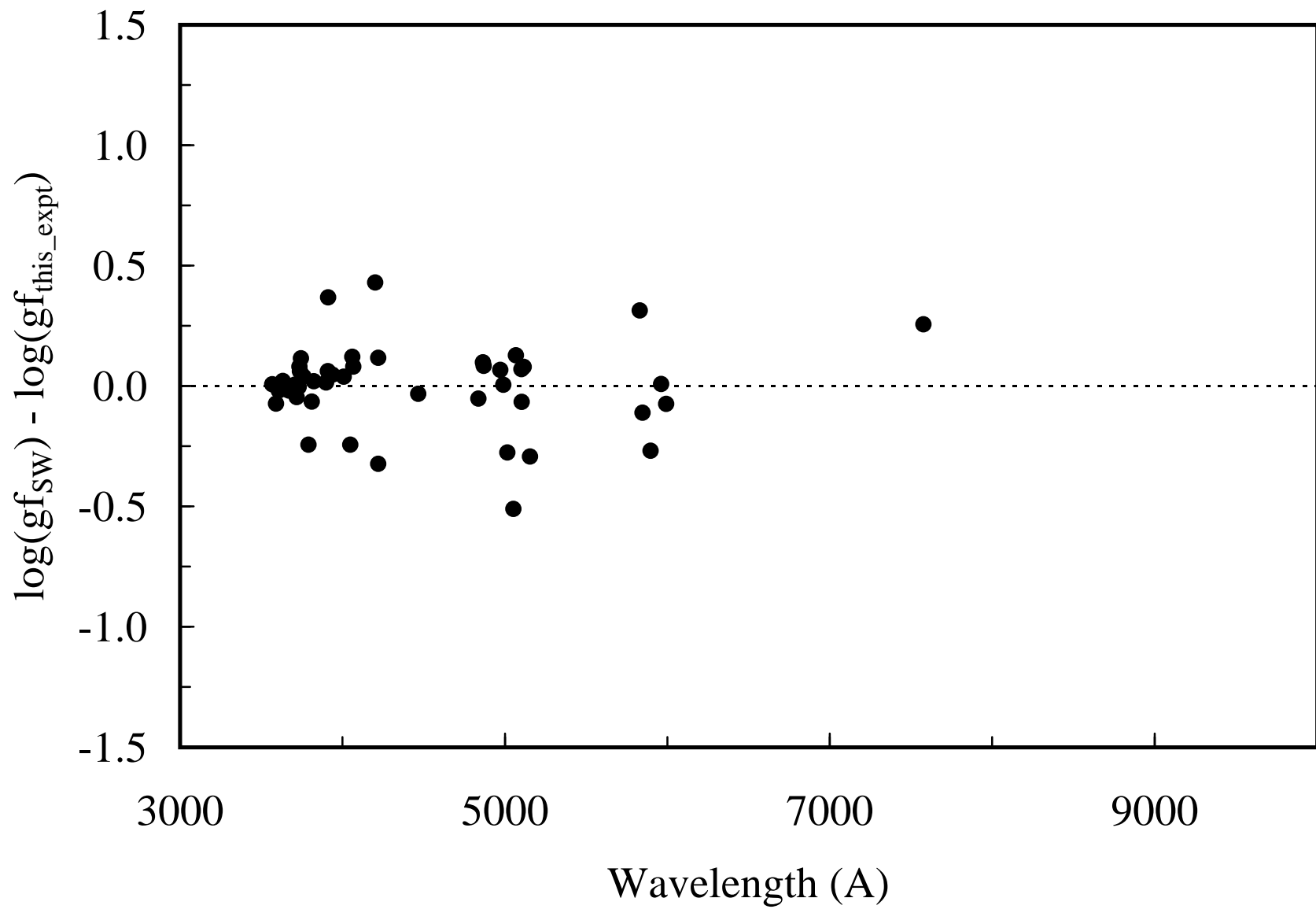


Table 5. Contributions of Sm from the s- and r-processes based on the Si = 10^6 scale.

Isotope	s-abundance ^a	%	r-abundance ^a	%	s-abundance ^b	%	r-abundance ^b	%
¹⁴⁷ Sm	0.0028	3.3	0.31	17.8	0.008	10.8	0.0317	18.2
¹⁴⁸ Sm ^c	0.038	44.5	0	0	0.282	37.0	0	0
¹⁴⁹ Sm	0.0051	5.9	0.31	17.8	0.0045	5.8	0.031	17.9
¹⁵⁰ Sm ^c	0.0217	25.2	0	0	0.019	25.0	0	0
¹⁵² Sm	0.018	21	0.053	30.4	0.016	20.7	0.053	30.5
¹⁵⁴ Sm	0	0	0.059	34	0.0005	0.6	0.058	33.4

Note. — ^aStandard Model: Käppeler et al. (1989), Burris et al. (2000), Simmerer et al. (2001).

^bStellar Model: Arlandini et al. (1989).

^cOnly s-process.

